Preclinical evaluation of HDAC inhibitors for epigenetic therapy of primary brain tumors

Inaugural-Dissertation

zur Erlangung des Doktorgrades

der Mathematisch-Naturwissenschaftlichen Fakultät

der Heinrich-Heine-Universität Düsseldorf

vorgelegt von

Viktoria Marquardt

aus Kassel

Düsseldorf, Oktober 2019

aus dem Institut für Pharmazeutische und Medizinische Chemie

der Heinrich-Heine-Universität Düsseldorf

Gedruckt mit der Genehmigung der

Mathematisch-Naturwissenschaftlichen Fakultät der

Heinrich-Heine-Universität Düsseldorf

Berichterstatter:

1. Prof. Dr. Thomas Kurz

2. PD Dr. Jörg Felsberg

Tag der mündlichen Prüfung:

12.12.2019

Table of contents

Summary

Advances in next generation genomic technologies have yielded remarkable progress in our understanding of the biology underlying brain tumors and helped to identify distinct molecular characteristics for the different entities. As further layers of heterogeneity within the entities are being unraveled, genomic sequencing and copy number profiling also identified frequent alterations of chromatin modifiers, suggesting that epigenetic deregulation is an important driver of oncogenic transformation. Epigenetic modifications, such as DNA methylation or histone acetylation, and the information they convey are essential for the regulation of all DNA-based processes including transcription, replication and repair. Abnormal expression patterns or genomic alterations in chromatin modulators can therefore have profound impact on cell identity and lead to the induction and progression of cancers. To improve survival of high-risk patients and reduce the significant long-term sequelae associated with conventional chemotherapeutic treatment, implementation of rational therapies are highly warranted. Moreover, reversing aberrant epigenetic signature in cancer using targeted inhibitors has increasingly gained attention in the last decades, as exemplified by the clinical approval of inhibitors of DNA methyltransferases (DNMT) and histone deacetylase (HDAC) for the treatment of various cancers.

To accelerate and facilitate the discovery of novel inhibitors with translational potential, we established an institutional drug-screening pipeline that allows for the simultaneous evaluation of hundreds of compounds in large cell line cohorts. The optimized workflow was streamlined by semi-automated dispensing of inhibitors and cell lines, providing high accuracy and reproducibility. Our unique panel of cell lines, derived from the most common malignant brain tumor entities of infancy, childhood and adulthood, was screened with an institutional HDAC inhibitor (HDACi) library. The library is composed of clinically tested and approved HDACi as well as a unique compound collection synthesized in-house. Evaluation of over 250 inhibitors in 34 cell lines provided notable insights regarding the susceptibilities of distinct entities and subtypes for inhibition of HDACs. The cross-entity

comparison showed that *MYC* amplified Group 3 medulloblastoma are particularly sensitive towards HDAC inhibition and that the clinically tested HDAC 1-3 selective inhibitor CI-994 was the most significantly active inhibitor among the commercially available compounds. Further *in vitro* evaluation demonstrated induction of apoptosis and decreased *MYC* expression levels following CI-994 treatment of *MYC*-driven medulloblastoma cells. Confirming our screening approach, we demonstrated significantly extended survival in two orthotopic xenograft mouse models of *MYC*-driven medulloblastoma. CI-994 treatment decreased not only tumor growth at the primary site, but more noteworthy, elicited significant activity against metastatic dissemination. RNA sequencing results of treated cells identified significant upregulation of NFκB pathway genes in CI-994 treated cells. We further utilized the established screening workflow for large-scale synergy interaction studies. By screening CI-994 in combination with a library of 199 clinically established chemotherapeutics as well as targeted agents currently under clinical evaluation, we could identify several promising interactions. Amongst already established combination partners for HDACi such as DNA methyltransferases or proteasome inhibitors, we also showed that the NFκB pathway inhibitor bardoxolone methyl acts highly synergistic in combination with CI-994. Corroborating our RNA sequencing data, the results from the synergy screening further underlined that the NFκB pathway is activated upon CI-994 treatment and is functionally relevant.

Zusammenfassung

Die signifikanten Fortschritte, die in den letzten Jahren im Bereich der *Next Generation Sequencing* Technologien erzielt wurden, haben wesentlich zu unserem Verständnis der zugrunde liegenden Biologie von Hirntumore und dem Auftreten spezifische molekulare Veränderungen beigetragen. Während weitere molekulare Heterogenität innerhalb der einzelnen Entitäten entschlüsselt werden konnte, wurden mittels Sequenzierung zudem häufige Veränderungen von Chromatin-Modifikatoren identifiziert. Epigenetische Deregulierung stellt daher einen wichtigen Treiber maligner Transformation dar. Epigenetische Modifikationen wie DNA-Methylierung oder Histon-Acetylierung und die damit übermittelten Informationen sind für die Regulation aller DNA-basierten Prozesse einschließlich Transkription, Replikation und Reparatur unerlässlich. Abnormale Expressionsmuster oder genomische Veränderungen in Chromatin-Modulatoren können daher einen erheblichen Einfluss auf die Zellidentität haben und zur Tumorentstehung beitragen. Um das Überleben von Hochrisikopatienten zu verbessern und die langfristigen Nebenwirkungen einer konventionellen, chemotherapeutischen Behandlung zu reduzieren, ist die Entwicklung rationaler, gezielter Therapien erstrebenswert. Darüber hinaus hat der Einsatz von Inhibitoren zur Umkehrung abormaler, epigenetischer Signaturen bei Krebs in den letzten Jahrzehnten zunehmend an Aufmerksamkeit gewonnen, wie die klinische Zulassung von Inhibitoren für DNA-Methyltransferasen (DNMT) und Histon-Deacetylase (HDAC) zur Behandlung verschiedener Krebsarten zeigt.

Um die Entdeckung neuartiger Inhibitoren mit translationalem Potenzial zu beschleunigen und zu erleichtern, haben wir eine institutionelle Plattform zum Wirkstoffscreening aufgebaut, die die gleichzeitige Evaluierung von Hunderten von Substanzen in großen Zelllinienkohorten ermöglicht. Der optimierte Arbeitsablauf wurde durch die halbautomatische Dosierung von Inhibitoren und Zelllinien optimiert, wodurch eine hohe Genauigkeit und Reproduzierbarkeit gewährleistet wird. Unsere einzigartige Kohorte von Zelllinien der häufigsten bösartigen Hirntumorentitäten im Säuglings-, Kinder- und Erwachsenenalter wurde mit einer institutionellen HDAC-Inhibitor (HDACi)-Bibliothek

untersucht. Die Bibliothek besteht aus klinisch getesteten und zugelassenen HDACi, sowie einer einzigartigen, institutionell entwickelten Wirkstoffsammlung. Die Evaluierung von über 250 Inhibitoren in 34 Zelllinien lieferte bemerkenswerte Erkenntnisse über die Sensitivität verschiedener Entitäten und Subtypen für die Hemmung von HDACs. Der Vergleich mit anderen Entitäten zeigte, dass *MYC*-amplifizierte Medulloblastom Zelllinien besonders empfindlich auf Inhibierung von HDACs reagiert und dass der klinisch getestete HDAC-Klasse-I-Inhibitor CI-994 der selektivste Inhibitor unter den kommerziell erhältlichen Substanzen war. Weitere *in vitro* Experimente zeigten die Induktion von Apoptose und reduzierte *MYC*-Expression nach CI-994 Behandlung von *MYC*-amplifizierten Medulloblastomzellen.

Die Behandlung von zwei orthotopen Xenograft-Mausmodellen mit CI-994 führte zu einem signifikant verlängertem Überleben. CI-994 Behandlung verringerte nicht nur das Wachstum des Primärtumors, sondern konnte außerdem eine Ausbreitung über Metastasen vermindern. Durch die Analyse von RNA-Sequenzierungsdaten CI-994 behandelter Zellen konnten wir zudem eine signifikante Hochregulation von Genen des NFκB Signalwegs identifizieren. Der etablierten Screening-Workflow konnten wir außerdem für Synergie-Interaktionsstudien nutzen. Durch das Screening von CI-994 in Kombination mit einer Bibliothek von 199 klinisch etablierten Chemotherapeutika sowie Wirkstoffen, die sich derzeit in der klinischen Prüfung befinden, konnten wir mehrere vielversprechende Wirkstoffkombinationen identifizieren. Neben bereits etablierten Kombinationspartnern für HDACi wie DNA-Methyltransferasen oder Proteasom-Inhibitoren konnten wir zusätzlich zeigen, dass der NFκB-Inhibitor Bardoxolone methyl in Kombination mit CI-994 synergistisch wirkt. Die Ergebnisse des Synergie-Screenings unterstützen somit die RNA-Sequenzierungsdaten und zeigen, dass der NFκB Signalweg nach CI-994 Behandlung aktiviert wird und funktionell relevant ist.

1 Introduction

Traditionally, cancer has been regarded as a disease of genomic imbalance. The accumulation of mutations in oncogenes or tumor suppressor genes as well as chromosomal alterations give rise to neoplastic cells with mutant genotypes.[1] Clonal expansion and the acquisition of distinct hallmark features like uncontrolled proliferation, acquired immortality and evasion of cell death impart selective advantages on mutated subclones of cells, enabling their dominance and outgrowth.[1] However, research during the last decades has unraveled the critical role of epigenetic deregulation in the initiation, progression and evolution of cancer.[2–5] Since single genetic variants cannot completely account for the complex, heterogeneous phenotype of neoplasia, oncogenic transformation and tumor progression is rather thought to involve both genetic and epigenetic alterations.[6,7] Initially defined by C. H. Waddington in 1942 as molecular pathways modulating the expression of a genotype into a particular phenotype, epigenetics nowadays is described as the heritable changes in gene expression without alteration of the DNA sequence.[8,9]

Changes in gene activity and cellular phenotype are shaped by epigenetic alteration in the organization of the chromatin. The genetic information of eukaryotic cell is packaged into macromolecular chromatin complexes composed of histone proteins and DNA. Regulation of the accessibility of the chromatin to transcription factors is regulated by covalent modification of its components, thereby altering the local structural dynamics of the chromatin.[10] Reversible epigenetic modifications are achieved by DNA methylation, modifications of histone proteins, nucleosome positioning and posttranscriptional gene regulation by noncoding RNAs, thereby defining the epigenetic landscape of the individual cells.[2] These heritable modifications and expression patterns are determined during the course of cell differentiation and are maintained during cell division, thus providing cells with distinct identities albeit sharing the same genome.[11]

The best studied epigenetic modifications are the methylation of the DNA base cytosine within so-called CpG island of gene promoter regions as well as the methylation and acetylation of lysine side chains of the histone tails.[10,12] Mediators of these modifications are

DNA and histone methyltransferases as well as histone acetyltransferases. Together with the corresponding counterparts, DNA and histone demethylases as well as histone deacetylases, they serve as epigenetic writers and erasers and define the epigenetic histone code.[13,14] Epigenetic readers are proteins that recognize these histone patterns and recruit additional protein complexes to regulate transcription.[15] In addition, the overall chromatin architecture is organized by chromatin remodelers and chromatin-associated proteins.[16] Altogether, these modifications play a critical role in the temporal and spatial regulation of transcription, replication and DNA repair and as a result of this epigenetic plasticity, dysregulation of chromatin modifying enzymes and abnormal expression patterns can contribute to tumorigenesis or are even thought to initiate neoplastic transformation by preceding genetic changes.[17,18]

Large scale genomic studies demonstrated that many adult and childhood cancers show deregulation in their epigenetic landscape.[6,7,19] Especially pediatric malignancies are characterized by a low overall mutational load in comparison to most adult cancers[20] and comprehensive epigenetic dysregulation caused by mutations of epigenetic modifiers or regulators was identified to play a pivotal role in many childhood cancers.[21,22] Although major improvements in cure rates for pediatric cancers have been achieved over the last decades, many cancer survivors suffer from severe long-term side effects caused by high-dose chemotherapeutic intervention. In addition, for some malignancies as well as in case of recurrence there are often no effective therapeutic options available.[23] Consequently, given the limitations of current treatment protocols and the potential to reverse cancer associated epigenetic alterations, the rational development and clinical evaluation of epigenetic drugs for the targeted treatment of cancer is increasingly recognized as a promising approach for pharmacological intervention.[24,25]

1.1 Brain tumors

Malignant brain tumors are the most common cause of cancer-related death in children and young adults.[26,27] Covering a broad spectrum of about 100 distinct malignancies, brain tumors do not only vary in their histological, demographical, and clinical features, but also show significant differences regarding their molecular characteristics.[28] The emergence of next generation sequencing methods and concomitant genomic studies of comprehensive brain tumor cohorts substantially increased the information about the distinct genetic and epigenetic alterations present in brain tumors.[29–33] Up to now, diagnostic characterization is still largely based on histopathological criteria defined by morphological evaluation and immunohistochemistry. However, further integration of the growing genetic understanding of brain tumors into their classification has the possibility to greatly increase diagnostic accuracy and objectivity, thereby improving prognosis and treatment options for a better management of patients.[28] In this regard, classification based on DNA methylation profiles has already been shown to be a valuable diagnostic tool for the identification of distinct central nervous system (CNS) tumor entities and subclasses.[34] As a result of the growing importance of molecular based characterization, the 2016 World Health Organization (WHO) classification of CNS tumors included for the first time molecular parameters into the definition of some brain tumors.[28] One of these selected entities is the embryonal brain tumor medulloblastoma (MB).

1.1.1 Medulloblastoma

Medulloblastoma is the most common malignant brain tumor in children. Originating from the cerebellum, medulloblastoma are invasive and fast growing tumors that are frequently metastatic already at diagnosis with spread through the cerebrospinal fluid (CSF) and along the surface of the brain and spinal cord.[35,36] Medulloblastoma generally form near the fourth ventricle between the brainstem and the cerebellum and are mainly diagnosed in infants and children, with a median age at diagnosis of five years. In adults, medulloblastoma is less common, accounting for around 1% of all adult brain tumors and incidence decreases with

increasing age.[37] Medulloblastoma are more common in males than females with a ratio of 1.8:1.[35] Historically, medulloblastoma have been classified based on four histological subtypes, namely classic, desmoplastic-nodular (D/N), large-cell–anaplastic (LCA), and medulloblastoma with extensive nodularity (MBEN).[28] However, genetic studies based on transcriptional and methylation profiling revealed distinct molecular subgroups that differ in their demographics, somatic mutations, transcriptomes and clinical outcome.[38–40] Molecularly defined, medulloblastoma is therefore divided into four consensus groups, namely, wingless (WNT), sonic hedgehog (SHH), Group 3 and Group 4.[41] Advancing the genomics approaches by integrating different layers of information obtained from DNA methylation and gene expression profiling revealed further heterogeneity within the subgroups dividing them in additional subtypes.[42–44]

Contemporary therapy consists of surgical resection of the tumor, followed by craniospinal irradiation with a boost to the tumor bed and adjuvant chemotherapy.[45] The use of these modalities in modern therapeutic protocols has resulted in a cure rate of approximately 70–85% among children aged $\geq$3 years.[45,46] Based on clinical criteria, patients with medulloblastoma are currently stratified into average-risk and high-risk groups. Average-risk medulloblastoma patients have less than 1.5 cm^2 post-operative residual tumor and no metastases, whereas high risk patients have metastatic dissemination at diagnosis and/or more than 1.5 cm^2 residual tumor.[45] Average and high-risk patients receive intense chemotherapy regime of various cycles of cisplatin, vincristine and cyclophosphamide or lomustine.[45] This treatment stratification approach led to improved survival rates for patients with high-risk disease, and allowed for the reduction of treatment exposure for patients with average-risk disease. Nevertheless, medulloblastoma patients have to deal with many long-term adverse sequelae. Deficits in neuro-cognitive and neuroendocrine function, hearing, fertility, cardiopulmonary fitness, and physical performance are some of the common side effects of therapy.[47–51] Medulloblastoma mostly recur as CNS metastases rather than at the primary site.[36] Long term survival after relapse is dismal and there is no standard therapy protocol available.[52]

1.1.1.1 Molecular subgroups of meduolloblastoma

WNT group

WNT signaling activated medulloblastoma is the least common subgroup accounting for around 10% of medulloblastoma cases. The WNT subgroup is characterized by a very favorable prognosis with long-term survival exceeding 90%, mortality is mainly attributed to complications of therapy or secondary neoplasm rather than recurrence. Metastatic spread at diagnosis and later is infrequent. [38,39,41] Progenitor cells from the lower rhombic lip of the dorsal brainstem are likely the cell of origin and WNT tumors are mostly located within the IV ventricle, infiltrating the dorsal surface of the brainstem.[53] WNT medulloblastomas are characterized by an activated WNT signaling pathway, which is almost universally caused by an activating somatic mutation in exon 3 of CTNNB1 (catenin beta 1). This alteration leads to a mutant form of the β-catenin protein which is resistant to degradation and induces the expression of WNT target genes.[43,54,55] The first evidence demonstrating the involvement of WNT signaling pathway in medulloblastoma came from genetic studies of patients with Turcot syndrome, predisposing them for familial adenomatous polyposis as well as colorectal adenomas and medulloblastoma.[55,56] In contrast to a higher risk associated with TP53 mutation in SHH tumors, TP53 mutation in WNT tumors does not infer worse prognosis.[57]

Albeit having a rather balanced genome, WNT medulloblastoma frequently show loss of one chromosome 6. Compared to the other subgroups this hallmark chromosomal aberration is found almost exclusively in WNT medulloblastoma.[58,59] Finally, when integrating gene expression and methylation data, the WNT subgroup can be further distinguished into two subtypes: WNT α is enriched for children with monosomy 6 whereas WNT β mainly consist of older patients who are diploid for chromosome 6. Survival between these two groups is comparable (Figure 1).[42]

Subgroup	WNT		SHH			
Subtype	WNT α	WNT β	SHH α	SHH β	SHH γ	SHH δ
Subtype proportion						
Subtype relationship						
Clinical data — Age	(>3-10, >10-17)	(>10-17, >17)	(>3-10, >10-17)	(0-3)	(0-3)	(>17)
Clinical data — Histology			LCA Desmoplastic	Desmoplastic	MBEN Desmoplastic	Desmoplastic
Clinical data — Metastases	8.6%	21.4%	20%	33%	8.9%	9.4%
Clinical data — Survival at 5 years	97%	100%	69.8%	67.3%	88%	88.5%
Copy number — Broad	6⁻		9q⁻, 10q⁻, 17p⁻		Balanced genome	
Copy number — Focal			MYCN amp, GLI2 amp, YAP1 amp	PTEN loss		10q22⁻, 11q23.3⁻
Other events			TP53 mutations			TERT promoter mutations

Age (years): 0-3, >3-10, >10-17, >17

Figure 1. Overview of the wingless (WNT) and sonic hedgehog (SHH) medulloblastoma subgroups. The WNT subgroup can further be subdivided into two and the SHH subgroup into four subtypes respectively. The subtypes differ with regards to clinical data and copy number profiles. Adapted with permission from Cavalli et al. [42]

SHH subgroup

The SHH activated subgroup comprises 25-30% of medulloblastoma and the age distribution within the SHH subgroup shows a bimodal shape. The majority of SHH tumors are diagnosed both in infants and young children under the age of four and in adolescents and adults above age 16.[40,41,60] SHH tumor location is mostly restricted to the cerebellum, as the tumor cells derive from granule cell progenitors. [53,61,62] SHH activated medulloblastoma are characterized by a transcriptional and genetic overexpression signature of regulators and target genes of the SHH signaling pathway.[40,41,43] The occurrence of distinct genetic alteration and expression profile is highly dependent on the age of the patients, showing unique and distinguishable signatures for infants, children and adult SHH tumors.[60,63] Most of the identified germline or somatic mutations as well as amplification affect genes of the SHH signaling pathway, including mutations in *PTCH1* (patched 1), *SMO* (smoothened) and

6

SUFU (suppressor of fused) and amplifications of *MYCN* and *GLI1* or *GLI2* (glioma-associated oncogene homolog 1/2). [43,64,65] Germline *TP53* mutation is linked with Li-Fraumeni syndrome and *PTCH1* mutation causes Gorlin syndrome. These inherited or acquired germline mutations increases the lifetime cancer risk, predispose the infants and children to medulloblastoma and have an impact on therapy protocols as they limit the use of radiation.[57,66–68] Characteristic for adult SHH medulloblastoma are mutations in the *TERT* (telomerase reverse transcriptase) promoter.[69]

When integrating gene expression with DNA methylation data the SHH tumors can be divided into 4 distinct subtypes.[42] SHH α tumors encompass mainly children with *MYCN*, *GLI* and *YAP1* (yes-associated protein 1) amplifications and *TP53* mutations. Both the SHH β and γ subtype are enriched for infant SHH tumors, although displaying different outcome and cytogenetic features. SHH β tumors show worse survival compared to SHH γ which can be attributed to a higher rate of metastatic dissemination as a marker of poor prognosis. SHH β tumors are characterized by focal *PTEN* (phosphatase and tensin homolog) deletions and multiple focal amplification whereas SHH γ exhibit a rather balanced genome with no significant alterations. SHH tumors in adults can mainly be assigned to SHH δ and are characterized by a higher overall number of mutation, showing frequent mutation in *PTCH1* and *SMO*. Moreover the SHH δ subtype tumors show an enrichment for mutations of *TERT* promoter.[42]

Prognosis for patients with SHH activated tumors is intermediate with an overall survival of approximately 75%.[70] However, outcome is specifically determined by the *TP53* status. *TP53* wild-type tumors show a long term survival of 80% whereas patients with *TP53*-mutated SHH tumors have a dismal prognosis with about 40%. Patients with identified *TP53* mutation are treated with high risk therapy protocols, since these tumors are more likely to recur and show resistance to treatment (Figure 1).[68]

Group 3

Group 3 tumors account for approximately 25% of all medulloblastoma and occur predominantly in infants and young children. With a prevalence of up to 50%, they are frequently metastatic at diagnosis and occur more commonly in male than female.[41] They are mostly located in the fourth ventricle and show high rates of classic histology besides LCA histology.[71] Prominin 1+/lineage-neural stem cells or cerebellar granule-neuron cells of the external granule-cell layer are the proposed cells of origin.[72,73]

The tumors are transcriptionally dominated by high expression levels of MYC as well as the activation of γ-aminobutyric acid (GABA)-ergic and photoreceptor pathway.[38,41] *MYC* activation is the most common cytogenetic aberration and is driven by *MYC* loci amplification. As a result of genomic rearrangement it occurs frequently as a fusion with *PVT1* (plasmacytoma variant translocation 1).[58,74] Additional copy-number alterations affect the transcription factor *OTX2* (orthodenticle homeobox 2), which is mutually exclusive of *MYC* amplification. *OTX2* is a target TGF-β (transforming growth factor beta) signaling pathway, which contains numerous other less recurrent copy-number alterations.[58] An additional common feature found in Group 3 medulloblastoma is the activation of the growth factor independent 1 family of proto-oncogenes *GFI1* and *GFI1B* by a mechanism called enhancer hijacking. Somatic structural variants resulting in a repositioning of the coding sequence of *GFI1* or *GFI1B* next to active enhancer elements, including super-enhancers, promote their oncogenic activity.[75] Overall the Group 3 genome exhibits high levels of genomic instability with frequent arm-level copy number gains and losses such as isochromosome 17q and gain of chromosome 7.[58,76] With an overall survival of around 50% the prognosis for patients with Group 3 tumors are currently the worst out of the four subgroups.[40,77] Depending on the presence of metastases and *MYC* status, patients are either stratified as standard or very high risk. Metastases and/or *MYC* amplification impart a poor prognosis for patients with group 3 tumors. i17q is also a possible marker of dismal prognosis.[68,76] Group 3 tumors relapse almost exclusively via metastatic dissemination and rarely with recurrence of tumor at original location.[78]

Recent integrative genomic and methylation analysis proposed three subtypes within Group 3 medulloblastoma. Group 3α tumors are frequently diagnosed in infants and often present with metastasis already at diagnosis. Group 3β tumors have a high frequency of *GFI1* family oncogene activation, are enriched for *OTX2* amplification and show frequently loss of *DDX3*. Group 3γ has the worst prognosis, as it often exhibits *MYC* amplification and also show a high incidence of metastasis (Figure 2).[42]

Due to the largely dismal prognosis of Group 3 tumors, there is a major focus on identifying novel experimental therapeutics to improve survival rates in this subgroup. Since targeting *MYC* activity directly still remains challenging, there are several approaches to decrease the hyperactivity of *MYC* indirectly, for example suppressing *MYC* transcription by BET (bromodomain and extraterminal domain) inhibitors.[79] Besides there are a number of promising therapeutic avenues and ongoing preclinical trials for targeting Group 3 medulloblastoma, including inhibition of PI3K (phosphatidylinositol 3-kinases), HDAC, aurora kinase, and cell cycle checkpoint (CDK4/6).[80–83]

Subgroup	Group 3			Group 4		
Subtype	Group 3α	Group 3β	Group 3γ	Group 4α	Group 4β	Group 4γ
Subtype proportion		(pie chart: 3α, 3β, 3γ)			(pie chart: 4α, 4β, 4γ)	
Subtype relationship		α, β, γ			β, α, γ	
Clinical data — Age	(0-3, >3-10)	(>3-10, >10-17)	(0-3, >3-10)	(>3-10, >10-17)	(>10-17, >17)	(>3-10, >10-17)
Clinical data — Histology						
Clinical data — Metastases	43.4%	20%	39.4%	40%	40.7%	38.7%
Clinical data — Survival at 5 years	66.2%	55.8%	41.9%	66.8%	75.4%	82.5%
Copy number — Broad	7$^+$, 8$^-$, 10$^-$, 11$^-$, i17q		8$^+$, i17q	7q$^+$, 8p$^-$, i17q	i17q	7q$^+$, 8p$^-$, i17q (less)
Copy number — Focal		OTX2 gain, DDX31 loss	MYC amp	MYCN amp, CDK6 amp	SNCAIP dup	CDK6 amp
Other events		High GFI1/1B expression				

Age (years): 0-3, >3-10, >10-17, >17

Figure 2. Overview of Group 3 and Group 4 medulloblastoma. Group 3 and Group 4 medulloblastoma can further be subdivided into three subtypes respectively. The subtypes differ with regards to clinical data and copy number profiles. Adapted with permission from Cavalli et al. [42]

Group 4

Group 4 medulloblastoma is the most common subgroup accounting for 40% of medulloblastomatumors and it is mainly diagnosed in children.[41] Childhood Group 4 medulloblastoma have an intermediate prognosis similar to the SHH subgroup whereas adults with Group 4 medulloblastoma may have a significantly worse outcome.[40,60] There is a considerable male preponderance with male cases being up to three times more common than female cases and Group 4 medulloblastoma frequently metastatic at diagnosis.[39,40] Group 4 tumors are mostly of classic histology, rarely also LCA histology and they are located at the 4th ventricle.[70]

In contrast to the WNT or SHH subgroup, the underlying biology of Group 4 tumors remains poorly understood.[41] Unlike for WNT and SHH subgroup there are no familial syndromes that predispose for Group 4 medulloblastoma. The most common cytogenetic

aberration is i17q and most female patients frequently present with loss of one X chromosome. Less frequent aberrations are loss of chromosome 8, 10, 11 and 17p and gain of chromosome 4, 7 and 18.[30,58] Unlike *MYC*-amplified group 3 tumors, i17q does not correlate with poor outcome in group 4 and loss of chromosome 11 is a favorable prognostic marker.[76]Group 4 tumors are transcriptionally characterized by over-representation of neuronal and glutamatergic pathways, albeit a clear clinical relevance.[38,39,41] The tumors are considered copy number–driven tumors. The proto-oncogenes *MYCN* and *CDK6* (cyclin-dependent kinase 6) are recurrently amplified in Group 4.[84] Unlike SHH tumors, *MYCN* amplifications do not confer a poor prognosis in group 4 medulloblastoma.

In addition, Group 4 tumor can be subdivided into three subtype. Groups 4α exhibits *MYCN* and *CDK6* amplification, the latter can also be found in Group 4γ subtype. Group 4β is characterized by *SNCAIP* (alpha-synuclein interacting protein) duplication. However, no significant difference between the subtypes can be found regarding overall survival or metastatic dissemination (Figure 2). [42]

1.2   Histone modifications

Chromatin is the basic scaffold for the functional organization of the eukaryotic genome into a compact, high-ordered complex. In the nucleus, DNA is packed into nucleosomes consisting of about 146 base pairs of double-stranded DNA wrapped around core histone octamers. These octamers are comprised of pairs of the histone proteins H2A, H2B, H3 and H4, while the linker histone H1 binds to the DNA strands outside the nucleosome.[85] Additionally to DNA methylation, modulation of the overall chromatin structure is not only essential for gene transcription but also DNA repair and replication.[10] The organization of the chromatin architecture is modulated by reversible modifications of the histone proteins, allowing the chromatin to assume distinct conformation of either highly condensed and transcriptionally inactive DNA (heterochromatin) or open and transcriptionally active DNA (euchromatin).[86] Modifications mainly take place at lysine, arginine and serine residues within the unstructured N-terminal tails of the histone proteins. At least eight different types

of covalent modifications are described, namely acetylation, methylation, phosphorylation, sumolyation, ubiquitylation, ADP ribosylation, deamination and proline isomerization. These modification not only influence chromatin structure but also serve as recognition sites for chromatin readers.[10,86]

1.2.1 Role of histone deacetylases

Acetylation of the ε- amino groups of lysines was first discovered as a post-translational modification of histones and has since then extensively been described in the context of gene transcription.[87] The acetylation of lysine is regulated by the opposing activities of histone acetyltransferases (HATs) and HDACs. The transfer of acetyl groups from acetyl-coenzyme-A to the ε-amino group of lysine side chains is catalyzed by HATs. Acetylation of histones leads to transcriptional activation as the positive charge of the lysine residue is neutralized, thereby interrupting the interaction to the negatively charged DNA backbone. The weakening of this interaction allows the DNA to unfold and become accessible to transcription factors. In contrast, the removal of the acetyl group from the lysine side chains of the histone proteins by HDACs leads to transcriptional repression due to chromatin condensation.[88] In addition to histones, proteomic studies analyzing the human acetylome showed that non-histone proteins are acetylated likewise, rendering acetylation an important modification for regulating stability, activity and protein-protein or protein-DNA interaction of proteins involved in diverse cellular function such as cell cycle, gene transcription, DNA damage repair, autophagy and cytoskeleton organization.[89,90]

Based on their sequence homology to the respective yeast orthologues, the 18 HDAC family members are grouped into four classes. Class I family of HDACs is comprised of HDAC1, -2, -3, -8, which are ubiquitously expressed and mainly located in the nucleus.[87] They share sequence similarity with the yeast reduced potassium dependency-3 (Rpd3) protein. As catalytic subunits, HDAC1-3 are recruited to multi-protein nuclear complexes that are crucial mediators of transcriptional repression and thus have been shown to be involved in tumorigenesis.[91] Besides their involvement in gene repression, HDAC class I members also

have non-histone targets. For example, HDAC1-3 have been shown to deacetylase p53, thereby altering the activity and stability of the tumor suppressor and hence influencing cell cycle and apoptosis induction.[92] HDAC8 has been shown to deacetylate the cohesion subunit SMC3 (structural maintenance of chromosomes), which is crucial for chromosome organization during cell cycle.[93]

Class II family members can be further subdivided into class IIa and class IIb, consisting of HDAC4, -5, -7, -9 and HDAC6, -10, respectively. They are homologous to the yeast histone deacetylase 1 (Hda1). While the class IIa enzymes are primarily localized in the cytoplasm, but based on their phosphorylation status can shuttle between cytoplasm and nucleus, the class IIb enzymes are mainly located in the cytoplasm. In contrast to class I, the expression of class II HDAC is tissue specific with high expression of class IIa enzymes in muscle, heart and brain tissue and of class IIb HDACs in kidney and liver tissue.[94] Class IIa HDACs were found in co-repressor complexes with HDAC3 and since the isolated enzymes only show minor or no deacetylase activity, it is discussed that class IIa HDACs primarily act as recruiters and that the deacetylase activity of the co-repressor complexes stem from HDAC3.[95,96] HDAC6 possess two catalytic domains that are involved in the deacetylation of non-histone substrates like α-tubulin and heat-shock protein 90 (Hsp90). HDAC10 has been shown to function as a polyamine deacetylase and in this context a role in autophagy has been suggested.[97,98] The class IV family member HDAC11 exhibits sequence homology to both class I and II proteins, is localized in the nucleus and the most recent identified HDAC class member. Up to now its physiological role remains largely unknown, however recent research identified HDAC11 to be a fatty-acid deacylase.[99] Class III family consists of the so called sirtuins and comprise SIRT 1 to 7, sharing sequence homology with the yeast silent information regulator-2 (Sir2) protein. In contrast to the Zn^{2+} dependent class I, II and IV metalloproteins, class III enzymes are dependent on nicotinamide adenine dinucleotide (NAD^+) for their catalytic activity.[87]

Dysregulation of deacetylase activity during tumorigenesis can greatly impair the finely balanced acetylation status of normal cells. Hyperacetylation of histones and nonhistone

proteins, leading to the silencing of tumor suppressors by transcriptional repression and induction of aberrant function of various proteins, have been shown to contribute to the malignant phenotype of multiple cancers.[100] Owing their ability to reverse the dysregulated acetylation homeostasis of cancerous cell, HDAC inhibitors (HDACi) have been emerging as promising epigenetic therapeutics. The targeting of HDACs has been shown to induce differentiation, cell cycle inhibition, apoptosis as well as increase the susceptibility to other chemotherapeutics in a large variety of cancers *in vitro* and *in vivo* (Figure 3).[94,101,102]
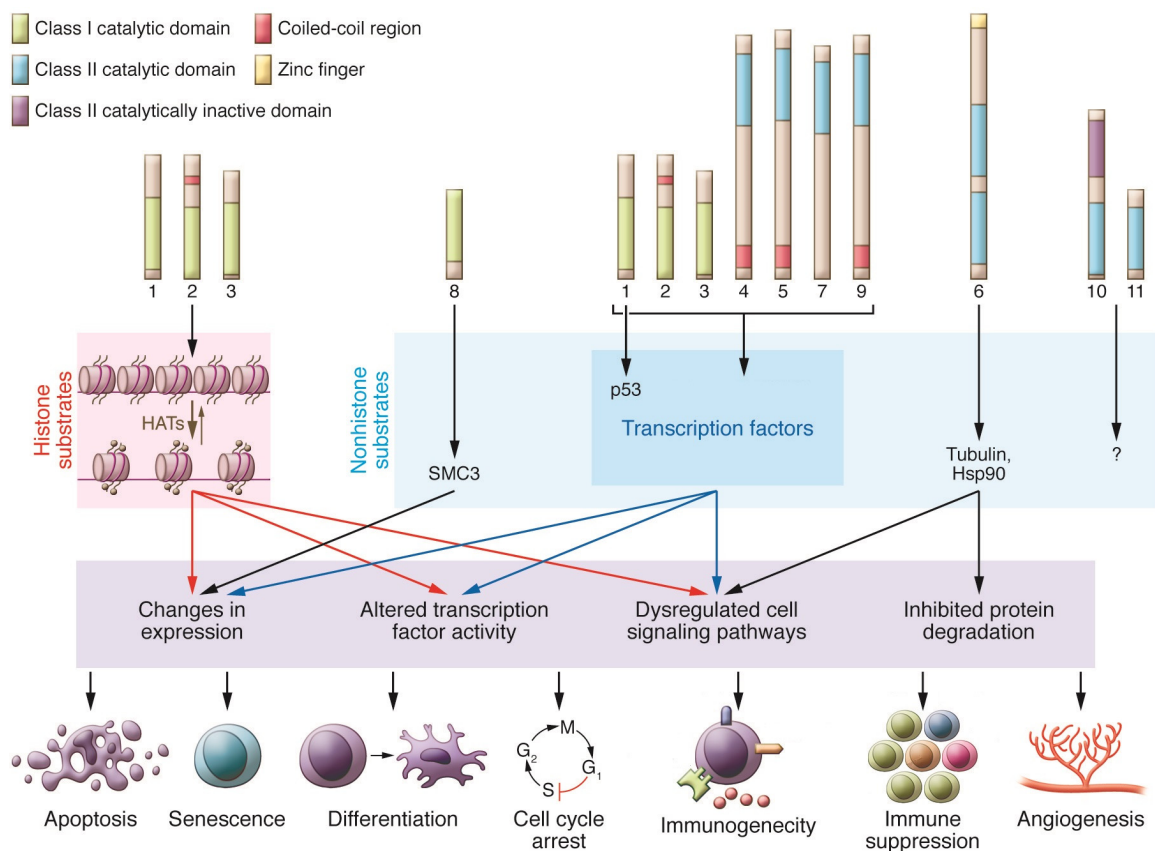
Figure 3. Molecular targets and pathways regulated by histone deacetylases. Illustration of the cellular substrates of HDACs, the involved downstream pathways and antitumoral effects of HDAC inhibition. Adapted with permission from West and Johnson.[101]

1.2.2 Histone deacetylase inhibitors

The classic pharmacophore of HDACi is determined by the relatively conserved regions within the catalytic pocket of the enzymes, mimicking the acetylated lysine side chain of the natural substrates. HDACi are therefore characterized by four main features, namely a zinc binding group (ZGB), a hydrophobic linker, a connecting unit (CU) and a cap group.[103] The

ZBG interacts with the zinc ion in the active site at the end of the narrow catalytic cavity and is connected to the Cap group via the aliphatic linker and the CU (Figure 4). The Cap group interacts with amino acids at the rim region of the catalytic site. Since the rim region shows certain diversity of the amino acid sequence between the HDAC isoforms, modifying the Cap group offers the potential to develop selective HDACi in particular.[103–105] According to the functional group of their ZGB, HDACi can mainly be classified into hydroxamic acids, benzamides, carboxylic acids, thiols, cyclic tetrapeptides or depsipeptides (Figure 4).
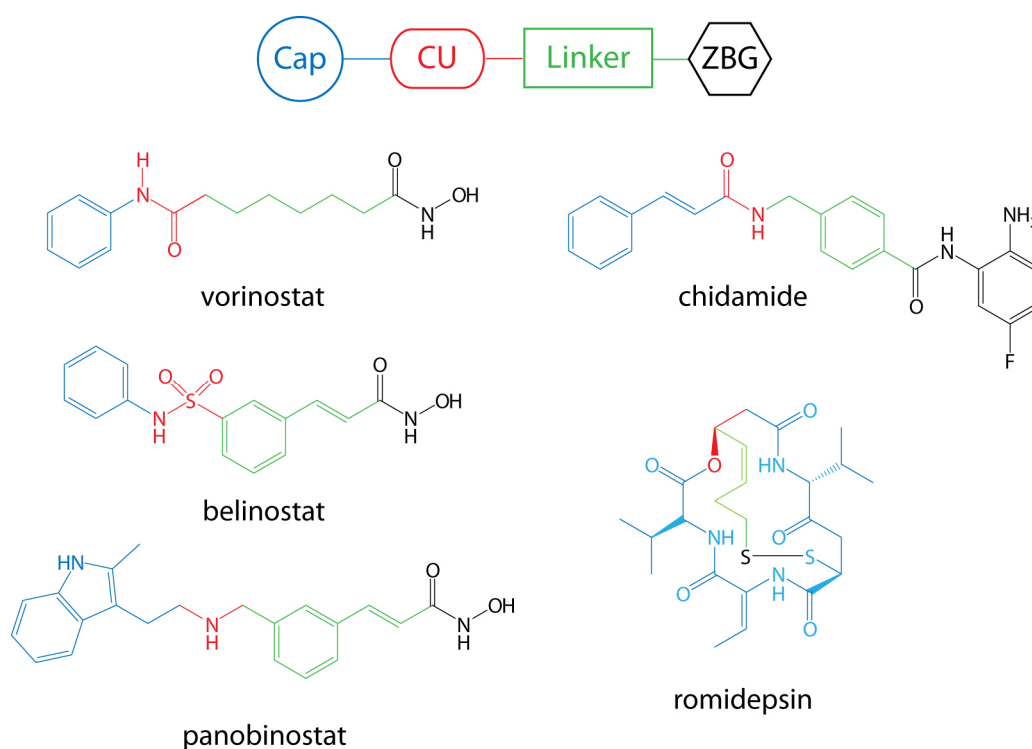
Figure 4. Pharmacophore model of histone deacetylase inhibitors and approved inhibitors.
The pharmacophore model of HDACi is composed of a cap group, a connecting unit (CU), a linker and the zinc binding group (ZBG). Chemical structures of the approved hydroxamic acids vorinostat, belinostat and panobinostat; the benzamide chidamide and depsipeptide romidepsin.[103]

To date, there are four HDACi approved by the US Food and Drug Administration (FDA). The hydroxamic acid vorinostat and the natural occurring depsipeptide romidepsin are approved for the treatment of cutaneous T-cell lymphoma (CTCL), the latter also for peripheral T-cell lymphoma (PTCL). The pan inhibitors belinostat and panobinostat are indicated for the treatment of PTCL and multiple myeloma, respectively. In addition, the benzamide chidamide has received approval from the chinese FDA for the treatment of

PTCL (Figure 4). Although there have been multiple trials of HDACi alone or in combination for the treatment of a variety of solid tumors, including brain tumors, only limited efficacy with in part wide range side effects were shown.[106–111] However, the approved HDACi as well as most of the evaluated compounds target multiple HDACs, rendering the identification of cancer relevant HDAC family members and the subsequent design of potent and selective inhibitors an ongoing challenge.[103,112]

For the rational design of selective inhibitors, the classical HDACi pharmacophore model can be extended to appreciate the discovery of additional binding cavities that are present in different HDAC isoforms. In addition to the substrate binding tunnel, class I HDACs have an additional subpocket, the so called foot pocket, that is targeted by benzamide-based HDACi, conferring selectivity for HDAC 1-3 in particular (Figure 5).
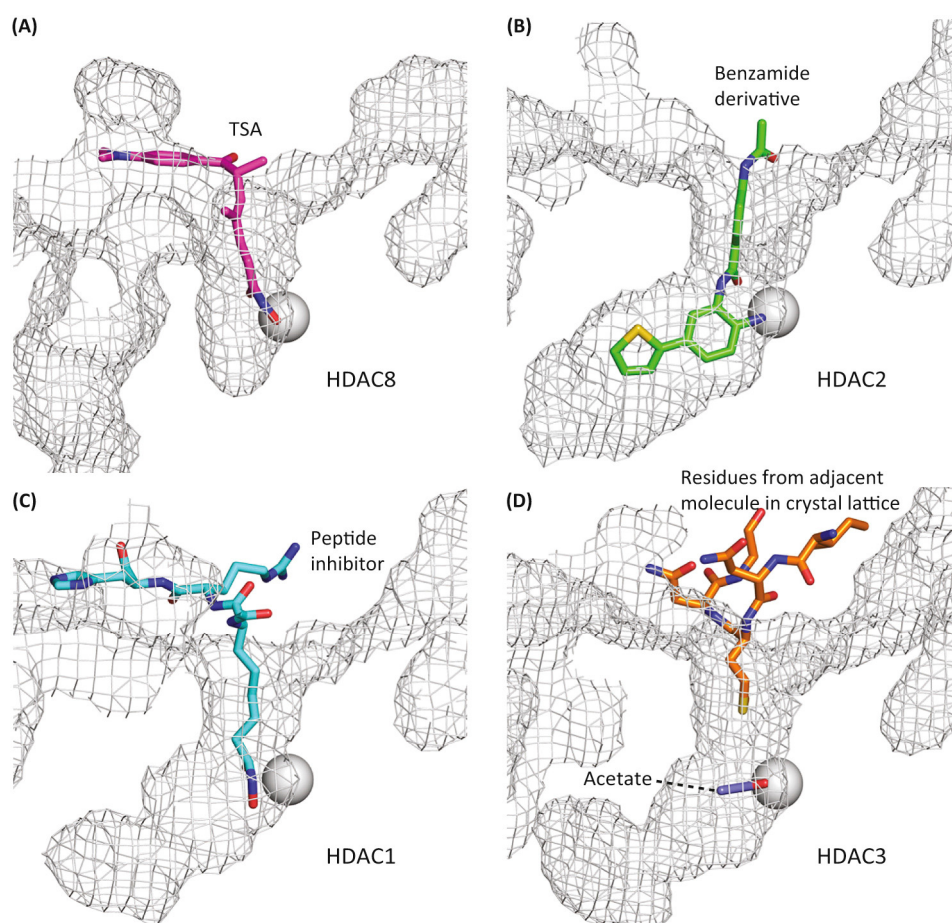
Figure 5. Structural differences between HDAC1-3 and HDAC8. (A) Trichostatin A bound to HDAC8. [113] (B) Benzamide based HDAC inhibitor bound to HDAC2.[114] (C) Peptide-based HDAC inhibitor bound to HDAC1.[115] (D) Interaction of HDAC3 with the deacetylase activation domain (DAD) of the SMRT complex.[116] Adapted with permission from Millard *et al.*[91]

The high sequence similarity between HDAC1 versus HDAC2 and HDAC3 (86% and 63%, respectively) renders the development of intra-class selective inhibitors challenging. However, despite the high similarity, distinct differences within the catalytic binding domains can be exploited to design selective HDAC1/2 and HDAC3 inhibitors. Starting from the clinically evaluated HDAC 1-3 inhibitor CI-994, the introduction of modifications at the C-5 or C-4 anilide position can be used to direct selectivity due to the structural difference of residue 118 (HDAC1/2: Ser, HDAC3: Tyr) (Figure 6).[117] The structural difference of HDAC8 can likewise be exploited for the design of selective inhibitors, for example by incorporating an α-amino ketone as the ZBG or with linkerless inhibitors.[118,119]
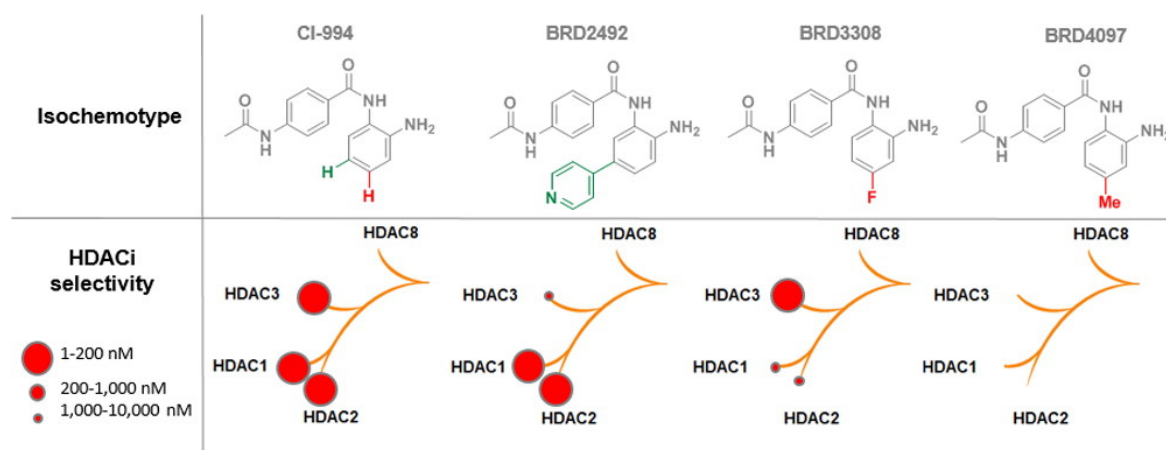
Figure 6. Set of *ortho*-aminoanilide based HDAC inhibitors with distinct selectivity profile. Structural differences within the catalytic binding domain of class I HDACs can be exploited to design intra-class selective inhibitors. Adapted with permission from Wagner *et al.*[117]

Similarly, the presence of a lower pocket in Class IIa enzymes, that is not found in the other isoforms, was shown to be amenable for the design of selective inhibitors for this subclass.[120] The HDAC6 isozyme has, in comparison to the other HDAC family members, a wider and more shallow entrance to the binding site. This structural feature can direct selectivity by incorporating bulky cap groups or branched linkers into the design of novel HDAC6 selective compounds.[121,122]

A novel approach for directing isoform-selectivity especially within the class I HDAC isozymes is based on their engagement in different transcriptional regulatory complexes. HDAC1-2 form the catalytic subunit of transcriptional co-repressor complexes like the

NuRD (nucleosome remodeling and deacetylase), MiDAC (mitotitic deacetylase) or CoREST (co-repressor of REST) complex while HDAC3 is exclusively engaged in the SMRT/NCoR (nuclear receptor corepressor) complex.[91] Chemoproteomic profiling revealed that HDACi show different affinities towards different complexes containing the same HDAC isozyme as the catalytic subunit.[123] Development of compounds that are directed against distinct protein complexes rather than the isolated enzyme, could therefore be a promising novel approach for selective inhibition of HDAC isozyme activity.

In addition, recent approaches to develop potent inhibitors include the design of hybrid compounds that simultaneously inhibit multiple cellular pathways and targets. Efficacy of single agent chemotherapeutics are often limited by concomitant activation of compensatory signaling pathways. The combination of complementary inhibitory functionalities, that target different networks, into one drug offers therefore the potential to overcome limited activity or acquired resistance of monotherapies.[124] Based on previously identified synergistic drug combinations, dual acting inhibitors were successfully developed that combine HDAC inhibitory functionality for example PI3K (phosphatidylinositol 3-kinase),[125] BET (bromodomain and extraterminal domain),[126] proteasome,[127] EGFR (epidermal growth factor receptor)[128] and topoisomerase inhibitor pharmacophores [129]. Due the flexibility within the rim region of HDACs, the incorporation of a second pharmacophore in the cap region of HDACi has been shown to be well tolerated for the design of dual-acting inhibitors.[130]

In addition to their application as anticancer agents, HDACi have been increasingly studied in the context of nonmalignant diseases. HDACi have been shown to have therapeutic activity as latency-reversing agents for the treatment of HIV.[131] Moreover HDACi have been extensively studied for the treatment of neurodegenerative diseases like Alzheimer[132] or Friedreichs Ataxia[133] and as anti-inflammatory and immune modulating agents.[134]

1.3 Drug discovery and development

Since the sequencing of the human genome, the further development of next generation sequencing (NGS) technologies and the concomitant emergence of cancer genomes characterization have greatly contributed to our understanding of cancer biology.[65,135–137] Classical chemotherapeutic intervention is up to now largely based on the use of rather unspecific, broad acting cytotoxic drugs like platinum agents, antimetabolites or alkylating drugs, affecting not only fast proliferating cancerous cells but also rapidly dividing normal cells. However, as the advancement in cancer genome characterization provides comprehensive insights about distinct genetic and epigenetic alterations and their functional roles during tumorigenesis of various cancer types,[20,138–140] it is particularly aspiring to identify and develop targeted therapeutics.

The discovery and development of new medications can be approached by two main strategies, namely phenotypic or target-based drug discovery approaches. Phenotypic based strategies using an animal or cell culture model of a disease for the identification of compounds that show a specific phenotypic effect, like reduced viability of cancer cells, are also called classic or forward pharmacology approaches. Historically, this approach has already been applied in the beginning of pharmacology by using mostly plant derived natural products without a clear understanding of the underlying mechanism. After the identification of compounds eliciting a phenotypic effect, the molecular targets have to be identified and validated.[141]

With the advent of molecular and structural biology as well as progresses in high-throughput screening (HTS) and combinatorial chemistry, the approach of target-based drug discovery has gained increasing attention. Starting point for this approach, also called reverse pharmacology, is the hypothesis that the modulation of a target biomolecule will result in a beneficial therapeutic effect. The identification of appropriate targets is achieved by integrating genomic, proteomic and metabolomic disease knowledge to determine druggable disease drivers.[142] Compounds modulating the selected target are then identified by screening of small molecule libraries (Figure 7).
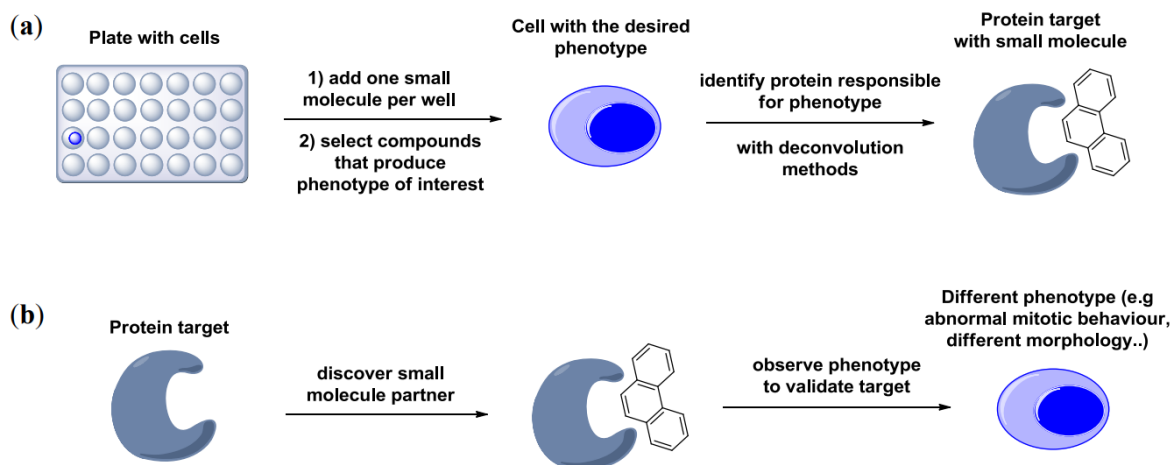
Figure 7. Phenotypic and target drug discovery approaches. The discovery of novel inhibitors can be approached by two distinct strategies, namely phenotypic-(a) and target-based (b) drug discovery. Adapted from Lenci *et al.*[143]

Following the initial hit identification of compounds showing the desired phenotypic or target modulation effect, these compounds are chemically modified to yield so called lead structures. By means of medicinal chemistry approaches, hit compounds are optimized with regards to their biological activity, physicochemical and pharmacokinetic properties as well as toxicology profile. To yield orally bioavailable lead candidates, the drug discovery process is aimed at evaluating the structure-activity relationship (SAR) of the hit compounds to define the functional groups that are pivotal for producing the target biological effect. In addition, taking principles like Lipinski's rule of five[144] and expansions thereof[145–147] into account, will likely reduce attrition rates during clinical trials due to increased drug-like physicochemical properties. In the case of reverse pharmacology, drug design is based on the knowledge about the target and often complemented by computational methods for in silico predictions of ADME properties (absorption, distribution, metabolism and excretion) and virtual library screening.

Overall, from the initial high-throughput screening of compound libraries to the final approved medication it is estimated that the drug discovery process takes about 13 years with costs of over one billion dollars.[148] As the cost of drug discovery and development have significantly increased over the last decades and failure rates in clinical phases remain

high[149,150], in particular for oncological trials[150], the approaches of drug repositioning and personalized medicine have gained increasing attention.

1.3.1 Drug repurposing and personalized medicine

The concept of drug repurposing identifies new indications for existing drugs, that have been developed for a certain disease, to treat another disease.[151] Although many repositioned drugs have been identified serendipitously or new indications were found due to unexpected side effect in clinical trials, the rational repositioning of drugs is increasing with the advancing molecular understanding of diseases. The approach of drug repositioning involves the identification of novel targets for approved inhibitors or the recognition of new oncogenic disease drivers that can be targeted by an approved drug.[151] Repositioning of investigational or approved drugs that have already passed clinical phases will likely reduce the risk of failure in future clinical trials due to known clinical and pharmacokinetic profiles. In addition, drug optimization studies, ADME profiling or early clinical phases can often be omitted and therefore time to approval as well as overall expenses will significantly decrease.[152]

Along with the rational identification of new drug indications, the emergence of cancer genomics led to the recognition of molecular heterogeneity within tumor entities and thereby contributed to the evolving field of personalized medicine. The approach of personalized medicine considers the individual genetic profile to guide clinical treatment decision. The identification of novel diagnostic and prognostic biomarker together with the knowledge about the distinct genetic and epigenetic profile can help to classify diseases into molecular subtypes, providing the perspective to improve survival by treatment of patients with targeted drugs. Moreover, biomarker based stratification of patients during clinical trials could reduce attritions rates due to lack of efficacy.[153]

2   Aim of the thesis

Among children and young adults, brain tumors are one of the most common causes of cancer related mortality. Many primary brain tumors cannot be cured by the current standard therapeutic options consisting of neurosurgical resection, radiotherapy and adjuvant chemotherapy. In addition, survivors often suffer from the long-term side effect of high-dose chemotherapeutic and radiotherapeutic intervention, rendering the development of new rational therapeutic options highly desirable. The nature of cancer and its biology depends both on genetic and epigenetic alterations of intact genomes. Especially research during the last decades has revealed that epigenetic dysregulation is a critical driver for oncogenic transformation. With regards to preclinical studies and early clinical trials showing that pharmacological inhibition of HDACs can represent a promising new approach for the epigenetic treatment of brain tumors, the aim of this study was the identification of novel HDAC inhibitors with distinct antitumoral activity.

For the purpose of evaluating an institutional HDACi library of over 200 compounds, the first goal was to establish a drug screening pipeline that delivers reproducible and accurate screening results in a high-throughput manner. Therefore, we first focused on the optimization of the screening pipeline by implementing semi-automated equipment that allows for the rapid and accurate screening of compound libraries. Next, the HDACi library should be evaluated concerning the antitumoral activity in our comprehensive panel of cell lines derived from the most common brain tumor entities. After elucidating distinct response patterns across the entities, a promising drug candidate is selected and further evaluated both *in vitro* as well as *in vivo*. In addition, a screen for synergistic interaction could yield promising drug combinations that could further enhance the anticancer activity.

With this unparalleled screening approach of evaluating a unique library of HDAC inhibitors in a broad cell line panel we hoped to identify drugs with promising translational relevance for future clinical application and pave the way for the rational design and further development of novel inhibitors.

3   Material and methods

3.1   Devices and software

The following devices and softwares were used in the thesis.

Table 1. List of devices used in this thesis

Device	Distributor
Bioanalyzer	Agilent (Böblingen, Germany)
cBot	Illumina (San Diego, USA)
Centrifuge 5403	Eppendorf (Wesseling-Berzdorf, Germany)
Centrifuge Haraeus Fresco 21	Thermo Fisher Scientific (Schwerte, Germany)
Centrifuge Multifuge 4KR	Thermo Fisher Scientific (Schwert, Germany)
CFX384 Touch Real-Time PCR Detection System	Bio-Rad Laboratories (Feldkirchen, Germany)
CytoFLEX Flow Cytometer	Beckman Coulter (Krefeld, Germany)
D300e Digital Dispenser	Tecan (Crailsheim, Germany)
Flow Safe 2020 biological safety cabinet	Thermo Fisher Scientific (Schwerte, Germany)
GeneAMP PCR System 2700	Applied Biosystems (Schwerte, Germany)
HiSeq 2500	Illumina (San Diego, USA)
Incubator C170	Binder (Tuttlingen, Germany)
LAS-300 Imaging System	Fujifilm (Duesseldorf, Germany)
Maxwell RSC Instrument	Promega (Mannheim, Germany)
Mini Gel Tank and Blot Module	Thermo Fisher Scientific (Schwerte, Germany)
Multidrop Combi Reagent Dispenser	Themo Fisher Scientific (Schwerte, Germany)
NanoDrop Spectrophotometer ND-1000	Peqlab (Erlangen, Germany)
Spark 10M Multimode microplate reader	Tecan (Crailsheim, Germany)
Vi-Cell-XR	Beckman Coulter (Krefeld, Germany)

Table 2. List of software used in this thesis

Software	Distributor
Adobe Illustrator	Adobe System (San José, USA)
CFX Manager	Bio-Rad Laboratories (Feldkirchen, Germany)
Combenefit (version 2.021)	Cancer Research UK Cambridge Institute (downloaded from www. sourceforge.net)
CytExpert	Beckman Coulter (Krefeld, Germany)
D300e control (version 3.3.1)	Tecan (Crailsheim, Germany)
D300e merge	Tecan (Crailsheim, Germany)
FILLit for Multidrop Combi	Thermo Fisher Scientific (Schwerte, Germany)
Gimp	Downloaded from www.gimp.org

GraphPad Prism 5 (version 5.03)	GraphPad Software (San Diego, USA)
ImageJ	National Institute of Health (Bethesda, USA)
Ingenuity Pathway Analysis (IPA)	Qiagen (Hilden, Germany)
Microsoft Office	Microsoft (Redmond, USA)
Morpheus	Broad Institute (Cambridge, USA) (https://software.broadinstitute.org/morpheus
Partek Flow and Partek Genomic Suite	Partek Incorporated (St. Louis, USA)
Spark control	Tecan (Crailsheim, Germany)

3.2   Cell lines and culture conditions

A total of 41 brain tumor cell lines and 12 cell lines from other neoplasia were included in this work. A detailed description of all atypical/teratoid rhabdoid tumors (ATRT, n=11), glioblastoma (GBM, n=11), medulloblastoma (MB, =14), diffuse intrinsic pontine glioma (DIPG, n=5), neuroblastoma (NB, n=10) and malignant peripheral nerve sheath tumor (MPNST, n=2) models and culture conditions is provided in the following Table 3 and Table 4. *MYC* amplified medulloblastoma cell lines were annotated as *MYC*-MB according to their initial model descriptions. Cell line authentication was conducted by short tandem report profiling and mycoplasma contaminations were ruled out by PCR-based evaluation.

All cell lines were incubated at 37°C at 5% CO_2. Adherent cells were passaged using Trypsin, pelleted for 5 min at 300 g and resuspended in appropriate medium in dilutions of 1:5 – 1:20. For cryopreservation cell pellets were resuspended in 0.8-1.5 mL freezing medium (medium + 10% DMSO), transferred to a cryotube and frozen in a cryobox with ispropanol at -80 °C for at least 24 h. For long term storage, the cryotubes were kept in the gas phase of liquid nitrogen. For recultivation, the cryotube were warmed in a water bath at 37 °C, the thawed cell suspension was resuspended in fresh medium, pelleted for 5 min at 300 g and the pellets were resuspended in fresh medium.

Table 3. Overview of cell lines used in this thesis

Cell line	Entity	Culture condition	Cells/well (384 well plate)
ATRT13808	AT/RT	M1	3500
BT-12	AT/RT	M2	1500
BT-16	AT/RT	M2	3500
CHLA-02-ATRT	AT/RT	M3	5000

CHLA-04-ATRT	AT/RT	M3	4000
CHLA-05-ATRT	AT/RT	M3	9000
CHLA-06-ATRT	AT/RT	M3	6500
CHLA-266	AT/RT	M2	4000
HHU-ATRT01	AT/RT	M1	3500
JC-ATRT	AT/RT	M1	7000
VU397	AT/RT	M1	4500
AM-38	GBM	M4	4000
LN-18	GBM	M5	1250
LN-308	GBM	M5	1750
LN-229	GBM	M5	1000
SJ-GBM2	GBM	M2	1500
T98G	GBM	M5	1250
TP365 MG	GBM	M5	1250
U138 MG	GBM	M5	3000
U251	GBM	M5	1250
U87	GBM	M5	2000
YH-13	GBM	M4	4000
CHLA-01-Med	*MYC*-MB	M3	10000
CHLA-01R-Med	*MYC*-MB	M3	10000
D283 MED	*MYC*-MB	M6	5000
D341 MED	*MYC*-MB	M7	5000
D425 MED	*MYC*-MB	M8	2500
MED8A	*MYC*-MB	M5	2000
HD-MB03	*MYC*-MB	M9	4000
MB3W1	*MYC*-MB	M10	4000
MB002	*MYC*-MB	M11	10000
CHLA-259	MB	M2	9000
DAOY	MB	M5	1000
ONS76	MB	M5	1000
UW-228-2	MB	M5	750
UW-228-3	MB	M5	1000
DIPG06	DIPG	M12	12500
DIPG17	DIPG	M12	4500
DIPG24	DIPG	M12	10000
DIPG25	DIPG	M12	9500
DIPG33	DIPG	M12	2000
CHP-134	NB	M13	4500
CLBGA	NB	M13	4500

IMR32	NB	M13	4000
Kelly	NB	M13	4000
LAN-5	NB	M13	5000
NB1	NB	M13	6000
NLF	NB	M13	4000
SH-SY5Y	NB	M13	5000
SK-N-AS	NB	M13	2500
SK-N-FI	NB	M13	4000
NLF	NB	M13	4000
SH-SY5Y	NB	M13	5000
SK-N-AS	NB	M13	2500
SK-N-FI	NB	M13	4000
sNF02.2	MPNST	M14	750
sNF96.2	MPNST	M14	1500

Table 4. Overview of media composition

Entry	Medium	Supplements
M1	NeuroCult NS-A Basal Medium	1% L-Glutamine, 1% P/S, 75 µg/mL BSA, 1% N-2 supplement, 2% B-27 supplement, 10 ng/mL EGF, 10 ng/mL FGF, Heparin
M2	IMDM	20% FBS, 1x IST
M3	DMEM/F-12	2% B-27 supplement, 20 ng/mL EGF, 20 ng/mL FGF
M4	MEM	20% FBS, 1% L-Glutamine
M5	DMEM	10% FBS, 1% P/S
M6	MEM	10% FBS, 1% P/S
M7	MEM	20% FBS
M8	Modified IMEM	10% FBS, 1% P/S
M9	RPMI 1640	10% FBS, 1% MEM NEAA
M10	DMEM/F-12	0.4% P/S, 2% B-27 supplement, 1% MEM Vitamin solution, 20 ng/mL EGF, 20 ng/mL FGF
M11	1:1 DMEM/F-12 and Neurobasal-A Medium	1% P/S, 1% Sodium bicarbonate, 1% Sodium pyruvate, 1% MEM NEAA 2% B-27 supplement, 10 ng/mL EGF, 10 ng/mL FGF, 10 ng/mL LIF, 0.25% Heparin
M12	1:1 DMEM/F-12 and Neurobasal-A Medium	1% P/S, 1% Sodium bicarbonate, 1% Sodium pyruvate, 1% MEM NEAA, 0.5% Glutamax, 2% B-27 supplement, 10 ng/mL EGF, 10 ng/mL FGF, 10 ng/mL PDGF-AA, 10 ng/mL PDGF-BB, 0.25% Heparin
M13	RPMI 1640	10 % FBS
M14	DMEM	10 % FBS

Table 5. List of cell culture consumables

Consumable	Distributor	Catalog number #
DMEM Medium	Thermo Fisher Scientific (Schwerte, Germany)	31966-021
DMEM/F-12 Medium	Thermo Fisher Scientific (Schwerte, Germany)	11320-033
MEM Medium	Thermo Fisher Scientific (Schwerte, Germany)	10370-047
Modified IMEM Medium	Thermo Fisher Scientific (Schwerte, Germany)	A10489-01
RPMI 1640 Medium	Thermo Fisher Scientific (Schwerte, Germany)	31870-025
IMDM Medium	Thermo Fisher Scientific (Schwerte, Germany)	12440-061
Neurobasal-A Medium	Thermo Fisher Scientific (Schwerte, Germany)	10888022
B-27 supplement, minus vitamin A	Thermo Fisher Scientific (Schwerte, Germany)	12587010
L-Glutamine	Thermo Fisher Scientific (Schwerte, Germany)	25030-024
MEM Vitamin Solution	Thermo Fisher Scientific (Schwerte, Germany)	11120037
MEM Non-Essential Amino Acid (MEM NEAA)	Thermo Fisher Scientific (Schwerte, Germany)	1140-035
Sodium bicarbonate	Thermo Fisher Scientific (Schwerte, Germany)	25080-094
Sodium pyruvate	Thermo Fisher Scientific (Schwerte, Germany)	11360-070
HEPES	Thermo Fisher Scientific (Schwerte, Germany)	15630-080
BSA Fraction V (7.5 % solution)	Thermo Fisher Scientific (Schwerte, Germany)	15260-037
Insulin-Transferrin-Selenium (IST)	Thermo Fisher Scientific (Schwerte, Germany)	41400-045
N-2 supplement	Thermo Fisher Scientific (Schwerte, Germany)	17502048
Epidermal Growth Factor (EGF), human recombinant	Thermo Fisher Scientific (Schwerte, Germany)	PHG0311
NeuroCult NS-A Basal Medium (Human)	Stemcell Technologies	05750
Heparin Solution (0.2 %)	Stemcell Technologies	07980
Penicillin (10.000 U/mL)-Streptomycin (10 mg/mL) (P/S)	Sigma-Aldrich (Taufkirchen, Germany)	P4333
Heat Inactivated Fetal Bovine Serum	Sigma-Aldrich (Taufkirchen, Germany) PAN Biotech (Aidenbach, Germany)	F9665 P30-3302
Fibroblast Growth Factor basic (FGF), human recombinant	Biomol (Hamburg, Germany)	50361.50

Leukemia Inhibitory Factor (LIF), human	Merck Millipore (Darmstadt, Germany)	LIF1010
Platelet-Derived Growth Factor AA (PDGF-AA), human recombinant	Shenandoah Biotechnology (Warwick, USA)	100-16
PDGF-BB, human recombinant	Shenandoah Biotechnology (Warwick, Germany)	100-18AF
0.25 % Trypsin-EDTA	Thermo Fisher Scientific (Schwerte, Germany)	25200056
Accutase	Corning (Wiesbaden, Germany)	25-058-CI
Dimethyl sulfoxide (DMSO)	Sigma-Aldrich (Taufkirchen, Germany)	D8418
Dulbecco's phosphate buffered saline (PBS)	Sigma-Aldrich (Taufkirchen, Germany)	P5493
Cell scraper	Corning (Wiesbaden, Germany)	3008
6 well	Greiner Bio-One (Frickenhausen, Germany)	657160
Cell culture flasks	Greiner Bio-One (Frickenhausen, Germany)	658195 658175 690175
Parafilm	Bemis (Oshkosh, USA)	PM996
Falcon	Greiner Bio-One (Frickenhausen, Germany)	188271 227261
Cryoconservation tubes	Corning (Wiesbaden, Germany)	430488
Disposable pipettes	Corning (Wiesbaden, Germany)	4487 4488 4489
Disposable aspiration pipettes	Sarstedt (Nümbrecht, Germany)	86.1252.011

3.3 Inhibitor libraries

The institutional HDACi library used in this work consists of 288 inhibitors: 266 compounds were synthesized in-house (Prof. Dr. Kurz, Institute of Pharmaceutical and Medicinal Chemistry, Heinrich-Heine University Düsseldorf), 20 inhibitors are commercially available and two inhibitors were kindly provided by the CHDI Foundation.

TC-H 106, CI-994, pyroxamide, SBHA, KD5170, TCS HDAC6 20b, scriptaid, sodium 4-phenylbutyrate, M 344, MC 1568, PCI 34051, NSC 3852 and valproic acid were part of the Tocriscreen Epigenetics Toolbox from Tocris (Wiesbaden-Nordenstadt, Germany). Entinostat, vorinostat, belinostat, tubastatin A, ricolinostat and panobinostat were purchased from Selleckchem (Muenchen, Germany). Romidpesin was a kind gift from MedChemExpress (Sollentuna, Sweden) and CHDI-00465983-0000-003 and CHDI-

00390576-0000-004 were kindly provided by the CHDI Foundation (New York, USA). Inhibitors from Tocris were provided as 10 mM DMSO stocks, the remaining compounds were reconstituted with DMSO to yield 10 mM stock solutions. CI-994 for *in vitro* and *in vivo* experiments were purchased from MedChemExpress. The first library version contained 218 inhibitors (HDACi_V1), the second 263 inhibitors (HDACi_V2) and the third 288 inhibitors (HDACi_V3) (Table 7 and Table 7).

The epigenetic library was purchased from Tocris, contained 80 inhibitors (2 negative controls) and was supplied as pre-dissolved 10 mM DMSO solution (Table 8). The clinical inhibitor library (HHU_CL) consists of 200 compounds, which are either approved as therapeutics or are evaluated in clinical phase III/IV trials, and was purchased from MedChemExpress as a customized library. The compounds were provided as 10 mM DMSO stock solutions (Table 9). Screening of the epigenetic library was performed by David Pauck and Mara Maue

Table 6. List of institutional HDACi

Inhibitor	HDACi classification	HDACi library	Inhibitor	HDACi classification	HDACi library
ABK85	Hydroxamic acid	HDACi_V3	LAK49	Hydroxamic acid	HDACi_V2_V3
ABK86	Hydroxamic acid	HDACi_V3	LAK51	Hydroxamic acid	HDACi_V2_V3
BLK027	Hydroxamic acid	HDACi_V1_V2_V3	LAK53	Hydroxamic acid	HDACi_V2_V3
BLK028	Hydroxamic acid	HDACi_V1_V2_V3	LAK55	Hydroxamic acid	HDACi_V2_V3
BLK029	Hydroxamic acid	HDACi_V1_V2_V3	LAK57	Hydroxamic acid	HDACi_V2_V3
BLK031	Hydroxamic acid	HDACi_V1_V2_V3	LAK59	Hydroxamic acid	HDACi_V2_V3
DDK100	Hydroxamic acid	HDACi_V1_V2_V3	LAK61	Hydroxamic acid	HDACi_V2_V3
DDK113	Hydroxamic acid	HDACi_V1_V2_V3	LAK63	Hydroxamic acid	HDACi_V2_V3
DDK114	Hydroxamic acid	HDACi_V1_V2_V3	LAK65	Hydroxamic acid	HDACi_V2_V3
DDK115	Hydroxamic acid	HDACi_V1_V2_V3	LAK67	Hydroxamic acid	HDACi_V2_V3
DDK116	Hydroxamic acid	HDACi_V1_V2_V3	LAK72	Hydroxamic acid	HDACi_V2_V3
DDK117	Hydroxamic acid	HDACi_V1_V2_V3	LAK74	Hydroxamic acid	HDACi_V2_V3
DDK118	Hydroxamic acid	HDACi_V1_V2_V3	LAK81	Hydroxamic acid	HDACi_V2_V3

DDK119	Hydroxamic acid	HDACi_V1_V2_V3	LMK082	Hydroxamic acid	HDACi_V1_V2_V3
DDK120	Hydroxamic acid	HDACi_V1_V2_V3	LMK101	Hydroxamic acid	HDACi_V1_V2_V3
DDK121	Hydroxamic acid	HDACi_V1_V2_V3	LMK121	Hydroxamic acid	HDACi_V1_V2_V3
DDK122	Hydroxamic acid	HDACi_V1_V2_V3	LMK129	Hydroxamic acid	HDACi_V1_V2_V3
DDK129	Hydroxamic acid	HDACi_V1_V2_V3	LMK130	Hydroxamic acid	HDACi_V1_V2_V3
DDK131	Hydroxamic acid	HDACi_V1_V2_V3	LMK131	Hydroxamic acid	HDACi_V1_V2_V3
DDK132	Hydroxamic acid	HDACi_V1_V2_V3	LMK132	Hydroxamic acid	HDACi_V1_V2_V3
DDK133	Hydroxamic acid	HDACi_V1_V2_V3	LMK140	Hydroxamic acid	HDACi_V1_V2_V3
DDK137	Hydroxamic acid	HDACi_V1_V2_V3	LMK156	Hydroxamic acid	HDACi_V1_V2_V3
DDK138	Hydroxamic acid	HDACi_V1_V2_V3	LMK157	Hydroxamic acid	HDACi_V1_V2_V3
DDK139	Hydroxamic acid	HDACi_V1_V2_V3	LMK158	Hydroxamic acid	HDACi_V1_V2_V3
DDK140	Hydroxamic acid	HDACi_V1_V2_V3	LMK162	Hydroxamic acid	HDACi_V1_V2_V3
DDK141	Hydroxamic acid	HDACi_V1_V2_V3	LMK163	Hydroxamic acid	HDACi_V1_V2_V3
DDK142	Hydroxamic acid	HDACi_V1_V2_V3	LMK168	Hydroxamic acid	HDACi_V1_V2_V3
DDK143	Hydroxamic acid	HDACi_V1_V2_V3	LMK172	Hydroxamic acid	HDACi_V1_V2_V3
DDK144	Hydroxamic acid	HDACi_V1_V2_V3	LMK173	Hydroxamic acid	HDACi_V1_V2_V3
DDK145	Hydroxamic acid	HDACi_V1_V2_V3	LMK174	Hydroxamic acid	HDACi_V1_V2_V3
DDK146	Hydroxamic acid	HDACi_V1_V2_V3	LMK187	Hydroxamic acid	HDACi_V1_V2_V3
DDK147	Hydroxamic acid	HDACi_V1_V2_V3	LMK189	Hydroxamic acid	HDACi_V1_V2_V3
DDK148	Hydroxamic acid	HDACi_V1_V2_V3	LMK192	Hydroxamic acid	HDACi_V1_V2_V3
DDK153	Hydroxamic acid	HDACi_V1_V2_V3	LMK193	Hydroxamic acid	HDACi_V1_V2_V3
DRK12	Hydroxamic acid	HDACi_V3	LMK195	Hydroxamic acid	HDACi_V1_V2_V3
DRK16	Hydroxamic acid	HDACi_V3	LMK200	Hydroxamic acid	HDACi_V1_V2_V3
EHK2	Carboxylic acid	HDACi_V1_V2_V3	LMK204	Hydroxamic acid	HDACi_V1_V2_V3
EHKXIII	Hydroxamic acid	HDACi_V1_V2_V3	LMK208	Hydroxamic acid	HDACi_V1_V2_V3
FHK257	Hydroxamic acid	HDACi_V1_V2_V3	LMK210	Hydroxamic acid	HDACi_V1_V2_V3
FHK262	Hydroxamic acid	HDACi_V1_V2_V3	LMK214	Hydroxamic acid	HDACi_V1_V2_V3
FHK281	Hydroxamic acid	HDACi_V1_V2_V3	LMK215	Hydroxamic acid	HDACi_V1_V2_V3

KF3OH	Hydroxamic acid	HDACi_V1_V2_V3	LMK216	Hydroxamic acid	HDACi_V1_V2_V3
KFK01	Hydroxamic acid	HDACi_V1_V2_V3	LMK218	Hydroxamic acid	HDACi_V1_V2_V3
KK19OH	Hydroxamic acid	HDACi_V1_V2_V3	LMK220	Hydroxamic acid	HDACi_V1_V2_V3
KK20OH	Hydroxamic acid	HDACi_V1_V2_V3	LMK225	Hydroxamic acid	HDACi_V1_V2_V3
KK21OH	Hydroxamic acid	HDACi_V1_V2_V3	LMK230	Hydroxamic acid	HDACi_V1_V2_V3
KP03Hy	Hydroxamic acid	HDACi_V1_V2_V3	LMK231	Hydroxamic acid	HDACi_V1_V2_V3
KP04Hy	Hydroxamic acid	HDACi_V1_V2_V3	LMK232	Hydroxamic acid	HDACi_V1_V2_V3
KP05Hy	Hydroxamic acid	HDACi_V1_V2_V3	LMK233	Hydroxamic acid	HDACi_V1_V2_V3
KP06Hy	Hydroxamic acid	HDACi_V1_V2_V3	MPK77	Benzamide	HDACi_V3
KP07Hy	Hydroxamic acid	HDACi_V1_V2_V3	NR4a-1	Hydroxamic acid	HDACi_V2_V3
KP08Hy	Hydroxamic acid	HDACi_V1_V2_V3	NR4a-2	Hydroxamic acid	HDACi_V2_V3
KP09Hy	Hydroxamic acid	HDACi_V1_V2_V3	NR4a-3	Hydroxamic acid	HDACi_V2_V3
KP10Hy	Hydroxamic acid	HDACi_V1_V2_V3	NR4a-4	Hydroxamic acid	HDACi_V2_V3
KP11OH	Hydroxamic acid	HDACi_V1_V2_V3	NR4a-5	Hydroxamic acid	HDACi_V2_V3
KP13AOH	Hydroxamic acid	HDACi_V1_V2_V3	NR4a-6	Hydroxamic acid	HDACi_V2_V3
KP14OH	Hydroxamic acid	HDACi_V1_V2_V3	NR4b-1	Hydroxamic acid	HDACi_V2_V3
KP15OH	Hydroxamic acid	HDACi_V1_V2_V3	NR4b-2	Hydroxamic acid	HDACi_V2_V3
KP16OH	Hydroxamic acid	HDACi_V1_V2_V3	NR4c-2	Hydroxamic acid	HDACi_V2_V3
KSK003	Hydroxamic acid	HDACi_V1_V2_V3	NR4d-2	Hydroxamic acid	HDACi_V2_V3
KSK005	Hydroxamic acid	HDACi_V1_V2_V3	NR4e-2	Hydroxamic acid	HDACi_V2_V3
KSK007	Hydroxamic acid	HDACi_V1_V2_V3	RVK2	Hydroxamic acid	HDACi_V2_V3
KSK009	Hydroxamic acid	HDACi_V1_V2_V3	SHeK1	Hydroxamic acid	HDACi_V1_V2_V3
KSK012	Hydroxamic acid	HDACi_V1_V2_V3	SHeK5	Hydroxamic acid	HDACi_V1_V2_V3
KSK013	Hydroxamic acid	HDACi_V1_V2_V3	SHeK6	Hydroxamic acid	HDACi_V1_V2_V3
KSK017	Hydroxamic acid	HDACi_V1_V2_V3	SN1	Hydroxamic acid	HDACi_V1_V2_V3
KSK019	Hydroxamic acid	HDACi_V1_V2_V3	SN2-NH-OH	Hydroxamic acid	HDACi_V1_V2_V3
KSK021	Hydroxamic acid	HDACi_V1_V2_V3	SN4	Other	HDACi_V1_V2_V3
KSK023	Hydroxamic acid	HDACi_V1_V2_V3	SN6	Other	HDACi_V1_V2_V3

KSK025	Hydroxamic acid	HDACi_V1_V2_V3	SN7	Other	HDACi_V1_V2_V3
KSK027	Hydroxamic acid	HDACi_V1_V2_V3	TOK04	Hydroxamic acid	HDACi_V3
KSK029	Hydroxamic acid	HDACi_V1_V2_V3	TOK07	Hydroxamic acid	HDACi_V3
KSK031	Hydroxamic acid	HDACi_V1_V2_V3	TOK08	Hydroxamic acid	HDACi_V3
KSK033	Hydroxamic acid	HDACi_V1_V2_V3	TOK11	Hydroxamic acid	HDACi_V3
KSK035	Hydroxamic acid	HDACi_V1_V2_V3	TOK16	Hydroxamic acid	HDACi_V3
KSK037	Hydroxamic acid	HDACi_V1_V2_V3	TOK27	Hydroxamic acid	HDACi_V3
KSK041	Hydroxamic acid	HDACi_V1_V2_V3	VSK258-NH-OH	Hydroxamic acid	HDACi_V1_V2_V3
KSK043	Hydroxamic acid	HDACi_V1_V2_V3	VSK258-OH	Caroxylic acid	HDACi_V1_V2_V3
KSK045	Hydroxamic acid	HDACi_V1_V2_V3	VSK317-NH-OH	Hydroxamic acid	HDACi_V1_V2_V3
KSK047	Hydroxamic acid	HDACi_V1_V2_V3	VSK319-NH-OH	Hydroxamic acid	HDACi_V1_V2_V3
KSK049	Hydroxamic acid	HDACi_V1_V2_V3	VSK322-NH-OH	Hydroxamic acid	HDACi_V1_V2_V3
KSK056	Hydroxamic acid	HDACi_V1_V2_V3	VSK326-NH-OH	Hydroxamic acid	HDACi_V1_V2_V3
KSK060	Hydroxamic acid	HDACi_V1_V2_V3	VSK327-NH-OH	Hydroxamic acid	HDACi_V1_V2_V3
KSK062	Hydroxamic acid	HDACi_V1_V2_V3	VSK328-NH-OH	Hydroxamic acid	HDACi_V1_V2_V3
KSK064	Hydroxamic acid	HDACi_V1_V2_V3	VSK333-NH-OH	Hydroxamic acid	HDACi_V1_V2_V3
KSK068	Hydroxamic acid	HDACi_V1_V2_V3	VSK334-NH-OH	Hydroxamic acid	HDACi_V1_V2_V3
KSK069	Carboxylic acid	HDACi_V1_V2_V3	VSK335-NH-OH	Hydroxamic acid	HDACi_V1_V2_V3
KSK075	Hydroxamic acid	HDACi_V1_V2_V3	VSK336-NH-OH	Hydroxamic acid	HDACi_V1_V2_V3
KSK077	Hydroxamic acid	HDACi_V1_V2_V3	VSK339	Other	HDACi_V1_V2_V3
KSK079	Hydroxamic acid	HDACi_V1_V2_V3	VSK340-NH-OH	Hydroxamic acid	HDACi_V1_V2_V3
KSK081	Hydroxamic acid	HDACi_V1_V2_V3	VSK341-NH-OH	Hydroxamic acid	HDACi_V1_V2_V3
KSK083	Hydroxamic acid	HDACi_V1_V2_V3	VSK347-NH-OH	Hydroxamic acid	HDACi_V1_V2_V3
KSK085	Hydroxamic acid	HDACi_V1_V2_V3	VSK354-NH2	Benzamide	HDACi_V1_V2_V3
KSK105	Hydroxamic acid	HDACi_V1_V2_V3	VSK356-NH2	Benzamide	HDACi_V1_V2_V3
KSK107	Hydroxamic acid	HDACi_V1_V2_V3	VSK360-NH2	Benzamide	HDACi_V1_V2_V3
KSK111	Hydroxamic acid	HDACi_V1_V2_V3	VSK361-NH2	Benzamide	HDACi_V1_V2_V3
KSK113	Hydroxamic acid	HDACi_V1_V2_V3	VSK363-NH2	Benzamide	HDACi_V1_V2_V3

KSK115	Hydroxamic acid	HDACi_V1_V2_V3	VSK364-NH2	Benzamide	HDACi_V1_V2_V3
KSK117	Hydroxamic acid	HDACi_V1_V2_V3	VSK365-NH2F	Benzamide	HDACi_V1_V2_V3
KSK119	Hydroxamic acid	HDACi_V1_V2_V3	VSK376-NH2	Benzamide	HDACi_V2_V3
KSK126	Hydroxamic acid	HDACi_V1_V2_V3	VSK377-NH2	Benzamide	HDACi_V2_V3
KSK135	Hydroxamic acid	HDACi_V1_V2_V3	VSK381-NH2	Benzamide	HDACi_V2_V3
KSK139	Hydroxamic acid	HDACi_V1_V2_V3	VSK383-NH2	Benzamide	HDACi_V2_V3
KSK143	Hydroxamic acid	HDACi_V1_V2_V3	VSK384-NH2	Benzamide	HDACi_V2_V3
KSK145	Hydroxamic acid	HDACi_V1_V2_V3	VSK385-NH2	Benzamide	HDACi_V2_V3
KSK150	Hydroxamic acid	HDACi_V1_V2_V3	VSK386-NH2	Benzamide	HDACi_V2_V3
LAK03	Hydroxamic acid	HDACi_V1_V2_V3	VSK387-NH2F	Benzamide	HDACi_V2_V3
LAK05	Hydroxamic acid	HDACi_V1_V2_V3	VSKKKK1-NH2	Benzamide	HDACi_V2_V3
LAK07	Hydroxamic acid	HDACi_V1_V2_V3	VSKKKK2-NH2	Benzamide	HDACi_V2_V3
LAK09	Hydroxamic acid	HDACi_V2_V3	VTK09	Hydroxamic acid	HDACi_V1_V2_V3
LAK11	Hydroxamic acid	HDACi_V1_V2_V3	VTK11	Hydroxamic acid	HDACi_V1_V2_V3
LAK13	Hydroxamic acid	HDACi_V1_V2_V3	VTK13	Hydroxamic acid	HDACi_V1_V2_V3
LAK15	Hydroxamic acid	HDACi_V1_V2_V3	VTK15	Hydroxamic acid	HDACi_V1_V2_V3
LAK17	Hydroxamic acid	HDACi_V1_V2_V3	VTK17	Hydroxamic acid	HDACi_V1_V2_V3
LAK19	Hydroxamic acid	HDACi_V1_V2_V3	VTK19	Hydroxamic acid	HDACi_V1_V2_V3
LAK21	Hydroxamic acid	HDACi_V1_V2_V3	VTK21	Hydroxamic acid	HDACi_V1_V2_V3
LAK23	Hydroxamic acid	HDACi_V1_V2_V3	VTK23	Hydroxamic acid	HDACi_V1_V2_V3
LAK25	Hydroxamic acid	HDACi_V1_V2_V3	VTK25	Hydroxamic acid	HDACi_V1_V2_V3
LAK27	Hydroxamic acid	HDACi_V1_V2_V3	VTK27	Hydroxamic acid	HDACi_V1_V2_V3
LAK29	Hydroxamic acid	HDACi_V1_V2_V3	VTK29	Hydroxamic acid	HDACi_V1_V2_V3
LAK31	Hydroxamic acid	HDACi_V1_V2_V3	VTK36	Hydroxamic acid	HDACi_V1_V2_V3
LAK31-COOH	Carboxylic acid	HDACi_V2_V3	VTK39	Hydroxamic acid	HDACi_V1_V2_V3
LAK31-NH2	Benzamide	HDACi_V2_V3	VTK42	Hydroxamic acid	HDACi_V1_V2_V3
LAK31-NHCH3	Other	HDACi_V2_V3	YAK31	Hydroxamic acid	HDACi_V3
LAK33	Hydroxamic acid	HDACi_V2_V3	YAK40	Hydroxamic acid	HDACi_V3

LAK35	Hydroxamic acid	HDACi_V2_V3	YAK52	Hydroxamic acid	HDACi_V3
LAK37	Hydroxamic acid	HDACi_V2_V3	YAK61	Hydroxamic acid	HDACi_V3
LAK39	Hydroxamic acid	HDACi_V2_V3	YAK63	Hydroxamic acid	HDACi_V3
LAK41	Hydroxamic acid	HDACi_V2_V3	YAK70	Hydroxamic acid	HDACi_V3
LAK43	Hydroxamic acid	HDACi_V2_V3	YAK72	Hydroxamic acid	HDACi_V3
LAK45	Hydroxamic acid	HDACi_V2_V3	YAK73	Hydroxamic acid	HDACi_V3
LAK47	Hydroxamic acid	HDACi_V2_V3	YAK77	Hydroxamic acid	HDACi_V3

Table 7. List of commercially available HDACi

Inhibitor	Isoform preference	HDACi classification	Catalog No.	HDACi library
Belinostat	Pan	Hydroxamic acid	S1085 (Selleckchem)	HDACi_V1_V2_V3
CI-994	Class I	Benzamide	5268 (Tocris)	HDACi_V1_V2_V3
Entinostat	Class I	Benzamide	S1053 (Selleckchem)	HDACi_V1_V2_V3
KD 5170	Pan	Mercaptoketone	5268 (Tocris)	HDACi_V1_V2_V3
M 344	Pan	Hydroxamic acid	5268 (Tocris)	HDACi_V1_V2_V3
MC 1568	Class IIa	Hydroxamic acid	5268 (Tocris)	HDACi_V1_V2_V3
NSC 3852	Pan	Other	5268 (Tocris)	HDACi_V1_V2_V3
Panobinostat	Pan	Hydroxamic acid	S1030 (Selleckchem)	HDACi_V1_V2_V3
PCI 34051	HDAC8	Hydroxamic acid	5268 (Tocris)	HDACi_V1_V2_V3
Pyroxamide	Pan	Hydroxamic acid	5268 (Tocris)	HDACi_V1_V2_V3
Ricolinostat	HDAC6	Hydroxamic acid	S8001 (Selleckchem)	HDACi_V3
Romidepsin	Class I	Depsipetide	HY-15149 (medchemexpress)	HDACi_V1_V2_V3
SBHA	Pan	Hydroxamic acid	5268 (Tocris)	HDACi_V1_V2_V3
Scriptaid	Pan	Hydroxamic acid	5268 (Tocris)	HDACi_V1_V2_V3
Sodium 4-Phenylbutyrate	Pan	Aliphatic acid	5268 (Tocris)	HDACi_V1_V2_V3
TC-H 106	Class I	Benzamide	5268 (Tocris)	HDACi_V1_V2_V3
TCS HDAC6 20b	HDAC6	Other	5268 (Tocris)	HDACi_V1_V2_V3
Tubastatin A	HDAC6	Hydroxamic acid	S8049 (Selleckchem)	HDACi_V1_V2_V3
Valproic acid, sodium salt	Pan	Aliphatic acid	5268 (Tocris)	HDACi_V1_V2_V3
Vorinostat	Pan	Hydroxamic acid	S1047 (Selleckchem)	HDACi_V1_V2_V3
CHDI-003	Class IIa	Hydroxamic acid	Obtained from CHDI Foundation	HDACi_V3
CHDI-004	Class IIa	Hydroxamic acid	Obtained from CHDI Foundation	HDACi_V3

Table 8. Tocris Epigenetic Toolbox

Inhibitor	Research area	Target	Catalog No.
(+)-JQ1	Epigenetic Readers	BET	4499
3-Aminobenzamide	Transcriptional Modulators	PARP	0788
5-azacytidine	Epigenetic Writers	DNMT1	3842
A 366	Epigenetic Writers	G9a/GLP	5163
AK 7	Epigenetic Erasers	SIRT2	4754
BIX 01294	Epigenetic Writers	G9a/GLP	3364
Bromosporine	Epigenetic Readers	pan-BRD	4758
C 646	Epigenetic Writers	p300/CBP	4200
CI-994	Epigenetic Erasers	HDAC1/3	2952
Daminozide	Epigenetic Erasers	KDM2/7	4684
Decitabine	Epigenetic Writers	DNMT	2624
EGCG	Epigenetic Writers	DNMT1	4524
EX 527	Epigenetic Erasers	SIRT1	2780
Fisetin	Epigenetic Writers	DNMT1	5016
Forskolin	Transcriptional Modulators	PKA	1099
GSK J1	Epigenetic Erasers	JMJD3/UTX	4593
GSK J4	Epigenetic Erasers	JMJD3/UTX	4594
H 89 dihydrochloride	Epigenetic Writers	MSK1	2910
I-BET 151 hydrochloride	Epigenetic Readers	BET	4650
I-CBP 112	Epigenetic Readers	CREBBP/EP300	4891
IOX 1	Epigenetic Erasers	pan-JMJD	4464
IOX 2	Transcriptional Modulators	PHD2	4451
JIB 04	Epigenetic Erasers	pan-JMJD	4972
Kaempferol	Epigenetic Writers	RSK2	3603
KD 5170	Epigenetic Erasers	HDAC1/3/4/6	4001
KU 55933	Epigenetic Writers	ATM/ATR	3544
KU 60019	Epigenetic Writers	ATM/ATR	4176
L002	Epigenetic Writers	p300	5045
LMK 235	Epigenetic Erasers	HDAC4/5	4830
Lomeguatrib	Epigenetic Writers	DNMT	4359
LY 303511	Epigenetic Readers	BET	2418
M 344	Epigenetic Erasers	pan-HDAC	2771
MC 1568	Epigenetic Erasers	HDAC 4/5/7/9	4077
Mitoxantrone dihydrochloride	Epigenetic Writers	DNMT1	4250
MS 436	Epigenetic Readers	BRD4	5173
NSC 3852	Epigenetic Erasers	pan-HDAC	2521
P 22077	Epigenetic Writers	USP7	4485
PCI 34051	Epigenetic Erasers	HDAC8	4643
PF 03814735	Epigenetic Writers	Aurora Kinase A/B	4821

PFI 1	Epigenetic Readers	BET	4445
PFI 3	Epigenetic Readers	SMARCA4/2	5072
PJ 34 hydrochloride	Transcriptional Modulators	PARP	3255
PRT 4165	Epigenetic Writers	E3 Ligase	5047
Pyroxamide	Epigenetic Erasers	HDAC1	4403
Resveratrol	Epigenetic Erasers	SIRT1	1418
Retinoic acid	Transcriptional Modulators	HDAC	0695
RG 108	Epigenetic Writers	DNMT	3295
RN 1 dihydrochloride	Epigenetic Erasers	LSD1	4977
SAHA	Epigenetic Erasers	pan-HDAC	4652
Salermide	Epigenetic Erasers	SIRT1/2	4127
SB 747651A dihydrochloride	Epigenetic Writers	MSK1	4630
SBHA	Epigenetic Erasers	HDAC1/3	3810
Scriptaid	Epigenetic Erasers	pan-HDAC	2421
SGC 0946	Epigenetic Writers	DOT1L	4541
SGC-CBP 30	Epigenetic Readers	CREBBP/EP300	4889
SGI 1027	Epigenetic Writers	DNMT1	5155
Sirtinol	Epigenetic Erasers	pan-SIRT	3521
SL 327	Epigenetic Writers	MEK	1969
SNS 314 mesylate	Epigenetic Writers	pan-Aurora Kinase	4584
Sodium 4-Phenylbutyrate	Epigenetic Erasers	pan-HDAC	2682
Splitomicin	Epigenetic Erasers	Sir2p	1542
TC-E 5003	Epigenetic Writers	PRMT1	5099
TC-H 106	Epigenetic Erasers	HDAC 1/2/3/8	4270
TCS HDAC6 20b	Epigenetic Erasers	HDAC6	4805
Temozolomide	Epigenetic Writers	DNA	2706
Tenovin-1	Epigenetic Erasers	SIRT1	3365
Tranylcypromine hydrochloride	Epigenetic Erasers	LSD1	3852
Triptolide	Transcriptional Modulators	RNA Polymerase II	3253
U0126	Epigenetic Writers	MEK	1144
UNC 0224	Epigenetic Writers	G9a	3861
UNC 0638	Epigenetic Writers	G9a	4343
UNC 0642	Epigenetic Writers	G9a/GLP	5132
UNC 0646	Epigenetic Writers	G9a/GLP	4342
UNC 1215	Epigenetic Readers	L3MBTL3	4666
UNC 926 hydrochloride	Epigenetic Readers	L3MBTL1	4516
Valproic acid, sodium salt	Epigenetic Erasers	pan-HDAC	2815
Zebularine	Epigenetic Writers	DNMT	2293
ZM 447439	Epigenetic Writers	Aurora Kinase B	2458

Table 9. Customized HHU Clinical Inhibitor Library

Inhibitor	Target	Catalog No.
3-Deazaneplanocin A hydrochloride	EZH2 HMTase	HY-12186
5-Azacytidine	Nucleoside antimetabolite/analog	HY-10586
5-Fluorouracil	Nucleoside antimetabolite/analog	HY-90006
6-Mercaptopurine	Nucleoside antimetabolite/analog	HY-13677
6-Thioguanine	Nucleoside antimetabolite/analog	HY-13765
ABT-199	Bcl-2 Family	HY-15531
Actinomycin D	DNA transcription	HY-17559
Afatinib dimaleate	EGFR	HY-10261A
AICAR	AMPK	HY-13417
Alisertib	Aurora Kinase	HY-10971
Altretamine	DNA alkylator/crosslinker	HY-B0181
Amonafide	Topoisomerase	HY-10982
Anacetrapib	CETP	HY-12090
API-2	DNA synthesis	HY-15457
Arctigenin	Others	HY-N0035
Axitinib	VEGFR	HY-10065
AZD-9291	EGFR	HY-15772
AZD-9291 mesylate	EGFR	HY-15772A
Bardoxolone methyl	IKK	HY-13324
Baricitinib phosphate	JAK	HY-15315A
BAY 80-6946	PI3K	HY-15346
Belinostat	HDAC	HY-10225
Bendamustine hydrochloride	Others	HY-B0077
Betahistine dihydrochloride	Histamine Receptor	HY-B0524A
Bexarotene	RAR/RXR	HY-14171
BIBF 1120	FGFR PDGFR VEGFR	HY-50904
Bleomycin sulfate	Others	HY-17565
BML-286	PDZ domain of dishevelled	discontinued
BMN-673	PARP	HY-16106A
Bortezomib	Proteasome	HY-10227
Bosutinib	Bcr-Abl Src	HY-10158
Brivanib	VEGFR	HY-10337
BSI-201	PARP	HY-12015
Busulfan	DNA alkylator/crosslinker	HY-B0245
Cabazitaxel	Microtubule/Tubulin	HY-15459
Cabozantinib S-malate	VEGFR	HY-12044
CAL-101	PI3K	HY-13026
Canertinib	EGFR	HY-10367

Capecitabine	Nucleoside antimetabolite/analog	HY-B0016
Carboplatin	DNA alkylator/crosslinker	HY-17393
Carfilzomib	Proteasome	HY-10455
Carmustine	DNA alkylator/crosslinker	HY-13585
Cediranib	VEGFR	HY-10205
CEP-32496	Raf	HY-15200
Chlorambucil	DNA alkylator/crosslinker	HY-13593
Chlormethine hydrochloride	Others	HY-B1253
CI-994	HDAC	HY-50934
Cisplatin	DNA alkylator/crosslinker	HY-17394
Cladribine	Adenosine Deaminase	HY-13599
Clofarabine	Nucleoside antimetabolite/analog	HY-A0005
Cobimetinib	MEK	HY-13064
Crizotinib	ALK c-Met/HGFR	HY-50878
CYT387	JAK	HY-17420
Cytarabine	Nucleoside antimetabolite/analog	HY-13605
Dabrafenib mesylate	Raf	HY-14660A
Dacarbazine	Nucleoside antimetabolite/analog	HY-B0078
Dapagliflozin	SGLT	HY-10450
Dasatinib	Bcr-Abl Src	HY-10181
Daunorubicin hydrochloride	Topoisomerase	HY-13062
Decitabine	DNMT	HY-A0004
Deforolimus	mTOR	HY-50908
Dinaciclib	CDK	HY-10492
Docetaxel	Microtubule/Tubulin	HY-B0011
Dovitinib	c-Kit	HY-50905
Doxorubicin hydrochloride	Topoisomerase	HY-15142
Elesclomol	Apoptosis inducer	HY-12040
Empagliflozin	SGLT	HY-15409
Entinostat	HDAC	HY-12163
Enzastaurin	PKC	HY-10342
Epirubicin hydrochloride	Topoisomerase	HY-13624A
EPZ-6438	EZH2 HMTase	HY-13803
Erlotinib hydrochloride	EGFR	HY-12008Y
Estramustine phosphate sodium	Microtubule/Tubulin	HY-13627
Etoposide	Topoisomerase	HY-13629
Everolimus	mTOR	HY-10218
FG-4592	HIF	HY-13426
Floxuridine	Nucleoside antimetabolite/analog	HY-B0097

Fludarabine phosphate	Nucleoside antimetabolite/analog	HY-B0028
Fosbretabulin disodium	Microtubule/Tubulin	HY-17449
Ganetespib	HSP90	HY-15205
GANT-61	GLI1	HY-13901
GDC-0994	ERK	HY-15947
Gefitinib	EGFR	HY-50895
Gemcitabine	Nucleoside antimetabolite/analog	HY-17026
GSK 525762A	BET bromodomain	HY-13032
GSK126	EZH2 HMTase	HY-13470
GSK343	EZH2 HMTase	HY-13500
Homoharringtonine	Others	HY-14944
Honokiol	Apoptosis inducer	HY-N0003
Idarubicin hydrochloride	Topoisomerase	HY-17381
Imatinib mesylate	c-Kit PDGFR	HY-50946
INK 128	mTOR	HY-13328
IPI-145	PI3K	HY-17044
Irinotecan	Topoisomerase	HY-16562
Isotretinoin	RAR/RXR	HY-15127
Itraconazole	Antifungal	HY-17514
Ixabepilone	Microtubule/Tubulin	HY-10222
Lapatinib	EGFR	HY-50898
LDE225	Smo	HY-16582A
LDK378	ALK	HY-15656
LEE011	CDK	HY-15777
Lenvatinib	VEGFR	HY-10981
LGK974	PORCN	HY-17545
LGX818	Raf	HY-15605
Linifanib	PDGFR VEGFR	HY-50751
Linsitinib	IGF-1R Insulin Receptor	HY-10191
Lomustine	DNA alkylator/crosslinker	HY-13669
Lonafarnib	Farnesyl Transferase	HY-15136A
Losmapimod	p38 MAPK	HY-10402
LY2835219	CDK	HY-16297
LY3009120	Raf	HY-12558
Marimastat	MMP	HY-12169
Masitinib	c-Kit PDGFR	HY-10209
MEK162	MEK	HY-B1253
Melphalan	DNA alkylator/crosslinker	HY-17575
Methotrexate	Antifolate	HY-14519

Mitomycin C	DNA alkylator/crosslinker	HY-13316
Mitoxantrone dihydrochloride	Topoisomerase	HY-13502A
MLN9708	Proteasome	HY-10452
Motesanib diphosphate	c-Kit VEGFR	HY-10229
MRK003	γ-secretase	discontinued
Nelarabine	Nucleoside antimetabolite/analog	HY-13701
Neratinib	HER EGFR	HY-32721
Nilotinib	Bcr-Abl	HY-10159
Obatoclax	Bcl-2 Family	HY-10969
Olaparib	PARP	HY-10162
OTX-015	BET bromodomain	HY-15743
Oxaliplatin	DNA alkylator/crosslinker	HY-17371
Paclitaxel	Microtubule/Tubulin	HY-B0015
Pacritinib	FLT3 JAK	HY-16379
Palbociclib	CDK	HY-50767
Palifosfamide	DNA alkylator/crosslinker	HY-14798
Panobinostat	HDAC	HY-10224
Pazopanib hydrochloride	PDGFR VEGFR	HY-12009
PCI-32765	Btk	HY-10997
Pemetrexed	Antifolate	HY-13781
Pentostatin	Adenosine Deaminase	HY-A0006
Perifosine	Akt	HY-50909
Pexidartinib	c-Fms c-Kit	HY-16749
PF-04691502	mTOR PI3K	HY-15177
Pipobroman	Others	HY-16398
Ponatinib	Bcr-Abl FGFR FLT3 VEGFR	HY-12047
Pralatrexate	Antifolate	HY-10446
Procarbazine hydrochloride	DNA alkylator/crosslinker	HY-13733
Quizartinib	FLT3	HY-13001
R406	Syk	HY-12067
R788 disodium hexahydrate	Syk	HY-13038B
Rapamycin	mTOR	HY-10219
Regorafenib	VEGFR	HY-10331
Retinoic acid	RAR	HY-14649
Rigosertib sodium	Polo-like Kinase (PLK)	HY-12037A
Romidepsin	HDAC	HY-15149
Rucaparib phosphate	PARP	HY-10617
Ruxolitinib (S enantiomer)	JAK	HY-50858A
Ruxolitinib phosphate	JAK	HY-50858

Selumetinib	MEK	HY-50706
Semagacestat	γ-secretase	HY-10009
Sorafenib tosylate	Raf	HY-10201A
Staurosporine	PKC	HY-15141
Streptozocin	DNA alkylator/crosslinker	HY-13753
SU 5416	VEGFR	HY-10374
Sunitinib	VEGFR PDGFR	HY-10255
TAK-632	Raf	HY-15767
TAK-715	p38 MAPK	HY-10456
Tariquidar	P-glycoprotein	HY-10550
Tasquinimod	HDAC	HY-10528
Temozolomide	DNA alkylator/crosslinker	HY-17364
Temsirolimus	mTOR	HY-50910
Teniposide	Topoisomerase	HY-13761
Thioridazine hydrochloride	5-HT Receptor Dopamine Receptor	HY-13765
Thio-TEPA	DNA alkylator/crosslinker	HY-17574
Tipifarnib	Farnesyl Transferase	HY-10502
Tipiracil hydrochloride	Thymidine synthase	HY-A0063
Tivantinib	c-Met/HGFR	HY-50686
Tivozanib	VEGFR	HY-10977
Tofacitinib citrate	JAK	HY-40354A
Topotecan hydrochloride	Topoisomerase	HY-13768A
Trametinib	MEK	HY-10999
Trifluorothymidine	Nucleoside antimetabolite/analog	HY-A0061
TSU-68	PDGFR	HY-10517
Tubastatin A hydrochloride	HDAC	HY-13271
Uramustine	DNA alkylator/crosslinker	HY-13544
Valproic acid sodium salt	HDAC	HY-10585
Valrubicin	Others	HY-13772
Vandetanib	VEGFR	HY-10260
Vatalanib dihydrochlorid	VEGFR	HY-12018
Veliparib dihydrochloride	PARP	HY-10130
Vemurafenib	Raf	HY-12057
Verteporfin	YAP	HY-B0146
Vinblastine sulfate	Microtubule/Tubulin	HY-13780
Vincristine sulfate	Microtubule/Tubulin	HY-N0488
Vinflunine tartrate	Microtubule/Tubulin	HY-B0628A
Vismodegib	Hedgehog	HY-10440
Volasertib	Polo-like Kinase (PLK)	HY-12137

Vorinostat	HDAC	HY-10221
VRT752271	ERK	HY-15816
WP1066	JAK STAT	HY-15312
Zibotentan	Endothelin Receptor	HY-10088
Zoledronic acid monohydrate	Others	HY-13777A
Zosuquidar trihydrochloride	P-glycoprotein	HY-50671

3.4 Preparation of library plates

The initially employed HDACi library (HDACi_V1) was composed of 218 inhibitors. For preparation of the library plates, inhibitors were distributed over a total of eleven library plates with 20 compounds on each plate plus vorinostat, entinostat and tubastatin A as control compounds. All inhibitors were dispensed in singlicates with ten concentrations covering a range of 0.005-25 µM (logarithmic distribution). giving the possibility to evaluate the compounds over a wide range of concentrations. All wells were normalized to the highest DMSO concentration of 0.25% and five wells were included that contain only DMSO. In addition to omitting the outer two rows and columns to avoid plate effects, the inhibitors were printed in a randomized manner. Moreover, for each of the eleven library plates a total of 50 replicates were pre-dispensed to allow for the screening of a larger panel of cell lines. Library plates were sealed with Parafilm and stored at -80°C. In a second and third pre-dispensing cycle, the library was extended by 45 and 25 inhibitors, respectively (HDACi_V2 and HDACi_V3). For the extensions, the plate setups were adapted to accommodate the increased number of inhibitors on the same number of library plates as before. Therefore, inhibitors were dispensed in eight instead of ten concentrations and vorinostat and panobinostat were employed as control inhibitors on every library plate (Table 10). HHU Clinical Inhibitor library plates and epigenetic library plates were prepared by David Pauck.

Table 10. Setup of the HDACi libraries

	HDACi_V1	HDACi_V2	HDACi_V3
# Inhibitors	218	263	288
Inhibitors/plate	23	28	28
# Library plates	11	10	11
Concentrations	10	8	8
Control inhibitors	vorinostat, entinostat and tubastatin A	vorinostat and panobinostat	vorinostat and panobinostat
Concentration range	0.005-25 µM		
DMSO	0.25%		
Pre-dispensed replicates	50		

3.5 Screening of cell lines with inhibitor libraries

One hour before addition of the prepared cell suspension, the assay plates were removed from -80°C and thawed at room temperature. Seeding of cell suspension into the plates was carried out using the Multidrop Combi Reagent Dispenser. For each cell line, the optimal seeding number per well was determined beforehand (Table 3) to ensure exponential growth during the exposure to the inhibitors for 72 h. The final assay volume was 30 µL per well.

The determination of the optimal cell seeding number was performed using a serial cell number dilution between 500 and 10000 cells/well in a clear 384 well plates. After 72 hours, the optimal cell number was microscopically determined (70-80% confluence). For suspension cell lines, the optimal cell number was identified using CellTiter-Glo (CTG) Luminescent Cell Viability Assay to identify a cell number within the log phase and before reaching a plateau (Table 3).

3.6 Evaluation of synergistic interaction

For evaluation of synergistic interaction, the respective IC_{10} and IC_{25} concentrations of CI-994 for MED8A and D425 were at first dispensed in addition to pre-dispensed assay plates of the clinical inhibitor library. Wells with IC_{10} or IC_{25} of CI-994 alone were set as the maximal cell viability to assess the synergistic effect of combined treatment. For synergism

validation, CI-994 plus a second inhibitor were dispensed in a 5x5, 8x8 or 12x12 matrix with adjusted inhibitor dilutions.

3.7 CellTiter-Glo Luminescent Cell Viability Assay

For the cell viability readout CellTiter-Glo reagent was prepared according to the manufacturer's instructions. The CellTiter-Glo reagent was diluted with PBS (1:4, v/v) for primary screens and used undiluted for validation screens. A total of 30 µL of the readout reagent was dispensed in each well (384 well plate) using the Multidrop Combi Reagent Dispenser After shaking the plates for 2 min and a subsequent incubation time of 10 min, luminescence was measured using a Spark 10M microplate reader

Table 11. Consumables for drug screening

Consumable	Distributor	Catalog No.
CellTiter-Glo Luminscent Cell Viability Assay	Promega (Mannheim, Germany)	G7573
White 384 well plates, sterile, TC treated White 96 well plate, sterile, TC treated	Corning (Wiesbaden, Germany) Thermo Fisher Scientific (Schwerte, Germany)	3570 136101
T8+ cassette	Tecan (Crailsheim, Germany)	30097370
D4+ cassette	Tecan (Crailsheim, Germany)	30097371
Multidrop tubing	Thermo Fisher Scientific (Schwerte, Germany)	24072670 24073295

3.8 RNA isolation, cDNA synthesis and quantitative real-time PCR

Extraction of RNA was conducted using Invitrogen Trizol or the Maxwell RSC Instrument as per manufacturer instruction. cDNA was synthesized from 0.5 µg RNA using M-MLV Reverse Transcriptase according to the manufacturer's instructions. Quantitative real-time PCR was performed using the CFX384 Touch™ Real-Time PCR Detection System with TaqMan probes for *MYC* and *TGM2* (transglutaminase 2) Samples were amplified in triplicate and relative quantification to housekeeping genes *PPIA (*peptidylprolyl isomerase) and *PGK1* (phosphoglycerate kinase 1) was assessed using the $\Delta\Delta C_T$ method.

Table 12. qPRC mix

Volume	Reagent
5 µl	TaqMan Master Mix
0.5 µl	Primer mix
3.5 µL	H_2O
1 µL	cDNA

Table 13. qPCR detection program

Step	Temperature	Time
1	50 °C	2 min
2	95 °C	10 min
3	95 °C	15 s
4	60°C	1 min
		Go to step 3 39x

Table 14. Consumables for RNA isolation, cDNA synthesis and qPCR

Consumable	Distributor	Catalog No.
Hard-Shell PCR plates 384-well, thin wall	Bio-Rad Laboratories (Feldkirchen, Germany	HSP3805
Nuclease free water	Thermo Fisher Scientific (Schwerte, Germany)	AM9916
Ethanol	VWR (Darmstadt, Germany)	20821.330
Isopropanol	VWR (Darmstad, Germany)	20842.330
Chloroform	Merck Millipore (Darmstadt, Germany)	1.02445
TRIzol Reagent	Thermo Fisher Scientific (Schwerte, Germany	15596-018
M-MLV Reverse Transcriptase	Promega (Mannheim, Germany)	M368C
M-MLV RT buffer 5x	Promega (Mannheim, Germany)	M531A
dNTPs 25 µmol	Promega (Mannheim, Germany)	U151B
RNasin plus, Rnase inhibitor 40 u/µL	Promega (Mannheim, Germany)	N2511
RNAse away	Fisher Scientific (Schwerte, Germany)	10666421
Maxwell® RSC simplyRNA Cells Kit	Promega (Mannheim, Germany)	AS1390
TaqMan Universal Master Mix II with UNG	Applied Biosystems (Schwerte, Germany)	4440038
TaqMan Primer	IDT (Leuven, Belgium)	*MYC*: Hs.PT.58.26770695 *TGM2*: Hs.PT.58.23141755 *PPIA*: HsPanc1.PT.39a.22214851 *PGK1*: Hs.PT.58.606641

3.9   Cell lysis, protein extraction and protein quantification

Cell lysates were generated after treatment of D425 and MED8A cells with CI-994 (5 µM and 7,5 µM) and the corresponding DMSO controls (0.1%) for 24 h and 48 h. Cells were lysed and protein was extracted using RIPA Lysis Buffer supplemented with protease and phosphatase inhibitor cocktail from Roche. Protein was quantified with the Bradford method using the Protein Assay Dye Reagent from Bio Rad. Samples were separated by SDS-PAGE and transferred to a nitrocellulose membrane from GE Healthcare by wet blot using the Mini Gel Tank and Blot Module from Thermo Fisher Scientific. The membrane was incubated with mouse anti-MYC (dilution 1:1000) or rabbit anti-TGM2 (dilution 1:1000), and mouse anti-Actin (dilution 1:5000) primary antibodies overnight at 4 °C. Following incubation with species-specific, peroxidase-coupled secondary antibodies (anti-rabbit-HRP, dilution 1:5000 or anti-mouse-HRP, dilution1:5000) for 1 h at RT, proteins were visualized using the SuperSignal West Femto Maximum Sensitivity Substrate and detected using the LAS-3000 Imaging System from Fujifilm. Experimental work for immunoblotting was kindly performed by Lena Blümel.

Table 15. Consumables for cell lysis, protein quantification and western blotting

Consumable	Distributor	Catalog No.
Antibodies	Thermo Fisher Scientific (Schwerte, Germany) Cell Signaling (Leiden, Netherlands) EMD Millipore (Darmstadt, Germany Cell Signaling (Leiden, Netherlands) Santa Cruz Biotech, Heidelberg, Germany	anti-MYC: MA1-980, 9E10 anti-TGM2: 3557S, D11A6 anti-Actin: MAB1501 anti-rabbit-HRP: 074S anti-mouse-HRP: H2014,
Protein Assay Dye Reagent Concentrate	Bio-Rad Laboratories (Feldkirchen, Germany)	500-0006
Novex Tris-Glycine SDS running buffer	Invitrogen (Schwerte, Germany)	LC2675
RIPA lysis buffer	Merck Millipore (Darmstadt, Germany)	20-188
PhosphoSTOP	Thermo Fisher Scientific (Schwerte, Germany)	04906837001
Protease inhibitor	Thermo Fisher Scientific (Schwerte, Germany)	04693132001
Novex WedgeWell 4-12 % Tris-Glycine Gel	Invitrogen (Schwerte, Germany)	XP04122BOX
Nitrocellulose membrane	Sigma-Aldrich (Taufkirchen, Germany)	10600002
SuperSignal West Femto Maximum Sensitivity Substrate	Thermo Fisher Scientific (Schwerte, Germany)	34095

| BSA | Sigma-Aldrich (Taufkirchen, Germany) | A9306 |
| Milk powder | Carl Roth (Karlsruhe, Germany) | T145.2 |

3.10 Cell apoptosis assay

To assess apoptosis induction, cells were plated into six-well plates and treated with 5 or 7.5 μM CI-994 or DMSO for 48 h. After the indicated incubation time, cells were harvested, stained with propidium iodide (PI, #P4864, Sigma-Aldrich, Taufkirchen, Germany) and FITC labeled Annexin V (#556419 and #51-66121E, BD Pharmingen, Heidelberg, Germany) as per manufacturer's instructions and analyzed by flow cytometry using a CytoFLEX flow cytometer.

3.11 Recombinant lentiviral vector construction for *MYC* overexpression

A lentiviral vector was used for gene delivery to induce stable overexpression of *MYC*. The plasmid LeGO-iG2 (a kind gift from Boris Fehse, derived from Addgene # 27341)[154] was used to construct the recombinant lentiviral vector. The cDNA sequence of *MYC* was amplified from the pcDNA3.3_c-*MYC* plasmid (a kind gift from Derrick Rossi, derived from Addgene #26818)[155] using PCR. PCR primers were designed to include the BamHI and EcoRI restriction endonuclease sites. The PCR product and plasmid LeGO-iG2 were digested with BamHI and EcoRI (NEB, Frankfurt am Main, Germany). The digested PCR product and plasmid were purified using Wizard SV Gel and PCR Clean-Up System (Promega, Mannheim, Germany) and were then ligated. The sequence of all expression vectors was confirmed by DNA sequencing and restriction enzyme analysis (data not shown). Experimental work for vector constructions was kindly performed by Nan Qin and Frauke Meyer.

3.12 Stable transduction

Stable overexpression of *MYC* in UW228-3 cells and stable expression of NFκB reporter construct pHAGE NF-κB-TA-LUCUBC-GFP-W (a kind gift from Darrell Kotton, derived

from Addgene # 49343)[156] in D425 MED and MED8A cells were achieved by lentiviral transduction. Pure populations of each stable cell line were sorted by flow cytometry for stable GFP expression using the MoFlo XDP (Beckman Coulter). Experimental work was kindly performed by Nan Qin.

3.13 NFκB reporter assay

To determine NFκB pathway activity, MED8A and D425 MED stably expressing the NFκB reporter were treated with 1ng/mL TNFα (#8902SC, Cell Signaling, Leiden, Netherlands) as a positive control. Furthermore, these cells were treated with either DMSO and 2.5, 5, or 7.5 μM of CI-994 alone or in combination with 0.1, 0.25 or 0.5 μM of bardoxolone methyl. The NFκB reporter activity was evaluated using ONE-Glo Luciferase Assay System (#E6110, Promega, Mannheim, Germany) for luminescence readout after 48 h. Fold increase in NFκB reporter activity was calculated relative to untreated or DMSO control.

3.14 RNA sequencing

Sample preparation. RNA was isolated using Trizol and processed using the TruSeq RNA Sample Preparation v2 Kit (#RS-122-2001, low-throughput protocol, Illumina, San Diego, USA) to prepare the barcoded libraries from 500 ng total RNA. Libraries were validated and quantified using DNA 1000 and high-sensitivity chips on a Bioanalyzer; 7.5 pM denatured libraries were used as input into cBot (Illumina, San Diego, USA), followed by deep sequencing using HiSeq 2500 (Illumina, San Diego, USA) for 101 cycles, with an additional seven cycles for index reading. Experimental work was kindly performed by Frauke Meyer.

Data analysis. Fastq files were imported into Partek Flow (Partek Incorporated, Missouri, USA). Quality analysis and quality control were performed on all reads to assess read quality and to determine the amount of trimming required (both ends: 13 bases 5´and 1 base 3´). Trimmed reads were aligned against the hg38 genome using the STAR v2.4.1d aligner. Unaligned reads were further processed using Bowtie 2 v2.2.5 aligner. Aligned reads were combined before quantifying the expression against the ENSEMBL (release 84) database by

the Partek Expectation-Maximization algorithm. Finally, statistical gene set analysis was performed using the non-parametric Kruskal Wallis test to determine differential expression at the gene level. Partek flow default settings were used in all analyses.

Pathway Analysis. Ingenuitiy pathway analysis (IPA, Qiagen) was conducted using genes with significant differential expression (p≤0.05 and fold change ±2). The significance cut-off for IPA was set to p≤0.05 for identification of canonical pathways and upstream regulators. Heatmap visualization and unsupervised hierarchical clustering were performed after normalizing mean expression to 0 with a standard deviation of 1 and using Pearson's dissimilarity algorithm and average linkage in Partek Genomics Suite (Partek Incorporated). Data analysis was kindly performed by Daniel Picard.

3.15 Orthotopic xenograft models for brain tumors

All mice were housed in specific pathogen-free conditions at a barrier facility at the Lokey Stem Cell Building (SIM1) at Stanford University School of Medicine (Stanford, CA, USA). All animal handling, surveillance, and experimentation was performed in accordance with and approval from the Stanford University Administrative Panel on Laboratory Animal Care (APLAC No. 26548).

D425 MED-GFP-Luc2 or MED8A-GFP-Luc2 cells were orthotopically injected into 6 to 10-week-old NOD scid gamma (NSG) mice. In brief, mice were anesthetized with 3% isoflurane (Minrad International, Buffalo, NY, USA) in an induction chamber. Anesthesia on the stereotactic frame (David Kopf Instruments, Tujunga, CA, USA) was maintained at 2% isoflurane delivered through a nose adaptor. A burr hole was placed 2 mm posterior to lambda on midline. A blunt-ended needle (75N, 26 s/2"/2.5 µL; Hamilton Co., Reno, NV, USA) was lowered into the burr hole to a depth of 3 mm below the dura surface and retracted 0.5 mm to form a small reservoir. Using a microinjection pump (UMP-3; World Precision Instruments, Sarasota, FL, USA), 3×10^4 D425 MED-GFP-Luc or MED8A-GFP-Luc cells were injected in a volume of 3 µL at 30 nL/s. After leaving the needle in place for 1 minute, it was retracted at 3 mm/min.

Tumor formation was followed by bioluminescence imaging on an IVIS spectrum instrument (Caliper Life Science, Hopkinton, MA, USA) and quantified with Live Image 4.0 software (Living Image, PerkinElmer, Waltham, MA, USA). Medulloblastoma-engrafted mice were given a daily treatment of CI-994 (30 mg/kg) or vehicle control per oral gavage until they reached morbidity. Mice experiments were kindly performed by Johanna Theruvath.

3.16 Data analysis

Inhibitor treatment was assessed using Graphpad Prism software (Version 5.03). Dose-response curves were generated using non-linear regression (log(inhibitor) vs. normalized response) with mean luminescence signals from DMSO control wells (≥ 3) as 100% cell viability, inhibitor response was calculated accordingly relative to the control. All data are presented as mean ± SD unless stated otherwise. Comparisons between different groups were made using GraphPad Prism software, employing Student's *t* test or ANOVA as appropriate. Statistical significance between different dose-response curves was assessed with regards to the fitted midpoints (Log IC_{50}) using the sum-of-squares F test. The statistical significance of Kaplan-Meier survival curves was evaluated using the log rank (Mantel-Cox) test. p-values ≤ 0.05 were considered significant. Synergistic interaction was calculated using Bliss synergy scores as generated by the Combenefit software (Version 2.02). Heatmaps were generated using the online tool Morpheus (https://software.broadinstitute.org/morpheus/) and unsupervised hierarchical clustering was performed by employing the Euclidean distance with complete linkage method. For inactive compounds or inhibitors with IC_{50} values >25 µM the highest tested concentration of 25 µM was used as a default value in the heatmap. Venn diagrams were created using the following webtool: http://bioinformatics. psb.ugent.be/webtools/Venn/.

4 Results

For the pre-clinical evaluation of new epigenetic, HDACi-based treatment options for primary brain tumors, we established and validated a semi-automated high-throughput screening workflow (see section 4.1). Our setup enabled the identification of active HDAC inhibitors by screening over 250 institutional and commercial inhibitors in a large panel of tumor cell lines (n>40) from different entities (see section 4.2). Hereby, we discovered the inhibitor CI-994 as a preferentially active inhibitor for *MYC*-driven Group 3 medulloblastoma and based on the screening results, CI-994 was further evaluated both *in vitro* and *in vivo* (see section 4.3).

4.1 Implementation of a semi-automated high-throughput screening pipeline

The identification of novel compounds with antitumoral activity represents one of the key challenges in translational research. Despite the emergence of transcriptomic and methylation profiling of brain tumors recognizing molecularly defined subgroups e.g. for medulloblastoma, atypical/teratoid rhabdoid tumor and ependymoma, treatment stratification and clinical trial design is still primarily based on histopathological criteria. However, as clinical trials are cost- and time-intensive, pre-clinical data based on drug screening results could help to identify clinically meaningful and particularly tumor (subgroup)-specific drug candidates, promoting patient stratification accordingly. Moreover, since many brain tumors display resistance to standard multimodal therapeutic approaches and curative second-line treatment options are often lacking, novel targeted therapeutics are clearly warranted. The interdisciplinary setup of this project within the departments of neuropathology, pediatric oncology and pharmaceutical and medicinal chemistry, grants access both to a unique compound library of HDAC inhibitors as well as a large cohort of brain tumor cell lines. Paired with the possibility for genome-wide profiling and next-generation sequencing methods, this setting offers ideal prerequisites for translational research. However, to fully exploit this potential, we will have to be able to perform an the evaluation of large compound libraries in a variety of cell ines.

4.1.1 Setup and optimization of the screening workflow

Driven by this lack of methodological connection we first optimized and implemented an institutional semi-automated screening workflow. In general, the screening workflow was designed to enable the screening of hundreds of compounds with a plethora of cell lines in days. Thus, to facilitate the workflow manual steps required are reduced to a minimum and tasks including the dispensing of inhibitors, cell lines and readout reagent are automated. The drug screening workflow was therefore streamlined using the D300e Digital Dispenser, the Multidrop Combi Reagent Dispenser and the Spark 10M Microplate Multimode Plate Reader.

The D300e Digital Dispenser is used for the dispensing of inhibitors by employing disposable dispenseheads, that allow for nL to pL dispension of inhibitors. Using this device, inhibitors are directly dispensed from stock solutions into the assay plates, thereby eliminating the need of preparing serial dilutions of inhibitors beforehand. To improve the reliability of the results, plate designs can be set up in a way that all wells are normalized to the highest dimethylsulfoxide (DMSO) concentration and inhibitors are dispensed in a randomized manner. The Multidrop Combi Reagent Dispenser is suitable for the use in a high-throughput format as it allows for the accurate dispensing of a wide range of volumes into different microtiter plate formats. In our setting, we used the Multidrop Dispenser for dispensing of the cell suspension as well as the readout reagent into the assay plates. The Spark 10M Multimode Microplate Plate Reader was employed for the readout of the luminescence signals. Equipped with a Spark-Stack microplate stacker, this setup further increased the efficiency of the whole workflow.

Implementing these semi-automated devices, the overall workflow for drug screening can be divided into four main working steps, namely

1. dispensing of inhibitors
2. dispensing of cell lines
3. dispensing of readout reagent
4. readout and analysis.

1. Dispensing of inhibitors

The generation of assay (library) plates with serial dilutions of the inhibitor libraries is facilitated by digital titration of compounds directly into the plates. This feature therefore eliminates the need of multiple steps necessary in the process of manual pipetting e.g. preparation of serial dilutions and intermediate dilution in media, thereby clearly improving the accuracy of testing as compared to the manual preparation of dilution series. Moreover, with the possibility of randomized dispensing of inhibitors and thereby avoidance of plate and edge effects, the inhibitors were tested in singlicates to reduce the required number of plates per library. To make full use of the D300e Dispenser and to even further decrease variability between the screens, the library plates were eventually pre-printed in quantities of up to 50 plates per library plate and stored at -80°C until needed for dispensing of cell lines. This clearly reduced the time demand per screening run and allowed for an accelerated testing of a large number of tumor cell lines.

2. Dispensing of cell lines

For each cell line, the optimal cell seeding number per well was determined beforehand to ensure exponential growth during the exposure to the inhibitors (Table 3). Based on this we were able to reach high comparability between cell lines. The final assay volume was 30 µL per well for 384 well plates and the incubation time was 72 hours at 37°C with 5% CO_2. These parameters ensured good growth of a variety of cell lines and was used as standard for all experiments.

3. Dispensing of readout reagent

For the readout we decided to use the broadly employed CellTiter Glo (CTG) Luminescent Cell Viability Assay to determine the number of viable cells after inhibitor treatment The assay is based on the quantification of adenosine triphosphate (ATP) as an indicator of metabolically active cells. The generated luminescent signal is proportional to the amount of ATP, which is in turn proportional to the number of viable cells. In contrast to the often employed MTT (3-(4,5-dimethylthiazol-2-yl)-2,5-diphenyltetrazolium bromide) assay

which needs multiple preparation steps with accompanying incubation time, the CTG assay is a one-step procedure highly suitable for high-throughput screens. The CTG reagent can directly be added to the cultured cells and after ten minutes of incubation time generates a stable luminescent signal which has a half-life of more than five hours.

4. Readout and data analysis

For the detection of the luminescent signals, measurement was performed after ten minutes of incubation. Afterwards for the analysis, raw luminescence signals were normalized to wells containing only DMSO (=100% cell viability) and dose response curves are generated using GraphPad Prism software employing non-linear regression (log(inhibitor) vs. normalized response). Based on these data, IC_{50} values (half maximal inhibitory concentration) were calculated (Figure 8).
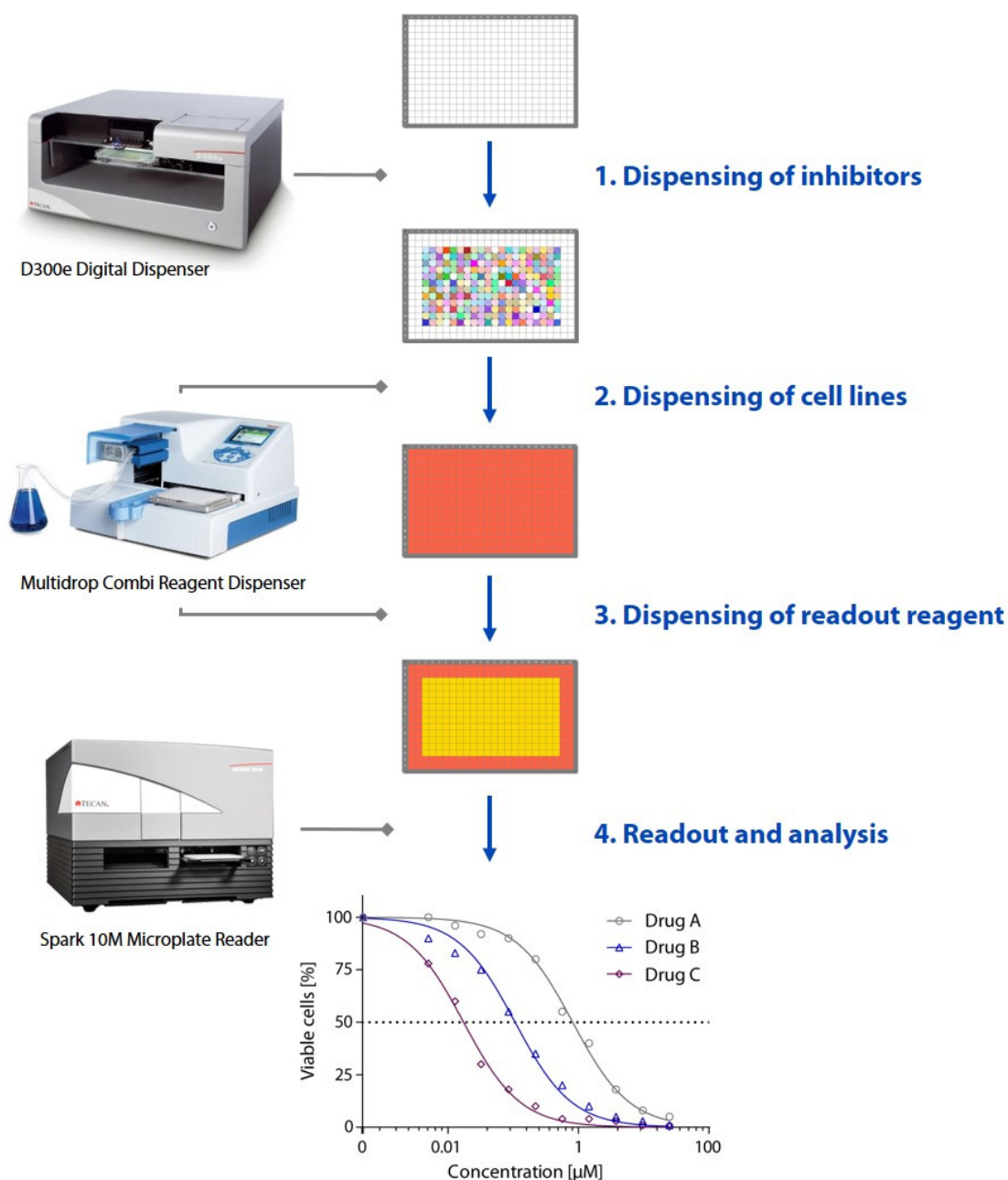
Figure 8. Optimized drug screening workflow. The established workflow can be subdivided into four main steps, starting with the dispension of the inhibitors to prepare the library plates (1.). After this, the plates can be stored at -80°C and thawed when necessary. The next workflow step is the seeding of cell lines into the plates, followed by an incubation time of 72 h (2.). For the readout, the readout reagent is dispensed into wells containing inhibitor treated cells (3.) and signals are read on a microplate reader (4.). Finally, analysis of the raw data is performed using nonlinear regression of the normalized signals to provide the appropriate dose-response curves (5.). The workflow was streamlined by the use of the D300e Digital Dispenser for dispensing of the inhbitors, the Multidrop Combi Reagent Dispenser for dispension of cell lines and readout reagent and the Spark 10M Multimode Microplate Reader is employed for the readout.

4.1.1.1 Validation of the dispensing method

The dispensing of inhibitors into well plates represents a rather time consuming step, especially for manual pipetting. In order to not only take advantage of the technical titration but also reduce the consumption of inhibitors, we evaluated if the assay plates can be pre-dispensed in a batch manner and stored at -80°C as compared to direct dispensing of inhibitors into the plates. For the evaluation of the feasibility of pre-dispensing of inhibitors and the subsequent storage of assay plates at -80°C, we selected eight HDACi from our institutional library covering a broad IC_{50} range. All inhibitors were tested in sNF96.2 cells, a robust and well-established cell line in our laboratory.

For the method of direct dispensing, the inhibitors were dispensed in a ten point dilution series onto assay plates already containing cells. The cells were seeded onto plates 24 h prior to inhibitor treatment. In contrast, for the second method, inhibitors were pre-dispensed into empty 384 well plates and subsequently stored at -80°C until needed. At least half an hour before application of cell lines, assay plates were removed from -80°C and thawed at room temperature. The prepared cell suspension was then dispensed onto the plates and they were incubated for 72 hours. Readout for both methods was cell viability as determined by CTG assay.

Our experiments clearly showed, that IC_{50} values derived from both methods are highly correlated (r=0.96, p=0.0002, Figure 9 A). Importantly, dose response curves generated by either method generally showed no significant difference with regards to the fitted mid-point ($logIC_{50}$), as exemplified for the inhibitor DDK137 (Figure 9 B). This clearly shows that our method pre-dispensing represents a viable and time- as well as cost-efficient method for the preparation of inhibitor plates.
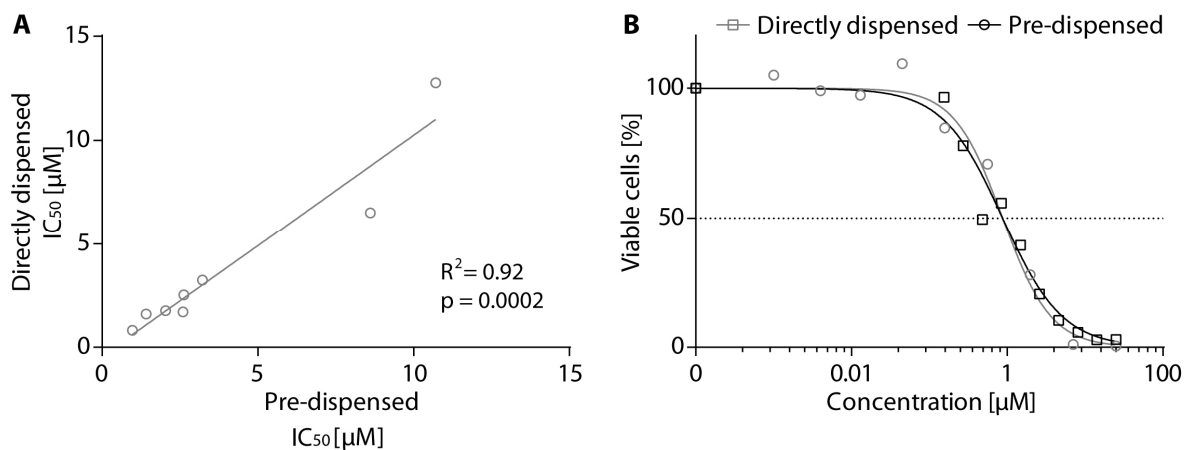
Figure 9. Comparison between direct and pre-dispensing of inhibitors. (A) IC_{50} values derived for sNF96.2 cells by either direct dispensing or pre-dispensing of inhibitors are highly correlated. (B) Exemplary dose response curve for the inhibitor DDK137 in sNF96.2 cells. No significant difference between the IC_{50} values derived by either method could be detected (p=0.36, sum-of-squares F test).

4.1.1.2 Validation of plate format

In a second step, the transferability of the assay from 96 to 384 well plates was evaluated in order to further increase the efficiency of the screening workflow. Again, selected inhibitors were tested on both formats using sNF96.2 cell lines and the derived IC_{50} values were compared. Importantly, a significant correlation between the two plate formats could be detected (r=0.89, p=0.0002, Figure 10 A). In addition, IC_{50} values derived from assaying directly dispensed inhibitors on 96 well plates are highly correlated to those pre-dispensed onto 384 well plates (r=0.98, p<0.0001, Figure 10 B).
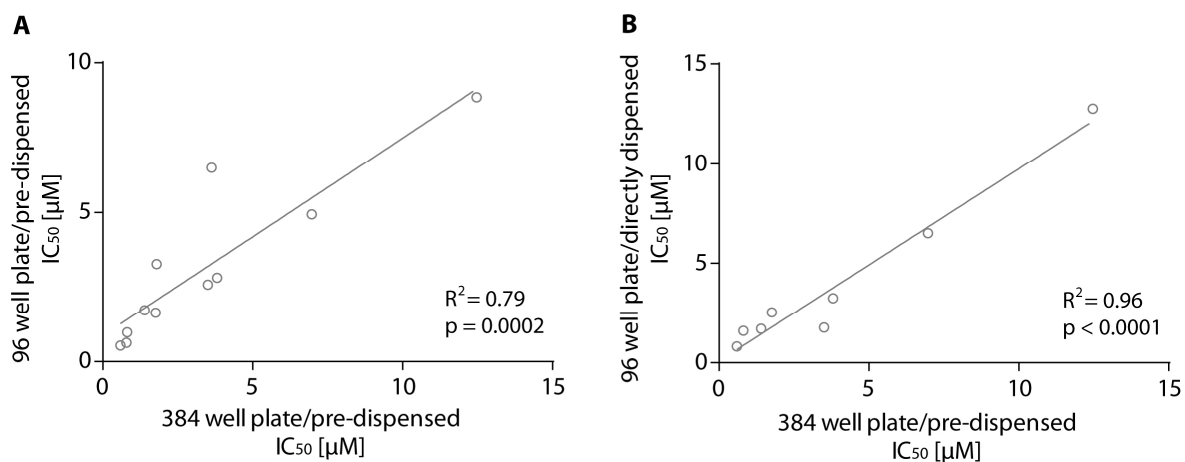
Figure 10. IC_{50} value comparison between 96 and 384 well plates. (A/B) IC_{50} values generated by evaluating sNF96.2 cells either on 96 well plates (inhibitors directly dispensed (A) or pre-dispensed (B)) or 384 well plates (inhibitors pre-dispensed) are highly correlated.

4.1.1.3 Validation of storage stability of pre-dispensed assay plates

As a final validation, the storage stability of the assay plates with pre-dispensed serial dilutions of the inhibitors and thus the reproducibility of IC_{50} values after storage of assay plates at -80°C were tested. IC_{50} values for directly dispensed inhibitors are significantly correlated with IC_{50} values generated after storage at -80°C (7 weeks, r=0.98, p<0.0001, Figure 11 A). The good correlation is maintained also at different time points after printing and storage of assay plates (r=0.99; p<0.0001, Figure 11 B), thereby underlining the robustness of the workflow.
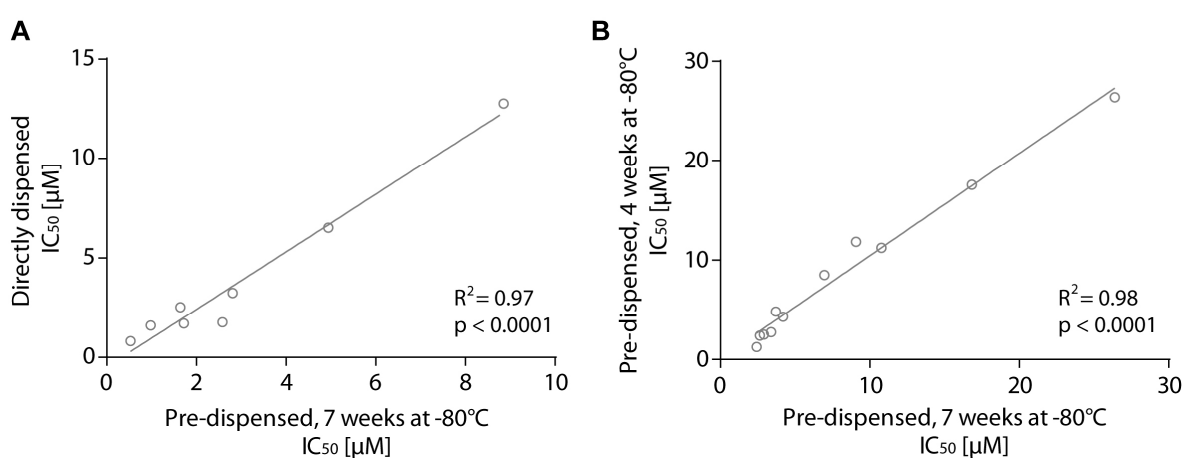
Figure 11. Comparison between direct and pre-dispensing of inhibitors. IC_{50} values for inhibitors directly and pre-dispensed for sNF96.2 cells are significantly correlated. (A) Correlation of IC_{50} values generated by direct dispensing and pre-dispensing of inhibitors. (B) No significant changes in IC50 values could be detected at different time points.

4.1.2 Adapted workflow for evaluation of synergistic inhibitor combinations

Single drug treatment is often associated with emerging resistance and limited efficacy. To circumvent this issue, combinations of multiple drugs are being administered at the same time. In many cases, it is being observed that the efficacy of combined drugs is not just additive, but often synergistic. This means that the effect of both combined is potentiated as compared to the sum of effects, when being administered separately. Hence, often lower doses of each drug can be used. for a treatment and potential side effects or emerging resistance can be avoided. In order to be able to identify synergistic inhibitor combinations, the established drug screening workflow was adapted accordingly to enable the evaluation

of potentially synergistic drug combinations with pre-printed inhibitor libraries (Figure 12). Based on the previously established protocol for drug screening, the following steps have been adapted:

1. Drug combination

Starting from pre-printed plates with serial dilutions of an inhibitor library, the drug of interest (drug X) was dispensed with IC_{10} or IC_{25} concentrations in each well. In addition to these combination plates, the cell lines were also screened with regular library plates without additional inhibitor.

Steps 2 and 3 of the workflow, including the dispensing of cell lines followed by incubation for 72 h and the dispensing of readout reagent were performed as described before.

4. Analysis

Cell viability of the combination plates are normalized to wells containing only drug X (=100%), thereby deducting the effect of drug X alone. For the regular library plates, signals are normalized as usual to DMSO only wells and the resulting dose-response curves are overlaid with the combination curves. This normalizing step allows for the differentiation between additive and synergistic effects, since in the case of additivity, the resulting curves will overlap (Figure 12 Graph A) and for synergistic drug combinations there will be a shift towards lower IC_{50} (Figure 12 Graph B).

For further validation of the identified favorable drug combinations, a more detailed evaluation is performed. For this purpose, the two drugs of interest are tested in extended concentration matrices (e.g. 8x8, 10x10) to identify optimal concentration combinations. Analysis of the combinations with regards to synergism is then performed by calculating so called synergism scores or combination indices. The most commonly used approaches for the analysis are Highest single agent (HSA), Bliss synergy, Loewe additivity and Chou-Talalay.[157,158]
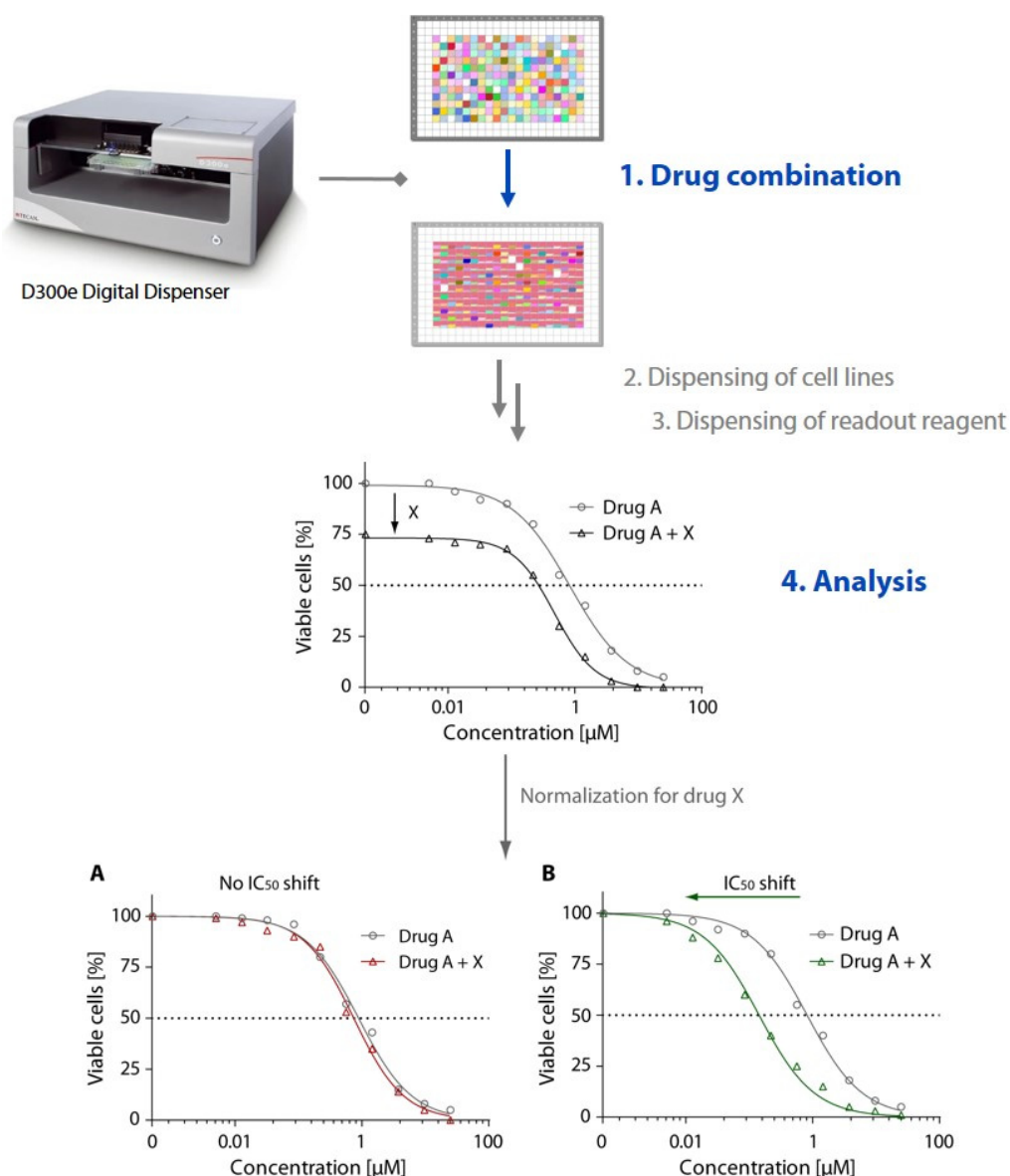
Figure 12. Modified workflow for the identification of synergistic drug combinations. For the screening for drug combination with synergistic potential, the drug of interest (depicted as drug X) is dispensed with one concentration (e.g. IC_{10} or IC_{25}) onto assay plates with pre-printed serial dilutions of an inhibitor library. Next, cell lines are added to library plates and combination plates and after incubation, readout signals are detected. For the discrimination of synergistic interactions from additive effects, signals are normalized to wells containing only the drug of interest and compared to the dose-response curves generated without the drug combination. Shifts in IC_{50} values of drugs from the inhibitor library can therefore likely be attributed to synergism.

4.1.3   Setup of the HDACi library screen and validation

After establishing and validating the technical aspects of the screening workflow, we expanded our screening approach toward the evaluation of a whole inhibitor library with over 200 compounds in a larger panel of cell lines. After two extensions, the institutional

HDACi library is now composed of a total of 288 compounds. Out of these, 267 compounds were synthesized in the laboratory of Prof. Dr. Kurz at the Institute of Pharmaceutical and Medicinal Chemistry (Heinrich-Heine University Düsseldorf), 2 inhibitors were provided by the CHDI foundation[120] and 20 inhibitors were obtained from commercial sources. The latter comprise the four FDA approved drugs vorinostat, belinostat, panobinostat and romidepsin as well as clinically tested compounds like entinostat, CI-994, ricolinostat and valproic acid. The majority of the commercial inhibitors are characterized as pan inhibitors but also include HDAC class I or class IIa as well as HDAC6 and HDAC8 selective compounds.

The institutional inhibitors were designed and synthesized in-house within the scope of different PhD projects. The largest majority of inhibitors belong to the class of hydroxamic acids followed by benzamides. A subset of the inhibitors were characterized concerning their biological activity against different cancer cell lines as well as with regards to their HDAC isoform profile and described in different previous publications. [159–164]

To ensure that results obtained from screening a library of over 200 compounds is as reproducible as shown before for a small number of selected inhibitors, two library screens with sNF96.2 cells were performed at different time points. In both screens, 100 compounds showed no or little activity with IC_{50} values exceeding the maximum concentration of 25 µM. For small subset of 12 inhibitors (5.5%) varying results were obtained between the screens with one of the two IC_{50} values above 25 µM. IC_{50} values for the remaining 106 compounds are in very good correlation between the two screens (r=0.91, p<0.0001, Figure 13), clearly confirming the robustness of the overall screening approach.
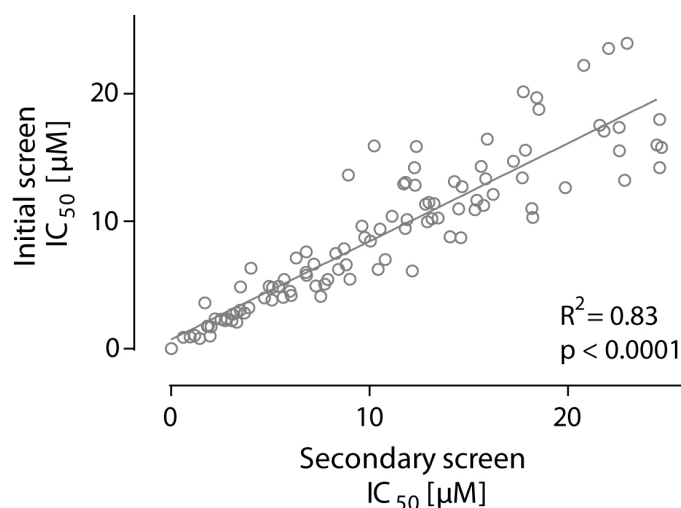
Figure 13. Correlation of IC$_{50}$ values of active inhibitors derived from two independent screens. The 218 inhibitors encompassing HDAC library was tested in an initial screen and re-screened after three weeks with sNF96.2 cells. The correlation graph shows the IC$_{50}$ values from 106 inhibitors. For 100 compounds both IC$_{50}$ values exceeded the maximum concentration of 25 µM and 12 inhibitors (5.5%) showed varying results with one of the two IC$_{50}$ values above 25 µM.

In addition to the initial tests of the screening workflow, the quality of individual library screens was evaluated based on different parameters. For the first library version the commercially available inhibitors entinostat, vorinostat and tubastatin A were dispensed on each of the eleven library plates as controls. These control inhibitors allow for the evaluation of possible inter-plate variation for one screen (Figure 14).
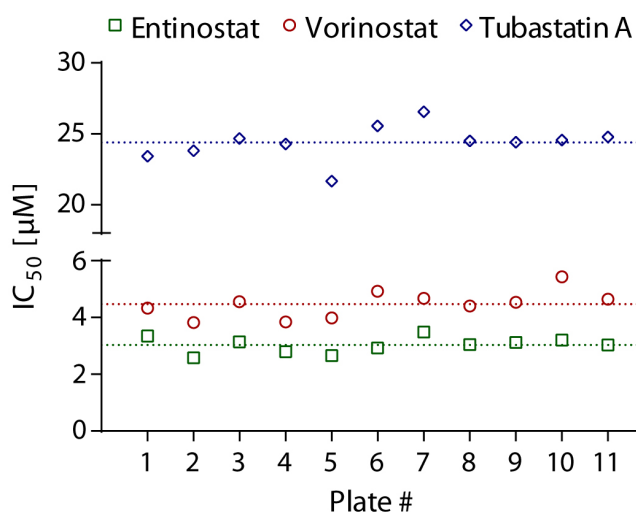
Figure 14. IC$_{50}$ value of control inhibitors across the HDACi library. The inhibitors entinostat, vorinostat and tubastatin A were dispensed on each of the eleven library plates as controls to check for inter-plate variability. The dashed lines depict the mean IC$_{50}$ value for each inhibitor across the plates (Entinostat 3.03 ± 0.28 µM; vorinostat 4.47 ± 0.47 µM; tubastatin A 24.38 ± 1.22 µM).

Figure 14 shows an example of the distribution of IC$_{50}$ values for the three inhibitors in sNF96.2 cells across the eleven library plates, nicely indicating low inter-plate variability with a standard deviation (SD) of $\leq$ 10%. For later HDACi library versions, tubastatin A was omitted as a control since it showed very low activity with IC$_{50}$ values often exceeding the highest tested concentration of 25 μM. Furthermore entinostat was substituted for panobinostat to also include a strong positive control on every plate. Panobinostat is a very potent inhibitor, which generally shows about 100% cell death at the highest concentrations.

4.2 HDACi response profiling in brain tumor models

After establishing and validating the screening workflow, we focused on the application of this robust setup for the identification of novel inhibitors for an epigenetic, HDACi-based therapy of brain tumors. For this, cell lines derived from the most common malignant brain tumors in childhood and adulthood, namely MB, DIPG, AT/RT and GBM were evaluated with the institutional HDACi library. As inhibitors from the initial HDACi library (HDACi_V1) were also included in the extensions (HDACi_V2 and V3), they have been screened with the complete set of cell lines, while newer inhibitors in the extension libraries were screened only with a subset of cell lines. For this reason, the following results will mainly focus on the 218 HDACi that were tested from the beginning across all cell lines screened. To provide a better overview of the inhibitors with potent activity or selective response, a total of 102 inhibitors (47%) were excluded from clustering analysis as they showed either no activity in any cell line (n=20 out of 218, 9%) or only minor and variable response in a subset of cell lines (mean IC_{50}>20 μM, n=82 out of 218, 38%) (Supplementary Figure 1).

Based on the unsupervised clustering of the drug activity (IC_{50} values) of the remaining 116 HDACi, we identified various interesting patterns of response. For inhibitors with no activity or IC_{50} values exceeding the highest tested concentration, 25 μM was set as a default value. Red therefore indicates inactivity and blue boxes show inhibitors with low μM to nM activity. The cell lines (columns) clustered into five main groups showing either relative sensitivity (clusters S1-S3) or resistance (clusters R1-R2) towards the inhibitors. Notably, clusters containing the most sensitive cell lines (cluster S1 and S2) are enriched for medulloblastoma. Cluster S3 is made up of a subgroups of AT/RT and DIPG cell lines. In the resistant clusters R1 and R2 the majority of GBM and AT/RT cell lines can be found in addition to two MB and DIPG cell lines (Figure 15).

Figure 15. HDACi response profiles in brain tumor cell lines. Heatmap indicating the response of AT/RT (n=11), DIPG (n=5), GBM (n=8), MB (n=4) and *MYC*-MB (n=6) cell lines to 116 out of 218 HDAC inhibitors. Cell lines (columns) and inhibitors (rows) were clustered based on the respective IC$_{50}$ [μM] values. For compounds that were inactive or showed only little reduction in cell viability, the highest tested concentration of 25 μM was used as a default value. Red therefore indicates inactivity while blue shows compounds with high activity. Unsupervised clustering divided cell lines into five and inhibitors into eight cluster. Cell line groups are denoted as R1, R2 or S1, S2, S3 (R= resistant, S=sensitive) based on their overall response profile. Inhibitor groups are named A-G, with clusters A-D containing broadly active drugs and clusters E-G showing variable activity across the cell lines. A total of 102 out of 218 (47%) inhibitors were excluded from the heatmap as they showed no activity in any cell line tested (n=20, 9%) or very little and varying activity (mean IC$_{50}$>20 μM; n=82, 38%) (Supplementary Figure 1). For the cell line DIPG25 one library plate failed quality control and therefore IC$_{50}$ values were left blank (as indicated by grey boxes in the heatmap).

65
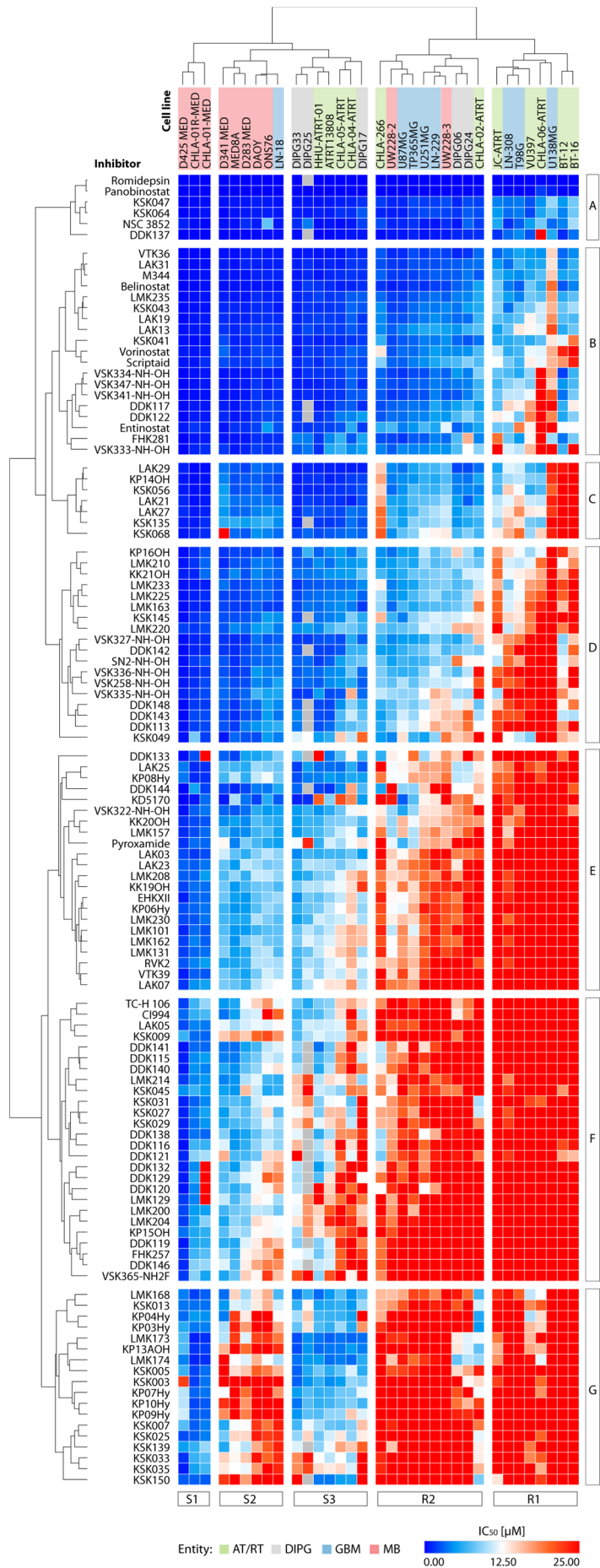
Inhibitors (rows) clustered into seven main groups with compounds exhibiting high to good activity across all cell lines and compounds with variable response between distinct cell lines and entities. The FDA approved drugs romidepsin and panobinostat were active across all cell lines with IC_{50} values in the very low nM range. They clustered together with the commercially available compound NSC 3852 (5-nitroso-8-quinolinol) and the institutional inhibitors DDK137, KSK047, KSK064 to form cluster A (Figure 16). This cluster is composed of the inhibitors exhibiting the strongest inhibitory response across the different entities.
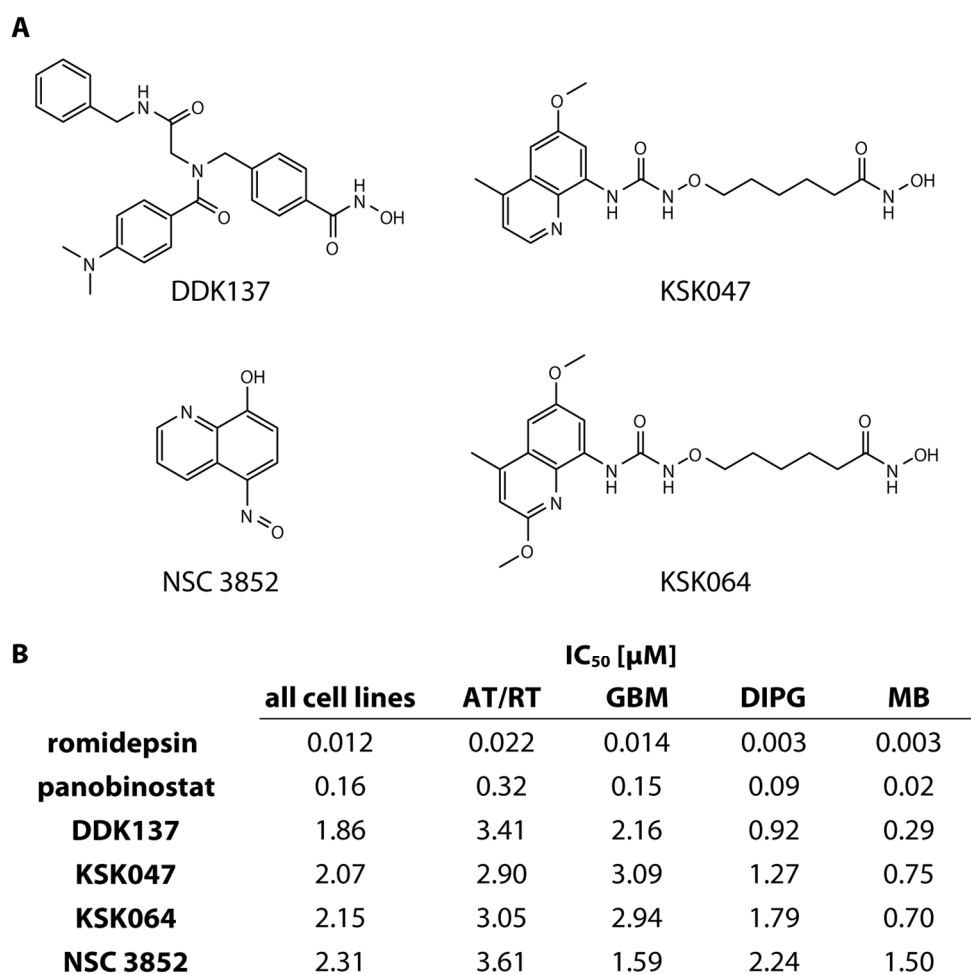
Figure 16. Representation of top active HDACi. (A) Chemical structures for the selected inhibitors (structures for romidepsin and panobinostat are depicted in Figure 4). (B) Corresponding mean IC_{50} value across all cell lines and for single entities.

B	IC_{50} [µM]				
	all cell lines	AT/RT	GBM	DIPG	MB
romidepsin	0.012	0.022	0.014	0.003	0.003
panobinostat	0.16	0.32	0.15	0.09	0.02
DDK137	1.86	3.41	2.16	0.92	0.29
KSK047	2.07	2.90	3.09	1.27	0.75
KSK064	2.15	3.05	2.94	1.79	0.70
NSC 3852	2.31	3.61	1.59	2.24	1.50

The natural product romidepsin act as a pro-drug; the disulfide bond is reduced by glutathione reductase to reveal a thiol that interacts with the zinc ion at the active site of HDACs.[165] In contrast to the pan HDAC inhibitors panobinostat and vorinostat,[166] romidepsin has been shown to be a potent inhibitor of particularly class I HDACs.[165] The

cinnamic hydroxamic acid analogue panobinostat as well as romidepsin are widely studied in clinical trials for several indications and have been approved for the treatment of PTCL and CTCL as well as PTCL and multiple myeloma, respectively. Compounds KSK047 and KSK064 are part of an inhibitor series with an alkoxyurea connecting-unit, that act as dual HDAC1/6 inhibitors with slight HDAC6 preference and have already been evaluated as potent inhibitors synergizing with cisplatin to inhibit tumor cell growth.[159] The peptoid-based compound DDK137 was evaluated likewise and found to be equally potent in inhibiting HDAC1 and HDAC6.[162,167] The quinoline compound NSC 3852 has been shown to induce differentiation and oxidative stress by ROS formation in breast cancer cell lines. Due to similar effects compared with SAHA and TSA treatment with modest *in vitro* HDAC activity the authors concluded that NSC 3852 mode of action could partially be attributed to inhibition of HDACs.[168,169] However, since the 8-quinolinol motif differs from the classic Zn^{2+} chelating motif of other HDACi and has not been thoroughly studied in this context, the good cytotoxicity of NSC 3852 might rather be attributed to the induction of ROS.

Clusters B and C are comprised of inhibitors with good activity across all cell lines with mean $IC_{50} < 10$ µM. Besides the FDA approved drugs vorinostat and belinostat, Cluster B contains also the clinically evaluated *o*-aminoanilide inhibitor entinostat. Clusters D-F are comprised of inhibitors with intermediate and variable activity, largely dividing the cell lines into the sensitive and resistant clusters. Inhibitor cluster G contains also compounds with variable response, however a different sensitivity pattern can be observed as compared to groups E and F. Interestingly, while cluster E and F show higher activity in the sensitive cell lines of cluster S1-S2 with good to intermediate response of cluster S3, inhibitors of cluster G and H seem to be selectively more active in a subset of MB in cluster S1 and in a subset of AT/RT and DIPG in cluster S3 with almost no activity in S2 (Figure 15).

4.2.1 Cross-entity comparison of HDACi response in brain tumor models

With the first unsupervised clustering analysis shown before (Figure 15), cell lines were grouped based on similarity between their response profiles, which likely is imparted by their

genetic and epigenetic background. However, while AT/RT, DIPG and GBM cell lines can be found across the different sensitivity/resistance cluster, MB cell lines clustered together quite closely showing a high overall sensitivity for HDAC inhibition. In a next step, we therefore had a closer look at the MB cell lines.

The MB cell lines in our screen can be grouped into *MYC*-amplified and non-amplified MB. The cell lines CHLA-01-MED, CHLA-01R-MED, D341 MED, D425 MED and MED8A are characterized by an amplification of *MYC* and D283 MED by a high copy number gain, therefore denoted as *MYC* MB cells in the following chapters. The MB cell lines DAOY, ONS-76, UW-228-2 and UW-228-3 show no *MYC* amplification with only very low endogenous expression levels and were therefore designated as non-*MYC* MB.[170]

Comparison of IC_{50} values of the active inhibitors ($IC_{50} < 25$ μM) for each cell line between these two MB subgroups clearly showed that the IC_{50} values in the *MYC* MB cell lines are on average significantly lower than in the non-*MYC* MB cell lines (p<0.001, Figure 17 A). Out of a total of 1308 IC_{50} values for the *MYC* MB cells, 943 IC_{50} values were below 25 μM (72%) whereas only 422 out of the 872 IC_{50} values (48%) for the non-*MYC* MB cells were below 25 μM. In addition, the median IC_{50} value (4.2 μM) across the *MYC* MB cell lines was considerably lower than in the non-*MYC* MB cells (median IC_{50} 8.8 μM). In addition, we also looked both at the activity of the inhibitors as well as the significance of the difference between the responses of the two subgroups. For this, we calculated a fold change by dividing the mean IC_{50} of the *MYC* MB cell lines by the mean IC_{50} of non-*MYC* MB cells. The fold change was then plotted against the p-value of the respective comparison (Figure 17 B). Positive values on the x-axis show inhibitors with higher activity in *MYC* MB cells and negative values inhibitors with higher activity in the other entities accordingly. To identify inhibitors with preferential activity we chose a fold change>1.5 and a p-value<0.05 as cut-off criteria. Thereby we could identify 71 inhibitors as significantly more active in the *MYC* MB and none showing a higher mean activity across the non-*MYC* MB cell lines. These finding is largely in agreement with previous publications, identifying HDACi as effective compounds in Group 3 *MYC*-driven MB.[80,81,171]
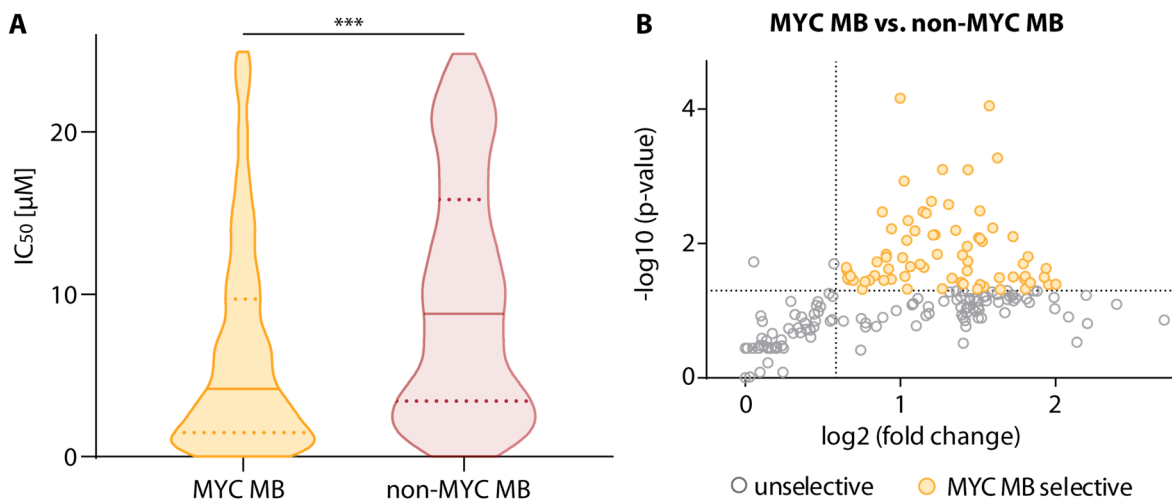
Figure 17. HDACi are significantly more active in *MYC*-driven compared to non-*MYC* medulloblastoma cell lines. (A) IC_{50} distribution of all active HDACi ($IC_{50}<25\mu M$) of each cell line in the *MYC* MB and non-*MYC* MB group (*MYC* MB: 943 out of 1308 IC_{50} values (72%); non-*MYC* MB: 422 out of 872 IC_{50} values (48%)). Bold lines mark the median IC_{50} value and the dashed lines the 25-75 percentile, respectively (*MYC* MB: median 4.2 µM, 25-75 percentile 1.5-9.7 µM; non-*MYC* MB: median 8.8 µM, 25-75 percentile 3.4-15.5 µM). (B) The HDACi responses in *MYC* MB cell lines were compared against AT/RT, DIPG and GBM For this purpose the fold change was calculated from the mean IC_{50} of each entity (log2, x-axis) and plotted against the corresponding p-value (- log10, y-axis). The dashed lines indicate a fold change>1.5 and a p-value<0.05. 71 inhibitors were significantly more active in the *MYC* MB cell lines, as depicted by the colored circles and non in the non-*MYC* MB cells. ***, p<0.001 (unpaired *t*-test).

In contrast to the aforementioned publications already describing the high sensitivity of *MYC*-driven MB towards HDAC inhibition, we identified this sensitivity not only in comparison with non-*MYC* MB cell lines but could further expand this observed response pattern as being unique among the different brain tumor entities. *MYC* MB show not only higher susceptibility when compared to non-*MYC* MB but also with regards to the other tested tumor entities. For a cross-entity comparison, we also looked at the mean response of the active inhibitors ($IC_{50}<25$ µM) in AT/RT, DIPG and GBM cell lines. With median IC_{50} values of 9.0 µM (AT/RT), 7.5 µM (DIPG) and 10.0 µM (GBM), these cell lines were also on average significantly less sensitive (p<0.001) than the *MYC* MB cells. In addition, considerably less inhibitors showed activity in these entities with only 39%, 50% and 36% of all IC_{50} being below 25 µM for AT/RT, DIPG and GBM, respectively (Figure 18 A)
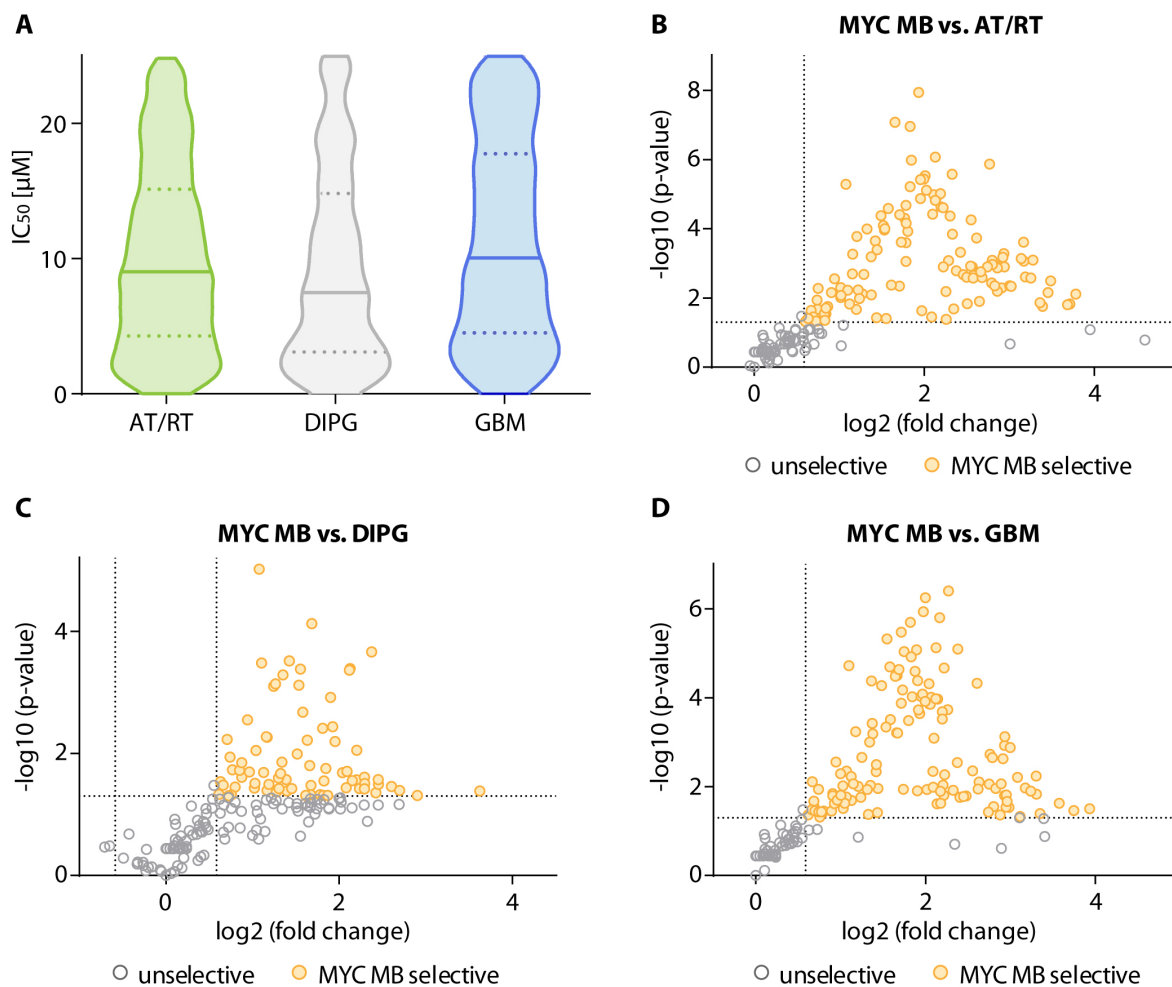
Figure 18. Comparison of the inhibitor response in *MYC* medulloblastoma vs. other brain tumor entities. (A) IC_{50} distribution of all active HDACi ($IC_{50}<25\mu M$) of each AT/RT, DIPG and GBM cell line (AT/RT: 940 out of 2398 IC_{50} values (39%); DIPG: 521 out of 1050 IC_{50} values (50%); GBM: 628 out of 1744 IC_{50} values (36%)). Bold lines mark the median IC_{50} value and the dashed lines the 25-75 percentile, respectively (AT/RT: median 9.0 µM, 25-75 percentile 4.3-15.1 µM; DIPG: median 7.5 µM, 25-75 percentile 3.1-14.8 µM); GBM: median 10.0 µM, 25-75 percentile 4.5- 17.7 µM). (B-D) 123, 76 and 136 inhibitors were significantly more active in the *MYC* MB cell lines in comparison to AT/RT, DIPG and GBM cells, respectively.

Like for the comparison with non-*MYC* MB, there was no inhibitor out of the 218 tested that showed higher mean activity in AT/RT or GBM (Figure 18 B/D). Only for the *MYC* MB *vs.* DIPG comparison, we could identify 14 inhibitors showing higher mean activity in the DIPG cell lines, however without significance (Figure 18 C).

For each of the entity comparison we identified a high number of inhibitors with preferential activity in *MYC* MB. Out of 218 inhibitors tested, 71, 123, 76 and 136 inhibitors were preferential active in *MYC* MB as compared to non-*MYC* MB, AT/RT, DIPG and GBM, respectively. To further narrow down the number of preferentially active inhibitors, we

increased the fold change cut-off to >2.5. Thereby we could identify14 compounds commonly detected in each comparison (Figure 19 A). Although these inhibitors showed in part varying activity in the *MYC* MB cell lines, the mean IC$_{50}$ values were in general significantly lower than in the other tested entities/subgroups (Figure 19 B).
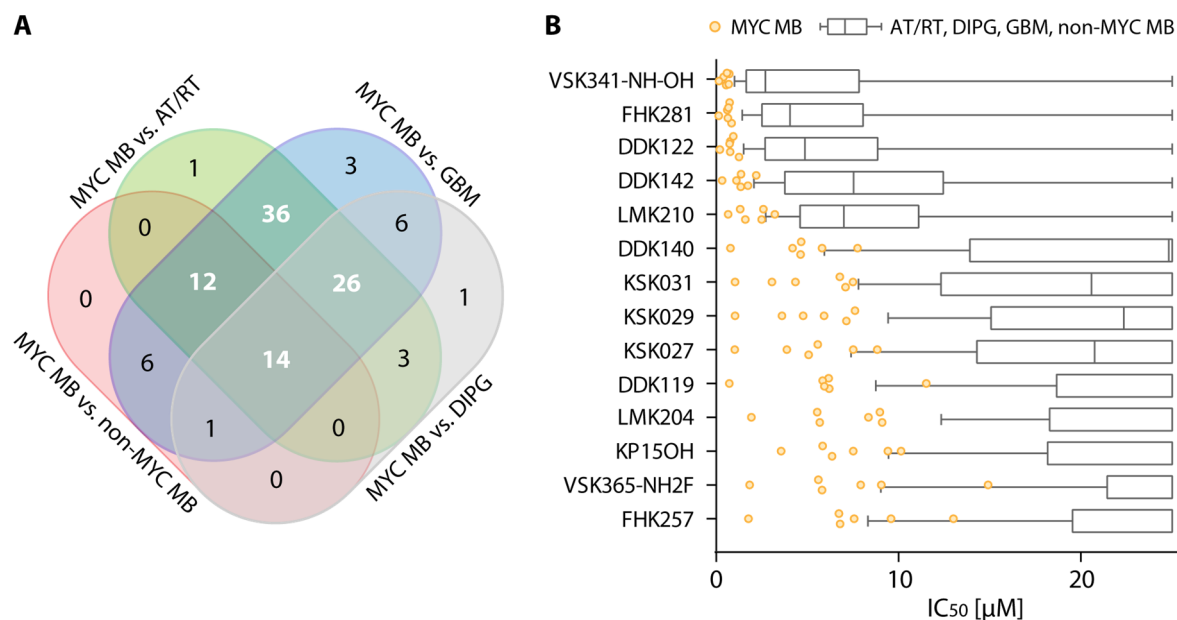
Figure 19. Identification of preferentially active inhibitors for *MYC*-driven medulloblastoma across the brain tumor entities. (A) Venn diagram depicting the overlap of significantly more active inhibitors for *MYC* MB from the individual entity comparisons with AT/RT, DIPG, GBM and non-*MYC* MB. Fourteen inhibitors were thereby identified as commonly more active in the *MYC* MB cells (B) Box plots representing the IC$_{50}$ distribution of the 14 inhibitors identified from the cross-entity comparison. The colored circles mark the respective IC$_{50}$ values for the six tested *MYC* MB cell lines and the boxplots show the median across AT/RT, DIPG, GBM and non-*MYC* MB cells together and the respective intequartile range with max/min whiskers.

The 14 identified inhibitors are mainly composed of hydroxamic acid based HDACi with one *o*-aminoanilide based inhibitor. Moreover, the group of preferential inhibitors consists of peptoid-based HDACi (Figure 20 A-B), terephthalic acid based inhibitors (Figure 20 C) and inhibitors with alkyl linker and differing linker groups (Figure 20 D). The compounds FHK257/281 and DDK119/122/140/142 are peptoid based inhibitors with a short benzylic linker and have already been evaluated for their HDAC inhibitory and cytotoxicity profiles. Their structures differ with regards to different functional groups at residues R[1] and R[2]. The two inhibitors VSK341-NH-OH and VSK365-NH2F are also HDACi with a peptoid-based cap group and an alkyl linker, that only differ with regards to their zinc chelating motif. The

study of Krieger *et. al* identified the hydroxamic acid VSK341-NH-OH as the most promising compound in their series of HDACi with potent inhibition of the class I HDAC1-3 and good inhibition of HDAC6.[163] In contrast but as expected, the *o*-aminoanilide based inhibitor VSK365-NH2F showed inhibition of HDAC1 but not of HDAC6.[172] Next, the three terephthalic acid based inhibitors KSK027/029/030 were so far only studied for their anti-plasmodial activity, but also showed inhibition of human HDAC1 and HDAC6 with moderate preference for the latter.[173] In our screening, the inhibitors exhibited a very similar inhibition profile, indicating that their shared linker structure and similar HDAC inhibition profile might be responsible for their activity. Lastly, the hydroxamic acids LMK204/210 and KP15OH share the same alkyl linker, but differ with regards to the connecting unit and cap group. LMK204/210 are derivatives of LMK235, that have been shown to inhibit class I and IIb HDACs with preference for HDAC6 and was able to reduce growth of urothelial carcinoma cells *in vitro*. The exerted effects on cell cycle and apoptosis induction were mainly attributed to the inhibition of class I HDACs. [164]

A

cmpd	R^1	R^2
FHK257	Ph	c-Hex
FHK281	3,5-Me-Ph	4-tolyl
DDK119	3,5-Me-Ph	t-Bu
DDK122	4-Me$_2$N-Ph	4-tolyl
DDK140	3,5-Me-Ph	n-Bu
DDK142	4-Me$_2$N-Ph	n-Bu

B

VSK341-NH-OH   VSK365-NH2F

C

cmpd	R^1
KSK027	Ph(CH$_2$)$_3$
KSK029	3,5-CH$_3$-PhCH$_2$
KSK031	1-naphthyl-CH$_2$

D

LMK204   KP15OH

LMK210

E

	IC$_{50}$ [μM]								
	MYC MB	non-MYC MB		AT/RT		DIPG		GBM	
VSK341-NH-OH	0.51	1.77	*	6.73	*	2.36	*	6.88	*
FHK281	0.61	2.11	*	8.33	**	7.46	*	4.49	**
DDK122	0.77	3.09	*	8.47	**	5.78	*	7.28	*
DDK142	1.34	4.70	*	10.91	**	6.59	*	13.26	**
LMK210	1.97	5.22	*	10.24	**	6.03	*	9.88	*
DDK140	4.63	16.55	*	20.26	***	19.74	*	22.36	***
KSK031	4.96	16.42	*	16.46	***	21.70	***	22.29	***
KSK029	5.01	15.64	*	19.41	***	21.75	***	21.81	***
KSK027	5.31	16.53	*	18.35	***	20.18	**	20.73	***
DDK119	6.06	20.04	**	21.59	***	19.36	*	23.80	***
LMK204	6.59	17.80	*	23.49	***	19.72	**	23.29	***
KP15OH	7.13	17.96	*	22.47	***	20.41	*	23.38	***
VSK365-NH2F	7.52	21.31	**	21.51	***	24.17	***	23.82	***
FHK257	7.57	19.99	*	21.27	***	19.15	*	24.37	***

Figure 20. Chemical structures and mean IC$_{50}$ values of selected inhibitors (A-D) Chemical structures of inhibitors identified as preferentially active in *MYC*-driven MB. (E) Mean IC$_{50}$ value of the selected inhibitors in the entities and corresponding significance for the comparison *MYC* MB *vs.* non-*MYC* MB, AT/RT, DIPG or GBM. *, p<0.05; **, p<0.01; ***, p<0.001 (unpaired *t*-test).

4.2.2 Evaluation of HDACi response in neuroblastoma cell lines

Besides brain tumor cell lines, we also evaluated the HDACi library in ten NB cell lines. Neuroblastoma is the most common extracranial solid tumor in children and amplification of MYCN is an established marker of negative prognosis, conferring high-risk disease.[174] MYCN belongs to the *MYC* family of transcription factors and is involved in the regulation of a variety of cellular functions like proliferation, cell growth and apoptosis. Aberrant expression or amplification therefore results, similarly to *MYC*, in oncogenic transformation.[175]

Due to the similar cellular functions of *MYC* and MYCN we were interested to see if MYCN amplification in NB confers a similar sensitivity pattern Therefore, we compared the response of MYCN NB with that of non-MYCN NB cells and obtained similar results as for the *MYC vs.* non-*MYC* comparison in MB. The MYCN-amplified cells NB showed a lower median IC_{50} of about 4.7 μM in comparison to 6.7 μM in the non-MYCN NB (Figure 21). Although this difference is significant, the fold change of 1.4 it is not as pronounced as in the MB cells, where the difference of the median IC_{50} exhibited a fold change of 2.1. In addition, when comparing both activity and significance of the individual inhibitor responses between the two groups, the HDACi are on average more active in the MYCN-amplified cells, however only two inhibitors passed our criteria for selective inhibitors (fold change>1.5 and p-value<0.05) (Figure 21). This is in strong contrast to the *MYC* MB vs non-*MYC* MB comparison where half of the inhibitors (n=111, 51%) were significantly more active in the *MYC*-amplified cells. These finding indicate that MYCN amplification in NB might be, unlike *MYC* amplification in MB, not the main factor that determines the response towards HDAC inhibition.
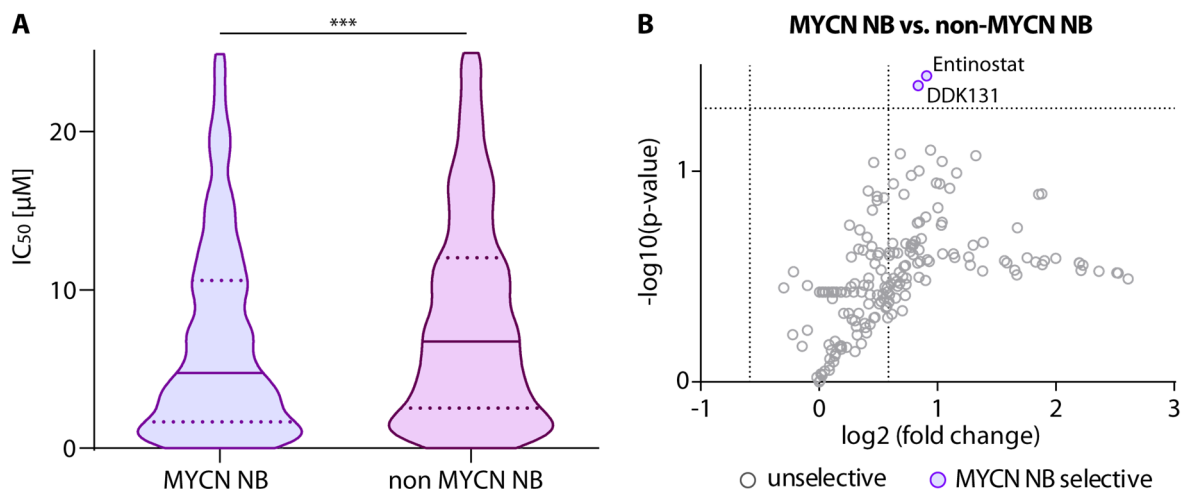
Figure 21. HDACi are significantly more active in MYCN NB compared to non-MYCN NB cell lines. (A) Violin plot depicting the IC_{50} distribution of all active HDACi (IC_{50}<25µM) of each cell line in the MYCN NB and non-MYCN NB group (MYCN NB: 804 out of 1095 IC_{50} values (73%); non-MYCN NB: 708 out of 1095 IC_{50} values (65%)). Bold lines mark the median IC_{50} value and the dashed lines the 25-75 percentile, respectively (MYCN NB: median 4.7 µM, 25-75 percentile 1.7-10.6 µM; non-MYCN MB: median 6.7 µM, 25-75 percentile 2.5-12.0 µM). (B) Volcano plot comparing the inhibitor response of MYCN amplified with non-amplified NB with regards to fold change and selectivity. ***, p<0.001 (unpaired *t*-test).

Finally, we also compared the inhibitor responses of MYCN amplified NB with *MYC* driven MB. Interestingly, this was the first entity comparison where *MYC* MB did not dominate the responsive inhibitors, but rather half of the inhibitors showed a more pronounced activity in MYCN NB. However, since both subgroups are very sensitive towards HDACi, we could only identify four and three inhibitors with significant activity in MYCN NB or *MYC* MB respectively (Figure 22).
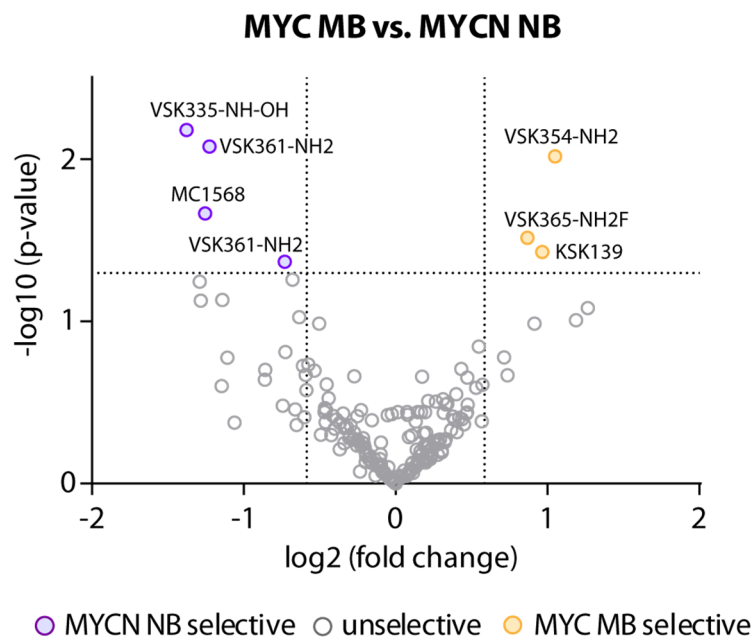
Figure 22. *MYC* MB and MYCN NB cell lines show comparable response patterns towards HDAC inhibition. The mean response across the *MYC* MB cells were compared with the MYCN NB cells. Thereby we could identify four and three preferentially active inhibitors for MYCN NB and *MYC* MB respectively.

4.2.3 Comparison of HDACi response with epigenetic inhibitor library

An additional comparison that underlines the strong rational to further investigate HDACi particularly in *MYC*-driven Group 3 MB was done by performing an additional screen with a library of epigenetic targeted inhibitors. This library is composed of inhibitors targeting a wide range of epigenetic modulators including epigenetic writers like DNA methyltransferases and Aurora kinases, epigenetic erasers like HDAC and histone lysine demethylases (KDMs) as well as epigenetic readers like BET bromodomain proteins and CREB binding proteins (CREBBP). This comprehensive library of 78 inhibitors was screened with a panel of MB, AT/RT and GBM cell lines to identify distinct response patterns. Out of the 78 inhibitors, 42 showed no response or only minor activity in a small number cell lines (Supplementary Figure 2). However, 32 inhibitors were more active in *MYC* MB measured by the fold change (Figure 23 A).
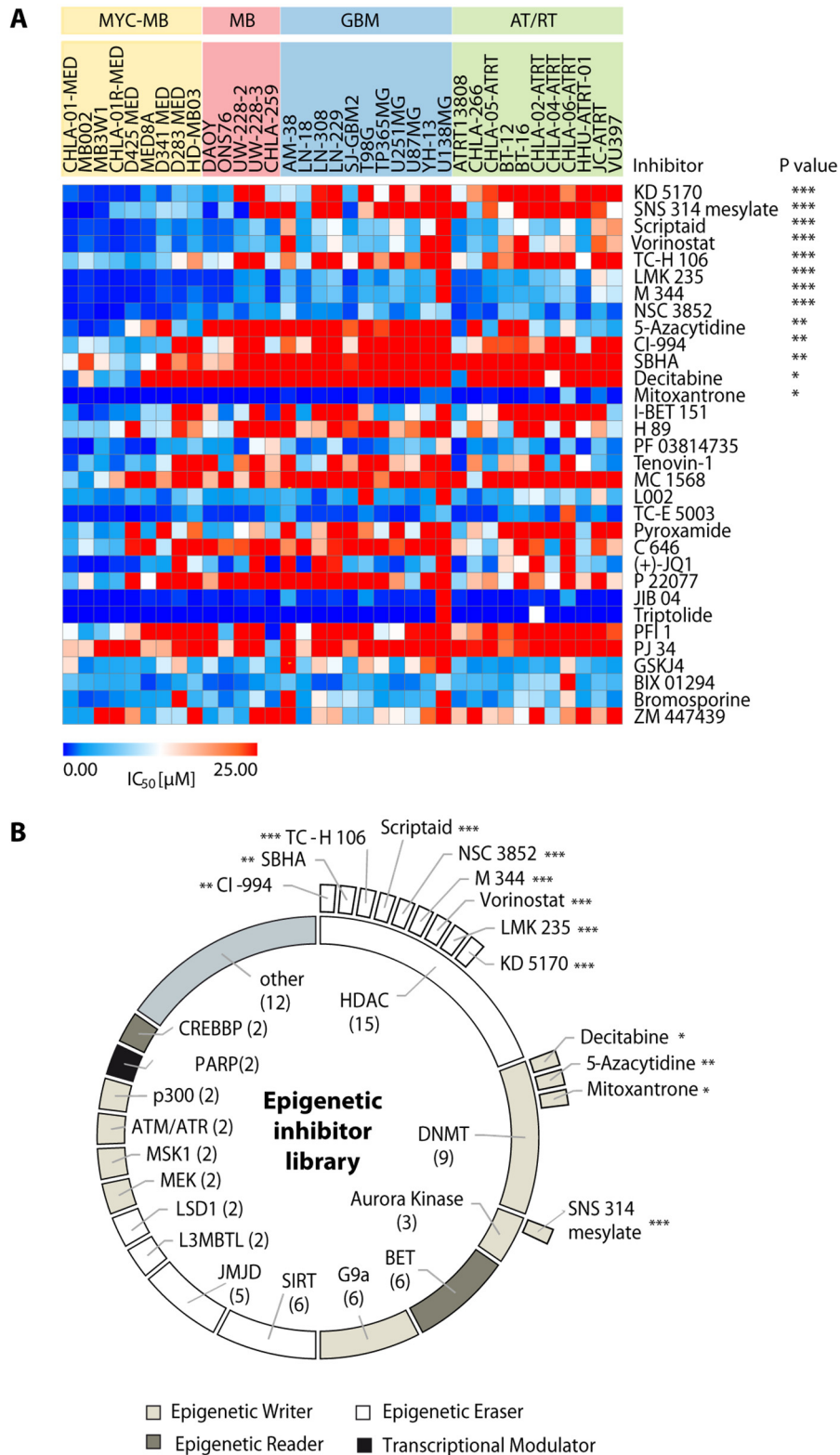
Figure 23. Confirmation of the high sensitivity of *MYC* MB towards HDAC inhibition in comparison to other epigenetic inhibitors. (A) Heatmap depicting the response profile of the 32 inhibitors with pronounced activity in *MYC* MB cells. (B) Composition of the epigenetic inhibitor library and labelling of the preferentially active inhibitors. *, p<0.05; **, p<0.01; ***, p<0.001 (unpaired *t*-test).

By comparing the mean response in *MYC* MB with the mean activity across the other tested cell lines, we could identify 13 inhibitors that were significantly more active in *MYC* MB. Among these significant inhibitors were three DNMT inhibitor and one Aurora kinase inhibitor, but the majority of the preferentially active compounds were HDACi (Figure 23 B) This finding further strengthen the observation, that *MYC*-driven MB are particularly sensitive to HDAC inhibition, even in comparison with other epigenetic inhibitors.

4.2.4 Response profile of extended inhibitor set

The initial HDACi library consisted of 218 compounds and was extended twice by 45 and 25 inhibitors (HDACi_V2 and HDACi_V3). However, these additional inhibitors were only tested with a subset of cell lines, more precisely with 10 cell lines (AT/RT=5, DIPG=5) in case of HDACi_V3 and 20 cell lines (NB=10, AT/RT=5, DIPG=5) for HDACi_V2 (Figure 24). Although these inhibitor were excluded from the analyses before, they nevertheless represent interesting compounds for further follow up studies.

The potent inhibitors LAK39 and LAK41 were in addition tested in three glioblastoma cell lines and assayed for their inhibition of HDAC1 and HDAC6. They exhibited an isoform profile comparable to vorinostat with a slight HDAC6 preference and increased cytotoxicity compared with vorinostat.[176] The β-peptoid-capped HDACi of the series NR4x were also further validated in neuroblastoma and glioblastoma cells and tested in a HDAC isoform assay. They were found to be non-selective compounds with high potency against HDAC1 and HDAC6 and showed strong antiproliferative effects in the tested cell line models.[161]

Figure 24. Inhibitor response profiles of extended HDACi libraries. The HDACi library was extended twice by 45 inhibitors (HDACi_V2) and 25 inhibitors (HDACi_V3) and screened with a subset of cell lines (NB=10, AT/RT=5, DIPG=5). For compounds that were inactive or showed only little reduction in cell viability, the highest tested concentration of 25 μM was used as a default value. Red therefore indicates inactivity while blue shows compounds with low μM to nM activity. The inhibitors were ranked according to their mean IC$_{50}$ value across all the tested cell lines.
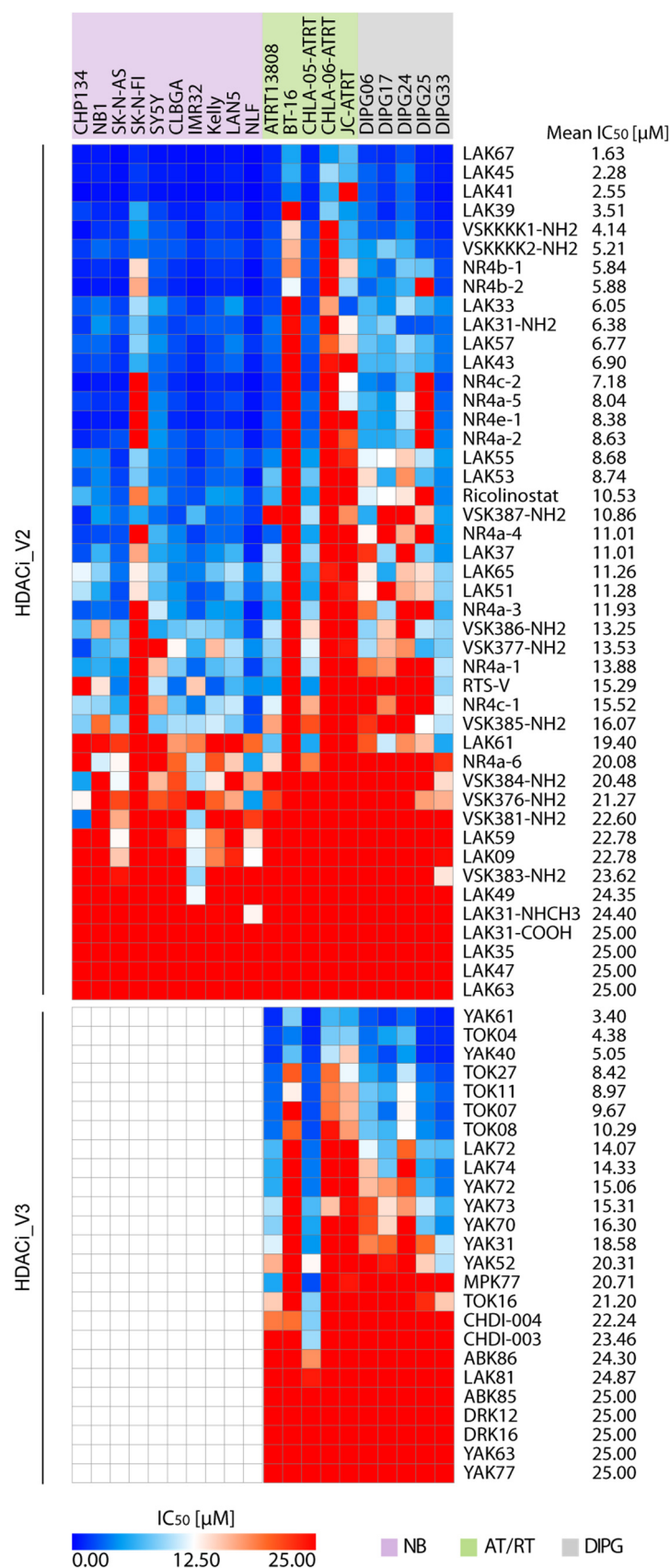
4.3 Selection of promising inhibitors and further evaluation

For a further, more detailed evaluation of a selected inhibitor and especially with regards to an *in vivo* application, we first chose to concentrate on the group of commercially available inhibitors. Among these, nine inhibitors were already evaluated in clinical trials with four inhibitors approved by the FDA for treatment of myeloma and lymphoma. These clinically tested and approved inhibitors likely have been optimized with regards to their pharmacokinetic profiles, have known toxicity and side effect profiles and have been characterized concerning their HDAC isoform profiles. In addition, based on the previously identified distinct responsiveness of *MYC* medulloblastoma towards HDAC inhibition, we focused particularly on the identification of an interesting drug candidate for this subgroup of brain tumors. Since the DIPG cell lines were screened at a later time point than the other entities, they are not included in the following analyses.

Unsupervised hierarchical clustering of the inhibitors divided the compounds into four groups. Since valproic acid, phenylbutyrate and MC 1568 failed to inhibit cell viability at the maximal concentration of 25 µM in any of the screened cell lines, they were omitted from the analysis. Like demonstrated before (Figure 15), the FDA-approved drugs vorinostat, panobinostat, romidepsin and belinostat showed substantial inhibition of cell viability across the tumor entities, with IC_{50} values in the low nM range for panobinostat and romidepsin. While the inhibitors tubastatin A, SBHA, PCI 34051 and TCS HDAC6 20b showed only minor activity in a few cell lines, the four inhibitors CI-994, TC-H 106, KD 5170 and Pyroxamide showed considerably lower IC_{50} values in the *MYC* medulloblastoma cells as compared to the other tested entities. Having a closer look at the inhibitors, we again compared the mean response of each inhibitor across the *MYC* medulloblastoma cell lines with the mean activity in non-*MYC* medulloblastoma, glioblastoma and AT/RT. Notably, again none of the HDACi were preferentially active in non-*MYC* medulloblastoma, glioblastoma or AT/RT cell lines in our *in vitro* screen. In contrast, 13 of the total 20 HDACi were identified as preferentially active in *MYC*-driven medulloblastoma (65%) as compared to the other brain tumor models, namely the inhibitors CI-994, KD5170, TC-H 106,

entinostat, LMK235, scriptaid, M344, vorinostat, pyroxamide, belinostat, SBHA, NSC 3852 and panobinostat (Figure 25). Notably, three HDAC 1-3 selective inhibitors (CI-994, TC-H 106 and entinostat) were among the top five most preferentially active inhibitors in *MYC*-driven medulloblastoma.
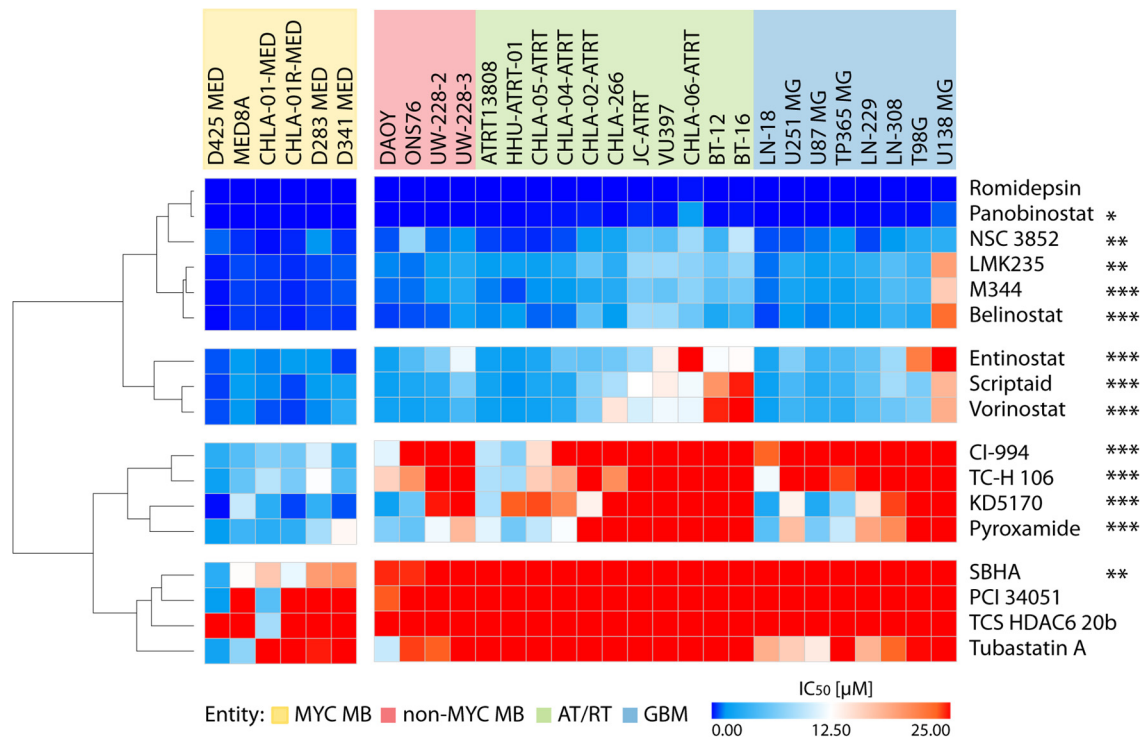
Figure 25. HDACi screen identifies preferentially active inhibitors for *MYC*-driven medulloblastoma. Heatmap representing the unsupervised clustering of 20 selected, commercially available HDACi based on their response in 29 brain tumor cell lines derived from *MYC* MB, non-*MYC* MB, AT/RT and GBM. *; p<0.05; **, p<0.01; ***, p<0.001 (unpaired *t*-test).

To select a candidate drug for further evaluation, we compared the overlap of preferentially active inhibitors that were identified in the *MYC* medulloblastoma *versus* non-*MYC* medulloblastoma, glioblastoma and AT/RT comparison respectively. Thereby we could identify three inhibitors that showed preferential activity in each comparison (Figure 26 A). Amongst the overlapping HDACi, the HDAC1-3 selective inhibitor CI-994 showed the most significant reduction of cell viability in *MYC*-driven MB (p=1.34·10^{-8}, fold-change 3.6, Figure 25 B). While CI-994 exhibited a mean IC_{50} of 5.97 μM in the *MYC*-driven medulloblastoma cell lines, the maximal inhibitor concentration of 25 μM induced on average less than 50% cell viability reduction in any of the other brain tumor entities (p<0.001,Figure 26 C).
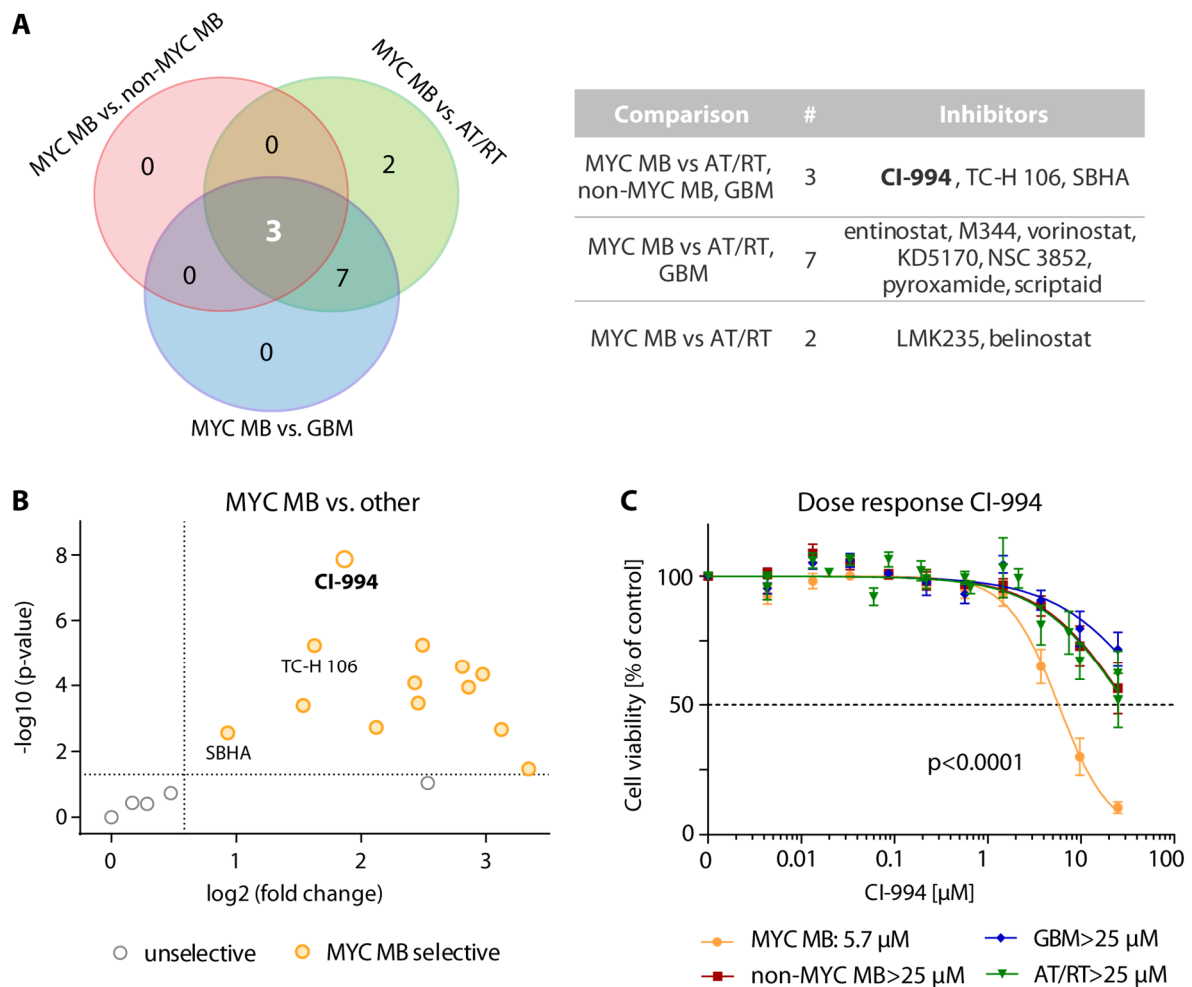
Figure 26. Selection of CI-994 for further validation. (A) Overlap of the significantly more active inhibitors in *MYC* MB in comparison to non-*MYC* MB, AT/RT and GBM. The inhibitor CI-994, TC-H 106 and SBHA were significant in each comparison. (B) CI-994 was identified as the most significantly active inhibitor in the comparison of *MYC* MB cell lines against the other tested cells (non-*MYC* MB, AT/RT and GBM). (C) Mean CI-994 dose-response curves for each entity or subgroup. CI-994 showed a mean IC_{50} of 5.7 µM for the six *MYC*-medulloblastoma cell lines, whereas in the other entities the highest concentration induced on average less than 50% reduction in cell viability.

In a validation screen of CI-994 with an extended concentration range of up to 50 µM, we verified the preferential activity of CI-994 in *MYC*-driven MB versus the other brain tumor entities as demonstrated by significantly lower IC_{50} values (Figure 27). In conclusion, our data indicate that CI-994 preferentially inhibits cell viability of *MYC*-driven MB *in vitro*.
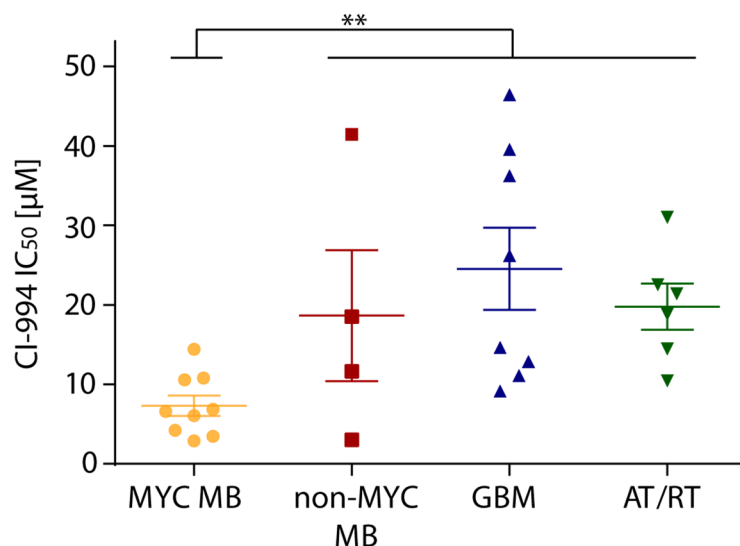
Figure 27. Validation of CI-994 activity. CI-994 was re-tested with an increased concentration range of up to 50 μM. The initial discovery cell line cohort was supplemented by three additional models of *MYC*-driven MB (cell lines), confirming the highly preferential response of CI-994 in *MYC*-driven medulloblastoma. Values shown represent mean ± SEM. **, $p < 0.01$ (Kruskal-Wallis test).

4.3.1 *In vitro* characterization of the selected HDACi CI-994

To elucidate the antitumoral effect of CI-994 in *MYC*-driven MB, we next determined the induction of apoptosis following treatment in two well-characterized *MYC*-amplified MB models, namely D425 MED and MED8A. To assess the induction of apoptosis, the cells were treated with 5 or 7.5 μM of CI-994 for 48 h, stained with annexin V and propidium iodide (PI) and subsequently analyzed by flow cytometry. We observed a significant increase in annexin V- and PI-positive cells in both cell lines upon inhibitor treatment at 7.5 μM ($p < 0.01$, Figure 28), indicating that induction of apoptosis contributes to the antitumoral activity of CI-994 as previously described in other entities.
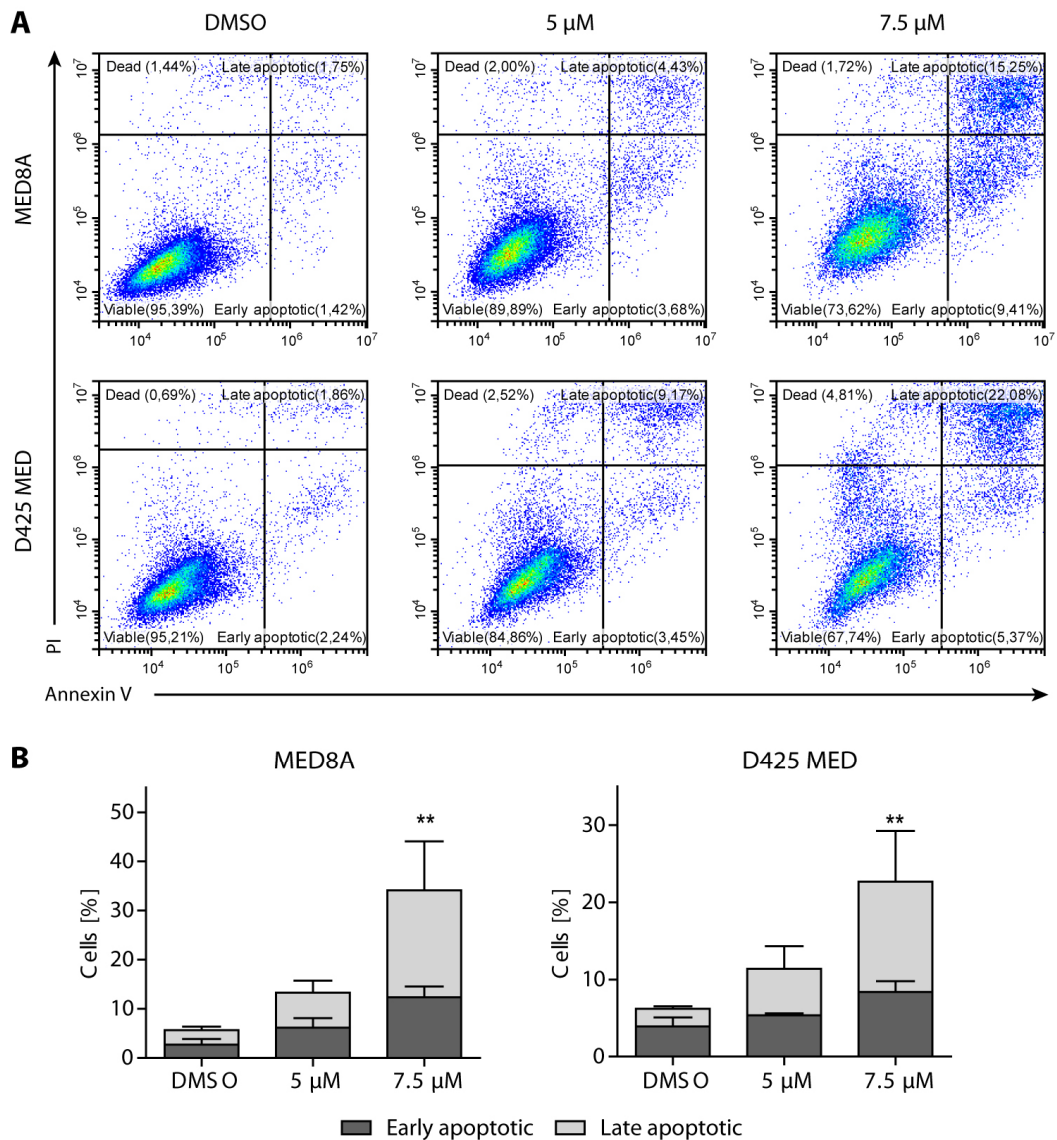
Figure 28. Induction of apoptosis following CI-994 treatment. (A) Representative FACS plots for MED8A and D425 MED cells treated for 48 h with 5 or 7.5 µM CI-994 or DMSO (0.1%) as a control. Cells were stained with PI and Annexin V FITC to assess cells undergoing apoptosis. (B) Bar graphs representing the proportion of cells in the stage of early or late apoptosis. Values shown represent mean ± SD of 3 replicates per condition. **, $p < 0.01$ (Dunn's Multiple Comparison Test).

Since CI-994 exhibited preferential activity against *MYC*-driven MB cells, we examined the impact of CI-994 treatment on *MYC* expression levels in D425 MED and MED8A. Notably, treatment with CI-994 significantly decreased *MYC* mRNA and protein levels in these two models ($p < 0.05$ for each comparison, Figure 29), suggesting that the antitumoral effect of the class I specific HDACi CI-994 is partly mediated by transcriptional repression of *MYC*.
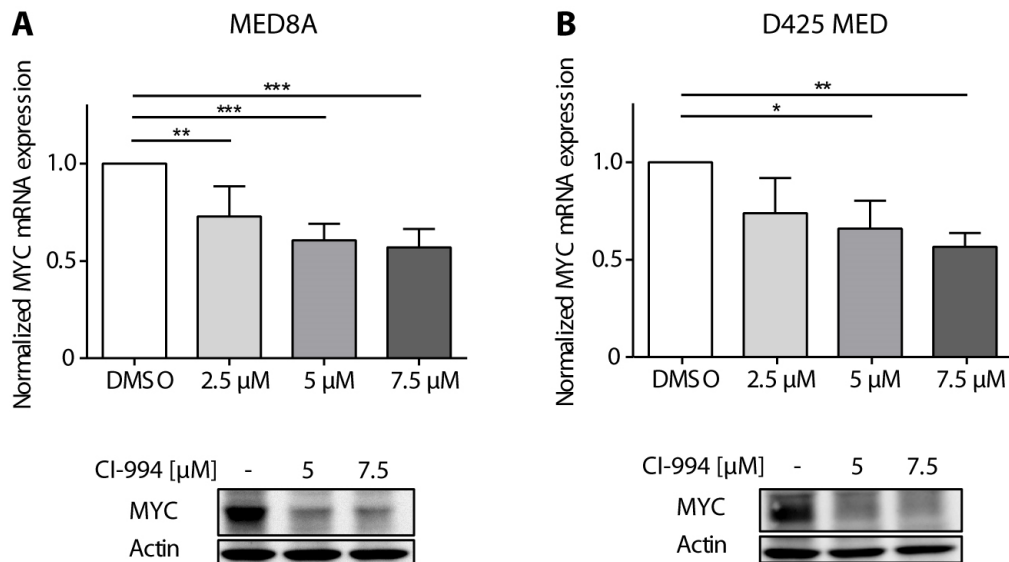
Figure 29. *MYC* expression is reduced following CI-994. (A) MED8A and D425 MED cells were treated with 2.5, 5 or 7.5 μM CI-994 or DMSO as a control for 48 h. *MYC* mRNA expression was normalized to housekeeping controls and calculated relative to DMSO control. Protein expression was evaluated after 48 h by immunoblotting with actin as control protein. (B) UW-228-3 cells with low endogenous expression of *MYC* were lentivirally transduced to overexpress *MYC*. Compared to the isogenic control cells, the overexpression cells (UW-228-3 *MYC* OE) were more sensitive towards CI-994 treatment. *; p<0.05; **, p<0.01; ***, p<0.001 (Dunn's Multiple Comparison Test).

To further investigate the relationship between sensitivity towards CI-994 and *MYC* expression levels, we performed lentiviral-based *MYC* overexpression in UW-228-3, a medulloblastoma cell line model without *MYC* amplification and low endogenous *MYC* levels. Treatment with CI-994 for 72 h resulted in a two-fold decrease in IC_{50} value of the *MYC* overexpressing cell line compared to the isogenic control (p<0.0001, Figure 30). Thus, our results indicate that the high activity of CI-994 in MB is in part *MYC*-dependent, further suggesting that aberrant *MYC* activation particularly in group 3 MB may comprise a predictive biomarker for the response to CI-994.

Based on previous findings that class I HDACs are overexpressed in group 3 MB,[81] the inhibition of this subset of HDACs has already been suggested to account for the antitumoral activity of pan HDACi in *MYC*-driven MB.[80] Therefore, with regards to our data and considering a potential reduction of unwanted side effects, we argue that class I selective HDACi should be considered over pan-HDACi and that future trial cohorts may incorporate *MYC* status as a predictive biomarker.
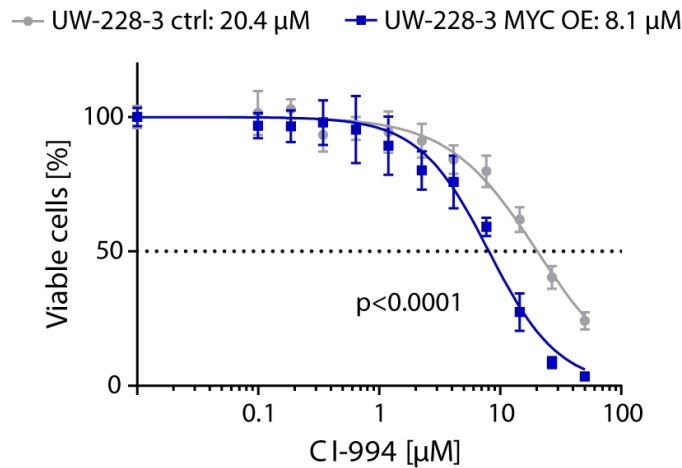
Figure 30. Sensitivity towards CI-994 is dependent on *MYC* expression level. Lentiviral based *MYC* overexpression in UW-228-3 (UW-228-3 *MYC* OE) led to significantly increased sensitivity towards CI-994 treatment as compared to the isogenic control with low endogenous *MYC* expression (UW-228-3 ctrl).

4.3.2 Evaluation of antitumoral activity of CI-994 *in vivo*

Considering the potent inhibitory effect of CI-994 *in vitro*, we next tested its efficacy in two orthotopic xenograft mouse models of *MYC*-driven MB *in vivo*. D425 MED and MED8A cells expressing GFP and luciferase were orthotopically injected into the cerebella of NSG (NOD scid gamma) mice. Tumor engraftment was detected by bioluminescence imaging (BLI) after seven days. Subsequently, tumor bearing mice were randomized to daily treatment with either vehicle control or CI-994 (30 mg/kg, p.o.) (Figure 31).
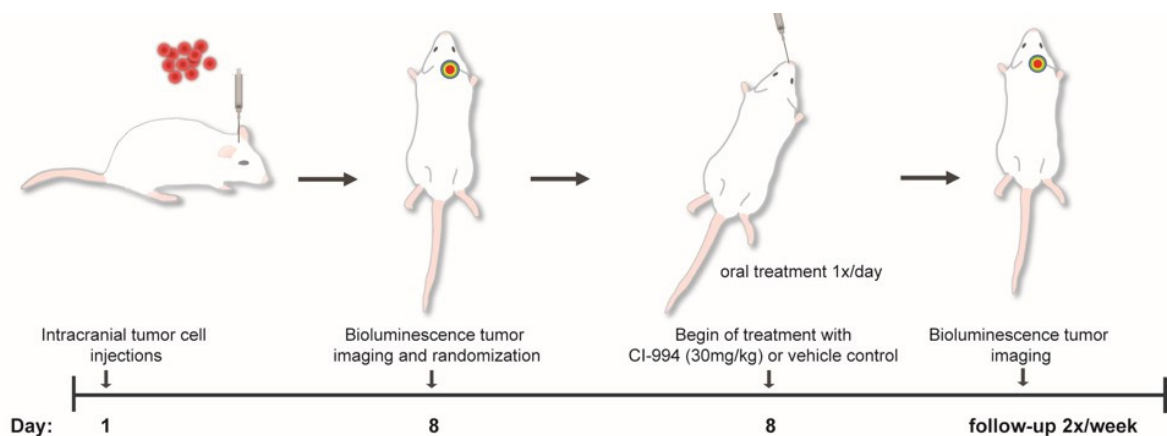
Figure 31. Treatment timeline for *in vivo* evaluation of CI-994. The *MYC*-amplified cell lines MED8A and D425 MED (expressing GFP and luciferase) were orthotopically injected and tumor engraftment was followed by bioluminescence imaging. Tumor bearing mice were randomized and received either CI-994 (30 mg/kg, p.o.) or vehicle daily.

Treatment with CI-994 significantly decreased tumor growth in both mouse models (Figure 32 A/B). In addition to the reduced tumor growth at the primary site, we detected a significant reduction of spinal dissemination in the CI-994 treatment group in both *MYC*-driven models (both models p<0.01, Figure 32 D). After tumor engraftment, control mice exhibited a median survival of 34 and 15 days for MED8A and D425 MED respectively. CI-994 treatment resulted in a significantly prolonged median survival of 41 days for MED8A (p=0.0026, Figure 32D) and 23 days for D425 MED (p=0.01, Figure 32 D). Thus, our data demonstrate antitumoral activity of CI-994 against the primary site, and, importantly, against the metastatic compartment of *MYC*-driven medulloblastoma *in vivo*. As metastatic recurrences are predominantly observed in group 3 medulloblastoma and effective therapeutic strategies are lacking, identification of a novel therapeutic agent targeting the metastatic compartment is particularly relevant.
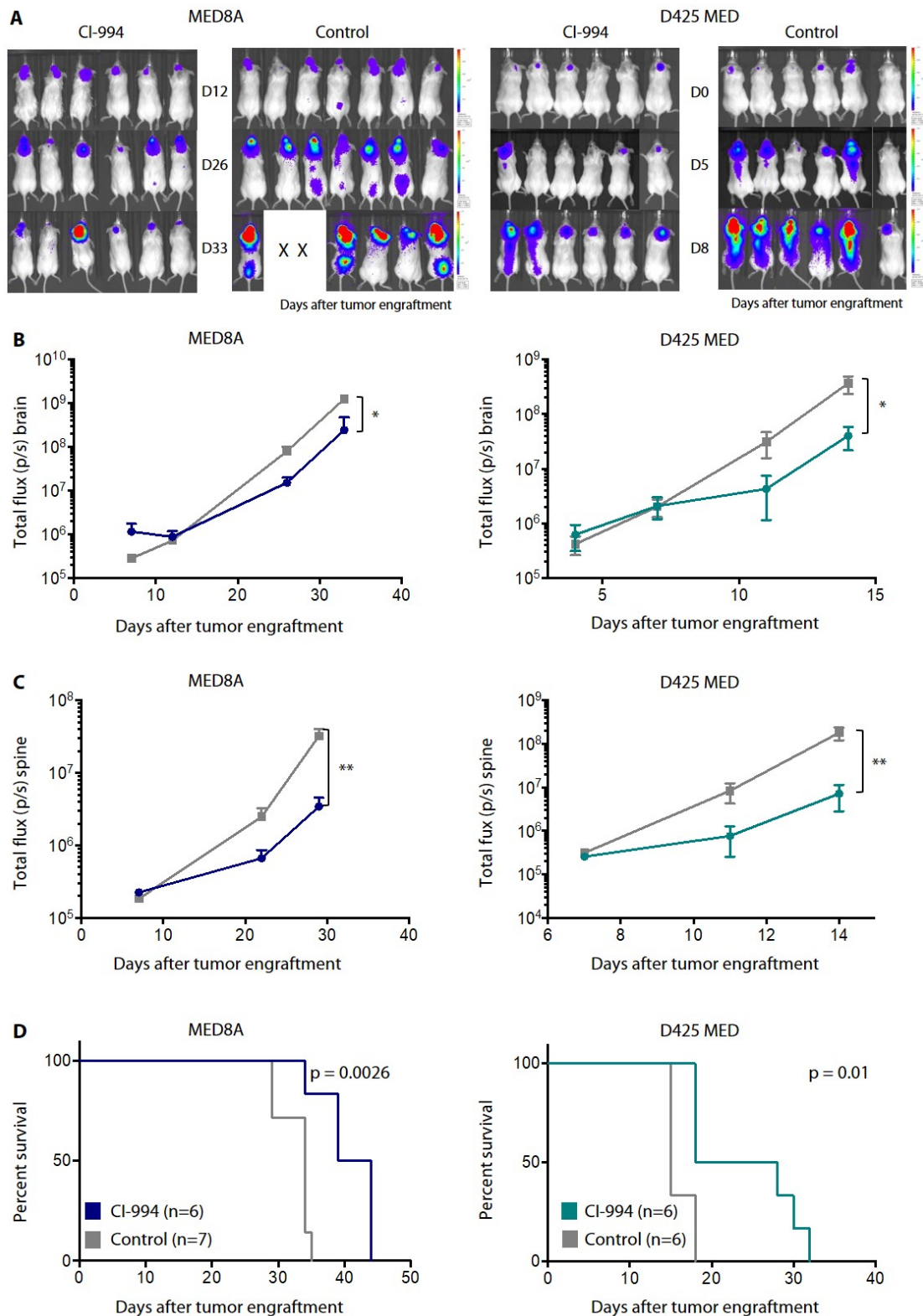
Figure 32. CI-994 treatment reduced tumor growth and formation of spinal metastases. (A) Bioluminescence imaging of MED8A and D425 MED xenografts. (B/C) Bioluminescence quantification of CI-994 treated and control mice. CI-994 treatment significantly inhibited tumor growth and reduced leptomeningeal dissemination in MED8A and D425 MED xenografts. (D) CI-994 treatment significantly increased median survival of MED8A and D425 MED xenografts from 34 days to 41 days and 15 days to 23 days, respectively. *, p<0.05; **, p<0.01.

4.3.3   Screen for synergistic drug combinations with CI-994

Since the administration of CI-994 as a single agent in *MYC*-driven MB resulted in a significant temporary, but not permanent treatment response, we next searched for compounds that would enhance the antitumoral activity of CI-994. For this purpose, we performed a synergism screen (as described in 4.1.2) using a customized clinical inhibitor library of 199 compounds that are either already approved as chemotherapeutics or are evaluated in clinical phase III/IV (Table 9). Compounds in this library effect a wide range of biological targets and signaling pathways, including inhibitors of proteasome, Bcl2-family, BET family, various receptors (EGFR, PDGFR, VEGFR) and kinases (CDK, PI3K, MEK , JAK, mTOR), thereby covering many cancer relevant targets. Besides these targeted agents, clinically well-established alkylating agents (like lomustine and melphalan), microtubuli inhibitors (like vincristine and paclitaxel) as well as platin based agents (cisplatin, carboplatin and oxaliplatin) and nucleoside analogues (like gemcitabine and cytarabine) are included.

The clinical compounds were screened as described above with eight different concentrations ranging from 0.005 – 25 µM in D425 MED and MED8A. Both models were also tested using the same clinical library setup, with the respective IC_{10} and IC_{25} concentrations of CI-994 (1.66/2.73 µM for MED8A and 1.45/2.10 µM for D425 MED) dispensed into each of the wells in addition. After 72 h of incubation, luminescent signals were detected as described before. To assess the additional decrease in cell viability due to synergistic interaction of CI-994 with each of the inhibitors, the cell viability was calculated relative to wells with CI-994 alone. With this approach additive or synergistic effects can be nicely visualized by overlaying the single agent dose response curve with the combination curve. For additive effects, the resulting combination curve will overlap with the single agent curve, synergistic effects however will lead to shift of the combination curve to lower IC_{50} values.

With this approach, we could identify 54 inhibitors for MED8A and 61 inhibitors for D425 MED that showed a decrease of the respective IC_{50} of at least 1.25 fold when tested in

combination with either IC_{10} or IC_{25} of CI-944. In both cell lines, a total of 17 clinical inhibitors showed a consistent shift indicating potential synergism for both the IC_{10} and IC_{25} concentrations (Figure 33).

Figure 33: Screen for synergistic interaction identified several favorable drug combinations with CI-994. (A) CI-994 was dispensed with the respective IC_{10} and IC_{25} concentrations for MED8A (1.66 and 2.73 µM) and D425 MED (1.45 and 2.10 µM) onto pre-printed clinical library plates with serial dilutions of 199 inhibitors in clinical use or evaluation. Signals of these combination plates were normalized to wells containing only IC_{10} or IC_{25} concentrations of CI-994. IC_{50} values were the compared to control plates of the clinical library without the additional CI-994 concentrations. By this approach 54 and 61 beneficial drug combinations (1.25 fold change in IC50) could be identified for MED8A and D425 MED, respectively. (B) Venn diagram depicting the overlap between the two cell lines and each condition, with 17 inhibitors commonly interacting synergistically with CI-994. (C) Six inhibitors were validated in seven *MYC* MB cell lines with a 6x6 concentration matrix. Bliss synergy scores were calculated and summed across the concentrations. Positive Bliss scores indicate synergistic interaction and negative values antagonism.

We identified several previously reported synergistic interactions for other HDACi in MB, including combinations with decitabine, doxorubicin and etoposide. In addition, we

observed CI-994-specific synergies, which have been reported in other cancer entities, including interactions with cytarabine, daunorubicine and mitoxantrone, as well as retinoic acid. Notably, several novel synergistic drug interactions with HDACi were identified for MB, including combinations with the proteasome inhibitors bortezomib and ixazomib, the EZH2 inhibitor GSK126 and the NFκB pathway inhibitor bardoxolone methyl.

Using a targeted validation approach we validated a synergistic interaction of CI-994 in five of the six evaluated drug combinations, namely bortezomib, decitabine, ixazomib, GSK126, and bardoxolone methyl, as measured by calculating Bliss Synergy scores (Figure 33 C). These results highlight specific compounds that can improve CI-994 efficacy against *MYC*-driven medulloblastoma *in vitro*.

4.3.4 Assessment of transcriptional changes following CI-994 treatment

To prioritize drug combinations to enhance CI-994 activity, we next aimed to elucidate the biological pathways driving resistance to CI-994 treatment. Global transcriptional perturbations induced by CI-994 treatment were determined using RNA sequencing. For this, the *MYC*-driven MB cell lines MED8A, D425 MED and D341 MED were treated with the respective IC_{50} concentrations of CI-994 or DMSO (0.1%) for 48 h

Treatment with CI-994 resulted in global gene expression changes in comparison to the DMSO treated control samples. Specifically, we identified 173 genes as differentially expressed in CI-994 versus DMSO-treated cells using a minimal fold-change ±2 and p≤0.05 as a cut-off. To elucidate canonical pathways and upstream regulators controlled by CI-994 treatment, we performed IPA on the differentially expressed gene sets. Among the canonical pathways and upstream regulators significantly dysregulated following CI-994 treatment, NFκB (nuclear factor kappa-light-chain-enhancer of activated B cells) pathway activation was consistently identified (Figure 34 A/B)

Moreover, 26 of 45 canonical pathways (58%) are functionally linked to NFκB pathway activity. This result further corroborates our finding that the NFκB pathway inhibitor bardoxolone methyl enhanced CI-994 efficacy in *MYC*-driven medulloblastoma models

(Figure 33), reinforcing the importance of this pathway in mediating resistance to CI-994. Furthermore, differentially expressed NFκB pathway genes were sufficient to subdivide all models into treatment groups using unsupervised hierarchical clustering (Figure 34 D). *TGM2* (transglutaminase 2) was the most upregulated gene in our analysis (fold-change 17.5, p<0.05, Figure 34 C).

A

Ingenuity Canonical Pathways	p value	Activation z-score
Rac Signaling	1.55E -04	2.449
Agrin Interactions at Neuromuscular Junction	1.10E -04	2.236
Estrogen -Dependent Breast Cancer Signaling	1.86E -04	2.236
JAK/Stat Signaling	2.63E -04	2.236
LPS -stimulated MAPK Signaling	3.31E -04	2.236
NF -κB Activation by Viruses	3.31E -04	2.236
RANK Signaling in Osteoclasts	6.76E -04	2.236
HGF Signaling	1.17E -03	2.236
Renin -Angiotensin Signaling	1.51E -03	2.236
IL-6 Signaling	1.86E -03	2.236
Gα12/13 Signaling	2.09E -03	2.236
HMGB1 Signaling	2.24E -03	2.236
PKC θ Signaling in T Lymphocytes	2.24E -03	2.236
P2Y Purigenic Receptor Signaling Pathway	2.24E -03	2.236
Integrin Signaling	3.98E -03	2.236
Colorectal Cancer Metastasis Signaling	7.24E -03	2.236
NF -κB Signaling	8.13E -03	2.236
B Cell Receptor Signaling	1.00E -02	2.236
Signaling by Rho Family GTPases	2.82E -02	2.236
ErbB2 -ErbB3 Signaling	1.10E -04	2.000

B

Upstream Regulator	Molecule Type	Activation z-score	p-value of overlap
TLR4	transmembrane receptor	2.200	0.0137
SMARCA4	transcription regulator	2.200	0.0263
F2	peptidase	2.176	0.0345
IFNA2	cytokine	2.172	0.0060
NFkB (complex)	complex	2.155	0.0109
MET	kinase	1.982	0.0054
CTNNB1	transcription regulator	1.981	0.0289
CXCL12	cytokine	1.951	0.0467
TGFB1	growth factor	1.834	0.0003
IFNG	cytokine	1.811	0.0019

C

ID	Prediction (based on measurement direction)	Expr Fold Change	Expected expression upon NFκB activation
TGM2	Activated	17.482	Upregulates
CLIP2	Activated	11.135	Upregulates
PLK2	Activated	4.455	Upregulates
RRAS	Affected	4.095	Regulates
JUN	Activated	2.871	Upregulates
PPARA	Activated	2.844	Upregulates
MSX2	Activated	2.272	Upregulates
NFKB2	Activated	2.172	Upregulates
ODC1	Inhibited	-2.132	Upregulates
HDGF	Affected	-2.530	Regulates

D

Figure 34. Expression of NFκB pathway genes is induced following CI-994 treatment. MED8A, D425 MED and D341 MED were treated either with IC_{50} concentrations of CI-994 or vehicle control and analyzed by RNA sequencing. Non-parametric supervised analysis identified 130 upregulated and 43 downregulated genes with a fold change ±2 and p≤0.05. The differentially regulated genes were analyzed by Ingenuity Pathway Analysis (IPA).Unsupervised hierarchical clustering of genes regulated by the NFκB complex.

We next confirmed the significant CI-994-mediated up-regulation of *TGM2* mRNA and protein levels in our two validation cell models D425 MED and MED8A cells (p<0.05 for each comparison, Figure 35)
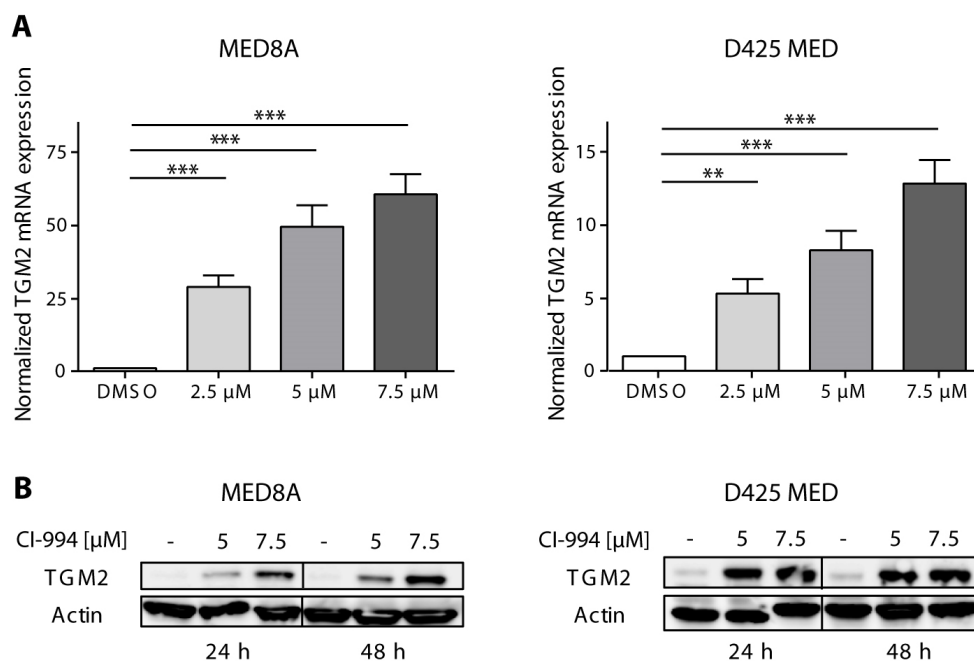
Figure 35. CI-994 treatment induces TMG2 expression. MED8A and D425 MED cells were treated with 2.5, 5 or 7.5 µM of CI-994 for 48 hours. (A) *TGM2* mRNA expression values are normalized to housekeeping controls and expression is calculated relative to DMSO control. (B) Representative western blot images for TGM2 and Actin as a loading control following CI-994 treatment for 24 and 48 hours. Values shown represent mean ± SD of three replicates per condition. *, p<0.05; **, p<0.01; ***, p<0.001 (Dunn's Multiple Comparison Test).

4.3.5 Evaluation of the synergistic drug combination with bardoxolone methyl

Given that CI-994 treated cells activate the NFκB pathway and that we independently identified the NFκB inhibitor bardoxolone methyl in our CI-994 synergism screen, we further examined this drug combination. We performed a more detailed synergism evaluation of bardoxolone methyl with CI-994 in MED8A and D425 MED using a 12x12 concentration matrix. This yielded highly synergistic interactions at multiple concentration combinations, as measured with Bliss synergy scores (Figure 36 A). Positive Bliss scores in blue indicate combinations where the effect is greater than expected based on sole additive effects of both drugs together.

Moreover, the addition of 0.60 µM or 0.25 µM of bardoxolone resulted in a dose reduction of CI-994 IC_{50} by 3 and 1.7 fold for MED8A and D425 MED, respectively (Figure 36 B/ C). A 4.7 and 4 fold IC_{50} reduction was achieved in the same manner by supplementing

bardoxolone methyl with 6 µM CI-994 in MED8A and D425 MED, respectively (Figure 36 B and C).
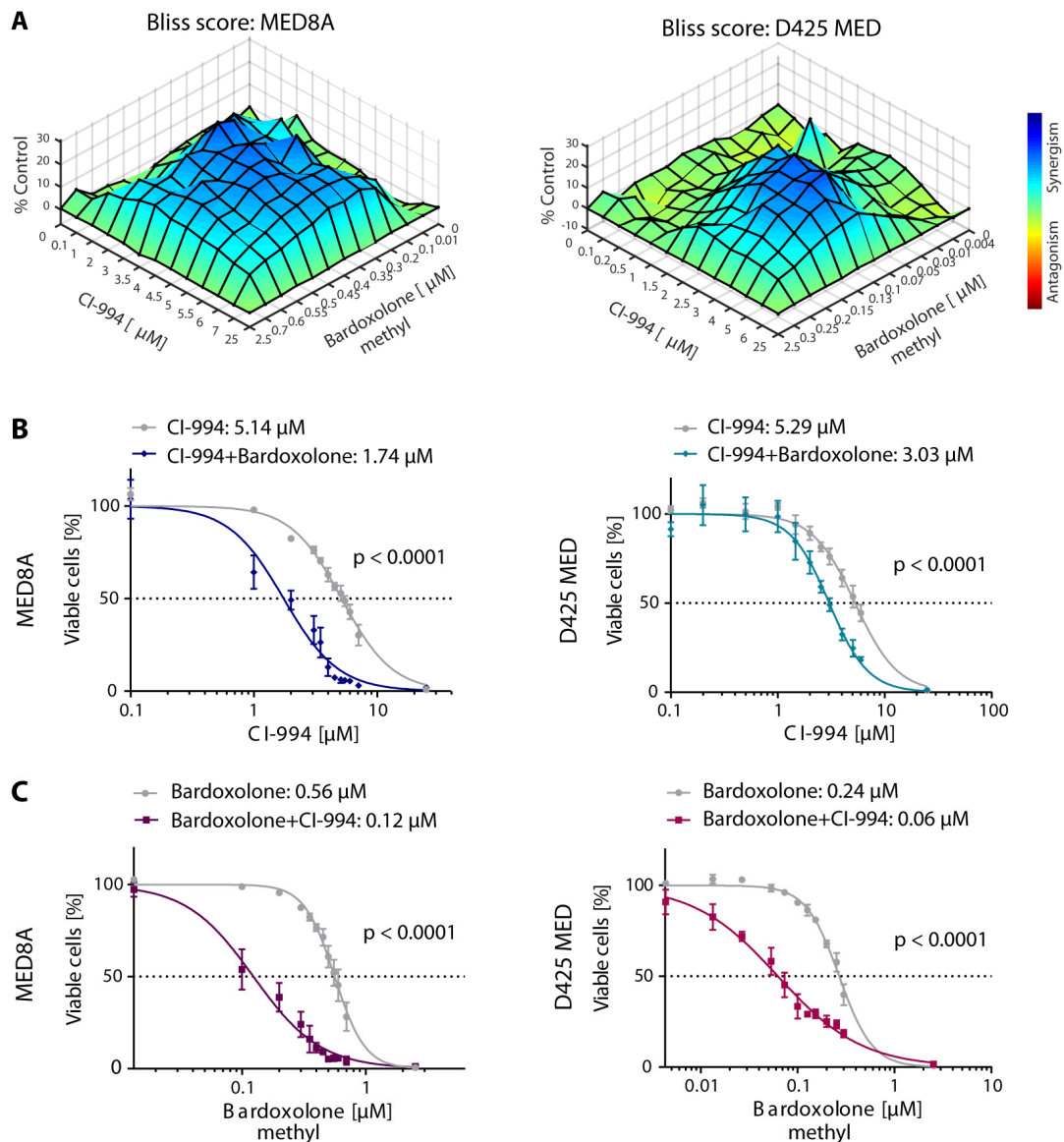
Figure 36. CI-994 synergizes with bardoxolone methyl to reduce cell viability of *MYC*-driven medulloblastoma cells. (A) CI-994 and bardoxolone methyl were tested in an extended 12x12 concentration matrices and analyzed using Bliss synergy score calculated by the Combenefit software. Blue color indicates synergistic drug combination. (B/C) Mean dose-response curves of CI-994 (alone and in combination with bardoxolone methyl) and bardoxolone methyl (alone and in combination with CI-994) showing the maximal IC_{50} shift for MED8A and D425 MED cells. Values shown represent mean ± SEM of four replicates per condition.

Moreover, we evaluated the effect of the combination treatment in two additional patient-derived *MYC*-driven (HDMB03 and MB002) and two non *MYC*-driven medulloblastoma (UW228-2 and ONS76) cell lines using the extended concentration matrix. While the two

MYC-driven cell lines confirmed the high sensitivity of *MYC* medulloblastoma for the combination treatment, we could detect no synergistic interaction across the broad concentration range in the non *MYC*-driven medulloblastoma cell lines (Figure 37).
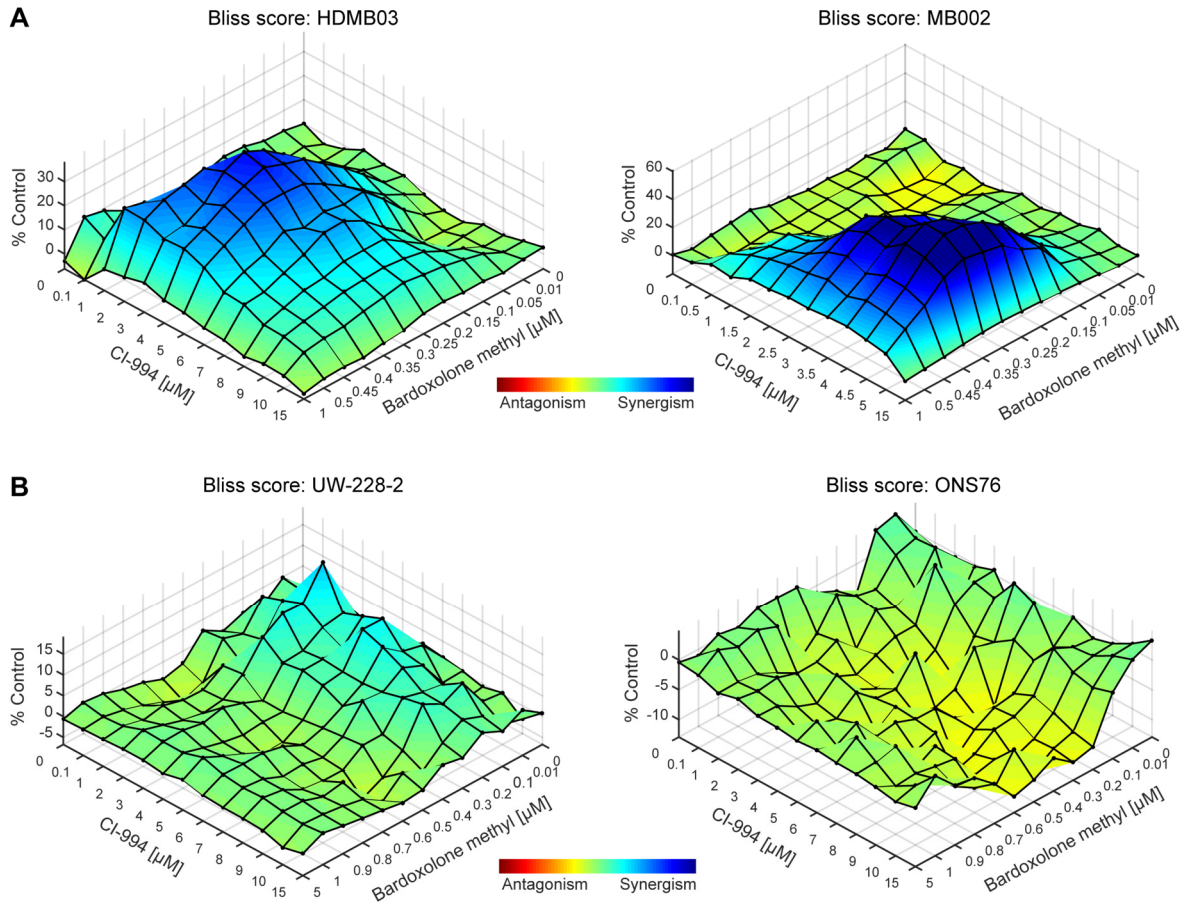
Figure 37 Synergism is observed in two additional *MYC*-driven MB models but not in non-*MYC* MB cells. CI-994 and bardoxolone methyl were tested in an extended 12x12 concentration matrices and results were analyzed using Bliss synergy score calculated by the Combenefit software. (A) Distribution of Bliss scores across concentration matrix in the *MYC*-driven MB cell lines HDMB03 and MB002, indicating synergistic interaction of the drug combination. (B) Combination of CI-994 with bardoxolone methyl in the two non-*MYC* MB cells UW-228-2 and ONS76 is not synergistic.

Next, we explored the impact of the CI-994 and bardoxolone methyl combination on NFκB activity to further validate the functional relevance of the NFκB pathway following CI-994 treatment. To this aim, we determined NFκB pathway activity directly using a luciferase based reporter assay. Stable expression of the NFκB reporter construct (pHAGE NF-κB-TA-LUCUBC-GFP-W), consisting of the NFκB consensus sequence upstream of the minimal promoter of the herpes simplex virus followed by the firefly luciferase reporter gene as well as the green fluorescent protein (GFP) reporter, were achieved by lentiviral transduction.[156]

This allows for the assessment of NFκB activation after treatment by measuring the luciferase expression levels.

For the evaluation of the pathway activity, we first treated the MED8A and D425 NFκB reporter cells with TNFα (tumor necrosis factor) as a positive control. TNFα is a proinflammatory cytokine with multiple functions belonging to the tumor necrosis factor (TNF) superfamily. The NFκB pathway can be activated through different intra- and extra-cellular stimuli including cytokines like TNFα. Treatment of the MED8A and D425 NFκB reporter cells with TNFα (1 ng/mL) resulted in a high induction of the NFκB pathway as measured with ONE-Glo Luciferase Assay System (Figure 38).
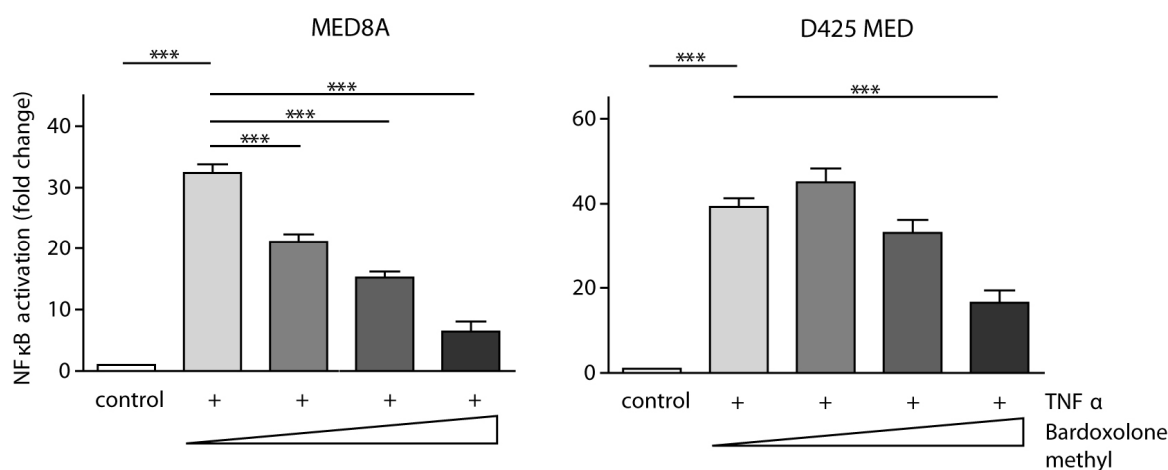
Figure 38. NFκB reporter cells are responsive towards activation by TNFα. MED8A and D425 NFκB reporter cells were treated with TNFα (1 ng/mL) to induce NFκB activity. Induction could be modulated by the addition of 0.1, 0.25 or 0.5 μM of bardoxolone methyl. (C/D) NFκB activity could be iduced by addition of 2.5, 5 or 7.5 μM CI-994 and was attenuated by co-treatment with bardoxolone methyl. Luminescence readout for assessing NFκB reporter activity was performed by using OneGlo reagent. Fold increase in NFκB reporter activity was calculated relative to DMSO controls. Values shown represent mean ± SD of four replicates per condition. *, $p < 0.05$; **, $p < 0.01$; ***, $p < 0.001$ (Dunn's Multiple Comparison Test).

After confirming that our NFκB reporter system works well in both models, we tested the pathway modulation by CI-994 alone and in combination with bardoxolone methyl. CI-994 treatment for 48 h resulted in a significant induction of the NFκB pathway, which was strongly attenuated by co-treatment with bardoxolone methyl (Figure 39).
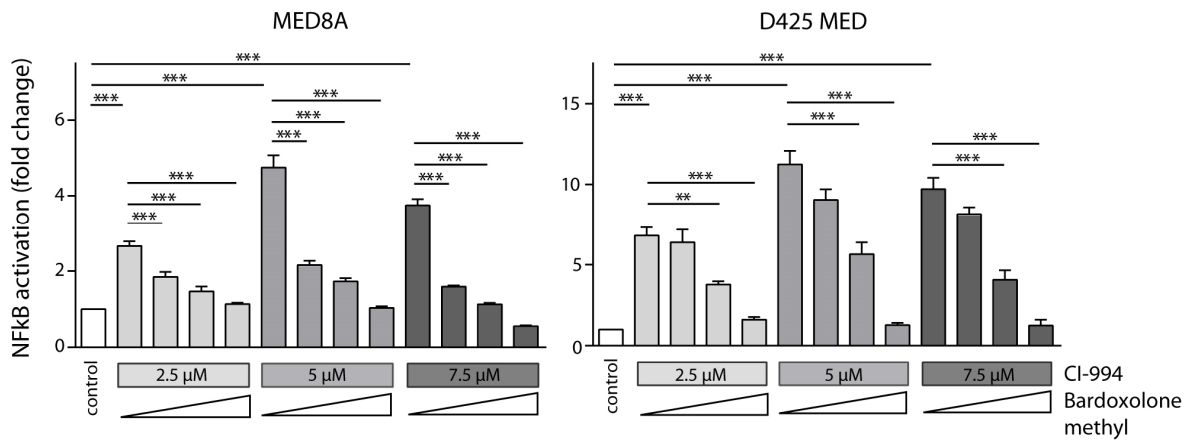
Figure 39. The NFκB pathway is induced by CI-994 and can be modulated by co-treatment with bardoxolone methyl. NFκB pathway activity could be induced by addition of 2.5, 5 or 7.5 µM CI-994 and was attenuated by co-treatment with bardoxolone methyl. Values shown represent mean ± SD of four replicates per condition. *, $p<0.05$; **, $p<0.01$; ***, $p<0.001$ (Dunn's Multiple Comparison Test).

Together with our RNA sequencing results, the findings from our synergy screen suggests that the NFκB pathway represents a therapeutically actionable target to overcome secondary resistance to class I HDACi and to potentially achieve long-term responses using combinatorial therapies for *MYC*-driven MB.

5   Discussion and conclusion

Alterations in cancer genomes and epigenomes strongly affect clinical responses to anticancer therapies and could therefore serve as biomarkers to identify the subset of patients that would most likely benefit from a targeted therapy. The discovery of Imatinib successfully illustrates the basic concept for the development of rationally designed drugs to target specific cancers. Imatinib selectively targets the protein product of the BCR-ABL translocation and its use in chronic myeloid leukemia has transformed the treatment of this disease by substantially improving the survival rates. However, many clinical and preclinical cancer drugs have not been connected with specific genomic alterations that could serve as biomarker and guide patient stratification accordingly. The treatment response of promising targeted drugs in clinical trials therefore often exhibited largely variable outcome for patients with the same histological cancer entity. Thus, precision medicine based on molecular classification of tumors holds the promise to enhance patient care and guide the implementation of novel therapy.

Systematic identification of biomarkers to guide choice of targeted therapy and improve clinical response is particularly desirable for pediatric brain tumors, as patient cohorts are relatively small and rationale treatment stratification in clinical trials therefore is particularly important. Although survival rates for many pediatric malignancies have improved over the last decades, the use of high-dose chemotherapy and radiotherapy is linked with significant long-term side effects substantially affecting the quality of life of survivors. However, identification of molecular targets that drive childhood cancer and the discovery of targeted drugs remains a challenging task. Results from adult cancer studies can often not be directly translated to pediatric cancers and patient numbers and therefore market size are often too low to drive development of therapies targeting pediatric tumors by pharmaceutical companies. Translational research in academia, especially at early stage preclinical development, therefore constitutes an important component in the identification of molecular targets and development of targeted drugs for pediatric brain cancers.

The development of novel drugs or the repurposing of existing medication generally involves large screening campaigns of compound libraries. However, the framework required for such approaches are often confined to pharmaceutical companies as they depend on cost- and maintenance intensive automated equipment. For the implementation of drug screening campaigns within translational academic settings, we therefore sought to establish a platform that comprise semi-automated devices that can be maintained in an academic laboratory.

Herein we describe the successful development and application of a screening platform for the evaluation of compound libraries in cellular screens and the subsequent identification as well as validation of a promising drug candidate. The reproducible and accurate evaluation of hundreds of compounds require automation of the dispensing steps, as manual pipetting is too time-intensive and prone to errors. For the dispensing of inhibitors we therefore employed the D300e Digital Dispenser that allows contact-less and low volume dispensing of compounds and operates as a benchtop device. The entire library was profiled in a broad dose-range format to provide a richly annotated dataset with multiparameter output. Application of cell lines were also performed semi-automated using the Multidrop Combi Reagent Dispenser. Finally, the platform was rounded up by the Spark 10M Multimode Microplate Reader which was equipped with an injector and microplate stacker, to further streamline the workflow and facilitate batch processing.

This screening approach is in contrast to many discovery screens performed in companies or by large joint research facilities. Generally, in a first screen only a single concentration of every inhibitor (in replicates) is tested and hit compounds are then determined by setting a certain threshold for activity. For very large inhibitor libraries with thousands of inhibitors this is clearly the only feasible way for a first hit discovery screen, however our dilution series approach provides more detailed data with a multiparametric output for each inhibitor. For novel inhibitors it is also interesting to evaluate their activity in normal cells. However, the possibilities to culture normal cells in vitro are inherently limited, as they often grow very slow or not at all and their lifespan is finite as compared to tumor cells. Tests with normal cells are therefore often performed at a later stage after the library screens. To identify

interesting drug candidates for further evaluation, we decided to base our selection on large cross-entity evaluation and comparison. Distinct response patterns of entities or subgroups can most likely be linked to the different underlying biology of the cells screened and therefore will have great translational potential and can inform clinically meaningful patient stratification.

The established drug screening platform was next employed for the evaluation of the institutional HDACi library in a large panel of cell lines derived from different brain tumor entities. As the majority of inhibitors in this library are experimental drugs without complete annotation about their isoform profile, toxicity or side effects in *in vivo* applications, we first concentrated on the commercially available and clinically tested inhibitors. Among these, the HDAC1-3 selective inhibitor CI-994 showed significant activity in *MYC* amplified Group 3 MB with no or little activity in the other tested entities.

CI-994 is an orally bioavailable class I specific HDACi, which crosses the blood-brain barrier, and has been demonstrated to reach therapeutic levels, as identified in our study, with peak plasma levels of 23.3 μM and peak cerebrospinal fluid (CSF) levels of 3.4 μM in non-human primate models.[177] Previous studies reported that CI-994 inhibits proliferation and induces apoptosis *in vitro* and *in vivo* in other tumor entities, including acute myeloid leukemia,[178] lung cancer,[179] prostate cancer[180] and colorectal cancer,[181] but was not examined in medulloblastoma up to now. Moreover, CI-994 was already evaluated in several clinical phase I trials;[182–185] two clinical phase II trials for advanced pancreatic cancer (NCT00004861, in combination with gemcitabine)[186] and advanced myeloma (NCT00005624) as well as one clinical phase III trial for treatment of patients with lung cancer (NCT00005093, in combination with gemcitabine).

Administration of CI-994 as a single agent resulted in transient thrombocytopenia as the dose-limiting toxicity (DLT) at the maximum tolerated dose (MTD) of 8 mg/m^2/day on a chronic schedule or 15 mg/m^2/day on an acute schedule.[184] In combination with gemcitabine,[182] carboplatin,[183] paclitaxel[183] and capecitabine,[185] CI-994 had comparable pharmacokinetics and the DLT were thrombocytopenia[182,185] together with neutropenia and

grade 3 respiratory insufficiency.[183] Peak plasma levels for single administration of CI-994 were determined to be 325 ng/mL and 570 ng/mL for the MTD.[184] In all clinical phase I trials distinct antitumoral activity of CI-994 alone or in combination with other chemotherapeutics was observed, ranging from complete response, partial response to stable disease.[182–185] In the case of the clinical phase II trial for advanced pancreatic cancer, no survival benefit could be observed for the combination of gemcitabine with CI-994.[186] However, these trials did not pre-select patients based on appropriate biomarkers or pre-evaluated rationale combination therapies.

Although pathologic activation of *MYC* is found in a large proportion of cancer and constitutes a major cancer driver, the oncoprotein is unfortunately not directly druggable by small molecule inhibitors. Alternative approaches to indirectly target *MYC* include for example the inhibition of BET family proteins. Transcription of *MYC* is induced by increased histone acetylation as BET proteins associate with the acetylated chromatin and facilitate transcriptional activation by assembling transcriptional complexes. Inhibition of bromodomains therefore leads to transcriptional repression of *MYC*, preventing the initiation of transcriptional progams influencing cell survival and proliferation.[187]

Although the diverse mechanisms of HDAC inhibitors still remain largely elusive and hard to decipher, in the course of this work we could show that treatment with HDAC inhibitors in general and with the HDAC1-3 selective inhibitor CI-994 in particular exhibit preferential activity in *MYC*-driven MB and is able to decrease *MYC* expression levels. Besides the induction of apoptotic pathways, the downregulation of *MYC* likely contributes to the antitumoral activity of CI-994. These notable findings could be further validated in two orthotopic xenograft mouse models of *MYC* MB. CI-994 significantly prolongs survival by decreasing tumor growth and leptomeningeal dissemination. However, as chemotherapeutic intervention generally involves multiple agents and CI-994 administered alone resulted only in a temporary but not permanent treatment response, we next performed RNA sequencing to elucidate pathways potentially limiting or even counteracting the antitumoral activity of CI-994 and thereby guiding drug combination selection.

Our transcriptomic data revealed a significant induction of the NFκB pathway following CI-994 treatment, which was detected in multiple curated gene sets and significant transcriptional activation was demonstrated using IPA. The NFκB pathway has not only been shown to be involved in mediating cancer cell survival but activation has been implicated in acquired resistance to chemotherapeutics.[188,189] Importantly, *TGM2*, a recently described target gene of the NFκB pathway,[190,191] was the most upregulated gene in our analysis. *TGM2* has been linked to apoptosis regulation and increased expression promotes cell survival in several cancers, including ovarian cancer,[192] pancreatic ductal adenocarcinoma,[193] melanoma[194] and glioblastoma.[195,196] Furthermore, *TGM2* upregulation has recently been demonstrated in the context of drug resistance to cisplatin in osteosarcoma[197] and non-small-cell lung cancer[198] and metastatic dissemination of breast cancer.[199,200] The finding of an NFκB pathway involvement in response to CI-994 treatment was further substantiated by the results of a screen for synergistic interaction.

In order to find drug combination partners for CI-994, we adapted the established screening workflow. CI-994 was tested in combination with a library of 199 clinically established or currently evaluated inhibitors targeting a wide range of pathways. With this unbiased screening approach we could identify multiple beneficial drug combinations. Amongst already described synergistic drug combinations with HDACi we could corroborate NFκB pathway activation upon CI-994 treatment by identifying synergistic interaction with the NFκB pathway inhibitor bardoxolone methyl. Bardoxolone methyl is an inhibitor of IκB and IKK proteins, showing potent pro-apoptotic and anti-inflammatory activities in solid tumors but has not been evaluated in medulloblastoma to date.[201,202] Interestingly, in addition two proteasome inhibitors exhibited significant synergism when combined with CI-994. Inhibition of the proteasomal degradation of IkB prevents the release of the NFκB complex and its translocation to the nucleus, thereby inhibiting the induction of NFκB target genes.[203]

Although *in vivo* evaluation of the combination treatment of CI-994 with bardoxolone methyl was performed, we could not detect an improved survival of the treated mice (data not shown). Bardoxolone methyl has been mainly studied in the context of chronic kidney

disease, where an improvement in renal function has been achieved. This effect was mainly attributed to the activation of the Keap1–Nrf2 pathway, which modulates inflammation and oxidative stress.[204] In addition, a proteomics study identified over 500 potential interacting partners with CDDO-Im, a closely related derivative of bardoxolone. Besides targeting the Nrf2 and NFκB pathway, CDDO-Im was shown to modulate different canonical signaling pathways including JAK/STAT, PTEN and mTOR pathway.[205] Therefore, taking the multitude of potential cellular targets into account, the negative results of the combination treatment might be attributed to low efficiency of the desired NFκB modulation and off-target pathways effects. The evaluation of additional NFκB pathway inhibitors with a more preferable inhibition profile should be envisaged to further substantiate the combination of HDACi with NFκB inhibitors as a promising therapy for *MYC*-driven MB.

In recent years several large screening approaches have been undertaken that aimed at the evaluation of not only inhibitor response in different entities but also link sensitivity with genomic data.[206–208] Moreover, insights of these studies are beginning to be integrated into larger databanks, containing information on drug sensitivity and possible molecular markers for responsiveness, as a public resource (e.g. https://www.cancerrxgene.org/).[209] Although these studies deliver invaluable information about the dependencies between drug response and genetic background of a large variety of cancer entities, pediatric brain tumors are considerably underrepresented in these studies.

With our unique collection of brain tumors, we could be able to fill this gap and provide a more detailed picture about the responsiveness of particularly childhood brain tumors to targeted therapies. However, to be able to integrate drug response with genetic data we will need to further annotate our cell line panel with regards to copy number, gene expression and mutational profiles. In line with providing a richly annotated cell line panel, a thorough characterization of the HDAC isoform/class selectivity of the HDACi library is an important next step. The institutional inhibitors can serve as important tool compounds to elucidate the role of single HDAC isozymes or class members in the tumorigenesis of brain tumors, however for this, isoform profiles are indispensable.

To conclude, with the establishment of the institutional drug screening pipeline we provided an invaluable tool for performing large scale library screens within an academic setting. The drug sensitivity data produced since the implementation of the workflow considerably surmount the data that would have been amenable by manual inhibitor testing. In addition, the batch processing of library plates and automated dispensing enabled the screening of large cell line panels. The screening approach was complemented by transcriptomic profiling of treated cells and evaluation of synergistic drug combinations. With this integrated large-scale pharmacogenomic approach we provide compelling experimental evidence to pursue further pre-clinical and clinical studies of HDAC1-3 selective HDACi particularly in *MYC*-driven medulloblastoma. Moreover, our data suggest that the combination with NFκB inhibitors could substantially increase the overall antitumoral activity of HDACi.

6 References

1. Hanahan, D. & Weinberg, R. A. Hallmarks of Cancer: The Next Generation. *Cell* **144**, 646–674 (2011).
2. Sharma, S., Kelly, T. K. & Jones, P. A. Epigenetics in cancer. *Carcinogenesis* **31**, 27–36 (2010).
3. Sandoval, J. & Esteller, M. Cancer epigenomics: beyond genomics. *Curr. Opin. Genet. Dev.* **22**, 50–55 (2012).
4. Baylin, S. B. & Jones, P. A. A decade of exploring the cancer epigenome — biological and translational implications. *Nat. Rev. Cancer* **11**, 726–734 (2011).
5. Feinberg, A. P., Koldobskiy, M. A. & Göndör, A. Epigenetic modulators, modifiers and mediators in cancer aetiology and progression. *Nat. Rev. Genet.* **17**, 284–299 (2016).
6. Shen, H. & Laird, P. W. Interplay between the Cancer Genome and Epigenome. *Cell* **153**, 38–55 (2013).
7. You, J. S. & Jones, P. A. Cancer Genetics and Epigenetics: Two Sides of the Same Coin? *Cancer Cell* **22**, 9–20 (2012).
8. Waddington, C. H. The Epigenotype. *Int. J. Epidemiol.* **41**, 10–13 (2012).
9. Berger, S. L., Kouzarides, T., Shiekhattar, R. & Shilatifard, A. An operational definition of epigenetics. *Genes Dev.* **23**, 781–3 (2009).
10. Kouzarides, T. Chromatin Modifications and Their Function. *Cell* **128**, 693–705 (2007).
11. Margueron, R. & Reinberg, D. Chromatin structure and the inheritance of epigenetic information. *Nat. Rev. Genet.* **11**, 285–296 (2010).
12. Esteller, M. Cancer epigenomics: DNA methylomes and histone-modification maps. *Nat. Rev. Genet.* **8**, 286–298 (2007).
13. Strahl, B. D. & Allis, C. D. The language of covalent histone modifications. *Nature* **403**, 41–45 (2000).
14. Jenuwein, T. & Allis, C. D. Translating the histone code. *Science* **293**, 1074–80 (2001).
15. Musselman, C. A., Lalonde, M.-E., Côté, J. & Kutateladze, T. G. Perceiving the epigenetic landscape through histone readers. *Nat. Struct. Mol. Biol.* **19**, 1218–27 (2012).
16. Clapier, C. R. & Cairns, B. R. The Biology of Chromatin Remodeling Complexes. *Annu. Rev. Biochem.* **78**, 273–304 (2009).
17. Berdasco, M. & Esteller, M. Aberrant Epigenetic Landscape in Cancer: How Cellular Identity Goes Awry. *Dev. Cell* **19**, 698–711 (2010).
18. Feinberg, A. P., Ohlsson, R. & Henikoff, S. The epigenetic progenitor origin of human cancer. *Nat. Rev. Genet.* **7**, 21–33 (2006).
19. Jones, P. A. & Baylin, S. B. The fundamental role of epigenetic events in cancer. *Nat. Rev. Genet.* **3**, 415–428 (2002).
20. Gröbner, S. N. *et al.* The landscape of genomic alterations across childhood cancers. *Nature* **555**, 321–327 (2018).

21. Filbin, M. & Monje, M. Developmental origins and emerging therapeutic opportunities for childhood cancer. *Nat. Med.* **25**, 367–376 (2019).

22. Lawlor, E. R. & Thiele, C. J. Epigenetic changes in pediatric solid tumors: promising new targets. *Clin. Cancer Res.* **18**, 2768–79 (2012).

23. Pui, C.-H., Gajjar, A. J., Kane, J. R., Qaddoumi, I. A. & Pappo, A. S. Challenging issues in pediatric oncology. *Nat. Rev. Clin. Oncol.* **8**, 540–549 (2011).

24. Dawson, M. A. & Kouzarides, T. Cancer Epigenetics: From Mechanism to Therapy. *Cell* **150**, 12–27 (2012).

25. Kelly, T. K., De Carvalho, D. D. & Jones, P. A. Epigenetic modifications as therapeutic targets. *Nat. Biotechnol.* **28**, 1069–1078 (2010).

26. Ostrom, Q. T. *et al.* American Brain Tumor Association Adolescent and Young Adult Primary Brain and Central Nervous System Tumors Diagnosed in the United States in 2008-2012. *Neuro. Oncol.* **18**, i1–i50 (2016).

27. Ostrom, Q. T. *et al.* CBTRUS Statistical Report: Primary Brain and Central Nervous System Tumors Diagnosed in the United States in 2008-2012. *Neuro. Oncol.* **17**, iv1–iv62 (2015).

28. Louis, D. N. *et al.* The 2016 World Health Organization Classification of Tumors of the Central Nervous System: a summary. *Acta Neuropathol.* **131**, 803–820 (2016).

29. Johann, P. D. *et al.* Atypical Teratoid/Rhabdoid Tumors Are Comprised of Three Epigenetic Subgroups with Distinct Enhancer Landscapes. *Cancer Cell* **29**, 379–393 (2016).

30. Jones, D. T. W. *et al.* Dissecting the genomic complexity underlying medulloblastoma. *Nature* **488**, 100–5 (2012).

31. Sturm, D. *et al.* Hotspot Mutations in H3F3A and IDH1 Define Distinct Epigenetic and Biological Subgroups of Glioblastoma. *Cancer Cell* **22**, 425–437 (2012).

32. Pajtler, K. W. *et al.* Molecular Classification of Ependymal Tumors across All CNS Compartments, Histopathological Grades, and Age Groups. *Cancer Cell* **27**, 728–743 (2015).

33. Mackay, A. *et al.* Integrated Molecular Meta-Analysis of 1,000 Pediatric High-Grade and Diffuse Intrinsic Pontine Glioma. *Cancer Cell* **32**, 520-537.e5 (2017).

34. Capper, D. *et al.* DNA methylation-based classification of central nervous system tumours. *Nature* **555**, 469–474 (2018).

35. Northcott, P. A. *et al.* Medulloblastoma. *Nat. Rev. Dis. Prim.* **5**, 11 (2019).

36. Phi, J. H. *et al.* Cerebrospinal fluid M staging for medulloblastoma: Reappraisal of Chang's M staging based on the CSF flow. *Neuro. Oncol.* **13**, 334–344 (2011).

37. Korshunov, A. *et al.* Adult and pediatric medulloblastomas are genetically distinct and require different algorithms for molecular risk stratification. *J. Clin. Oncol.* **28**, 3054–60 (2010).

38. Cho, Y.-J. *et al.* Integrative genomic analysis of medulloblastoma identifies a molecular subgroup that drives poor clinical outcome. *J. Clin. Oncol.* **29**, 1424–30 (2011).

39. Northcott, P. A. *et al.* Medulloblastoma comprises four distinct molecular variants. *J.*

Clin. Oncol. **29**, 1408–14 (2011).

40. Kool, M. *et al.* Molecular subgroups of medulloblastoma: an international meta-analysis of transcriptome, genetic aberrations, and clinical data of WNT, SHH, Group 3, and Group 4 medulloblastomas. *Acta Neuropathol.* **123**, 473–84 (2012).

41. Taylor, M. D. *et al.* Molecular subgroups of medulloblastoma: the current consensus. *Acta Neuropathol.* **123**, 465–472 (2012).

42. Cavalli, F. M. G. *et al.* Intertumoral Heterogeneity within Medulloblastoma Subgroups. *Cancer Cell* **31**, 737-754.e6 (2017).

43. Northcott, P. A. *et al.* The whole-genome landscape of medulloblastoma subtypes. *Nature* **547**, 311–317 (2017).

44. Schwalbe, E. C. *et al.* Novel molecular subgroups for clinical classification and outcome prediction in childhood medulloblastoma: a cohort study. *Lancet Oncol.* **18**, 958–971 (2017).

45. Gajjar, A. *et al.* Risk-adapted craniospinal radiotherapy followed by high-dose chemotherapy and stem-cell rescue in children with newly diagnosed medulloblastoma (St Jude Medulloblastoma-96): long-term results from a prospective, multicentre trial. *Lancet Oncol.* **7**, 813–820 (2006).

46. Packer, R. J. *et al.* Phase III study of craniospinal radiation therapy followed by adjuvant chemotherapy for newly diagnosed average-risk medulloblastoma. *J. Clin. Oncol.* **24**, 4202–8 (2006).

47. Mulhern, R. K. *et al.* Neurocognitive consequences of risk-adapted therapy for childhood medulloblastoma. *J. Clin. Oncol.* **23**, 5511–9 (2005).

48. Palmer, S. L. *et al.* Processing speed, attention, and working memory after treatment for medulloblastoma: an international, prospective, and longitudinal study. *J. Clin. Oncol.* **31**, 3494–500 (2013).

49. Packer, R. J., Zhou, T., Holmes, E., Vezina, G. & Gajjar, A. Survival and secondary tumors in children with medulloblastoma receiving radiotherapy and adjuvant chemotherapy: results of Children's Oncology Group trial A9961. *Neuro. Oncol.* **15**, 97–103 (2013).

50. Eaton, B. R. *et al.* Endocrine outcomes with proton and photon radiotherapy for standard risk medulloblastoma. *Neuro. Oncol.* **18**, 881–887 (2016).

51. Moxon-Emre, I. *et al.* Impact of craniospinal dose, boost volume, and neurologic complications on intellectual outcome in patients with medulloblastoma. *J. Clin. Oncol.* **32**, 1760–8 (2014).

52. Koschmann, C., Bloom, K., Upadhyaya, S., Geyer, J. R. & Leary, S. E. S. Survival After Relapse of Medulloblastoma. *J. Pediatr. Hematol. Oncol.* **38**, 269–73 (2016).

53. Gibson, P. *et al.* Subtypes of medulloblastoma have distinct developmental origins. *Nature* **468**, 1095–1099 (2010).

54. Ellison, D. W. *et al.* beta-Catenin status predicts a favorable outcome in childhood medulloblastoma: the United Kingdom Children's Cancer Study Group Brain Tumour Committee. *J. Clin. Oncol.* **23**, 7951–7 (2005).

55. Eberhart, C. G., Tihan, T. & Burger, P. C. Nuclear Localization and Mutation of β-

Catenin in Medulloblastomas. *J. Neuropathol. Exp. Neurol.* **59**, 333–337 (2000).

56. Hamilton, S. R. *et al.* The Molecular Basis of Turcot's Syndrome. *N. Engl. J. Med.* **332**, 839–847 (1995).

57. Zhukova, N. *et al.* Subgroup-specific prognostic implications of TP53 mutation in medulloblastoma. *J. Clin. Oncol.* **31**, 2927–35 (2013).

58. Northcott, P. A. *et al.* Subgroup-specific structural variation across 1,000 medulloblastoma genomes. *Nature* **488**, 49–56 (2012).

59. Clifford, S. C. *et al.* Wnt/Wingless Pathway Activation and Chromosome 6 Loss Characterise a Distinct Molecular Sub-Group of Medulloblastomas Associated with a Favourable Prognosis. *Cell Cycle* **5**, 2666–2670 (2006).

60. Remke, M. *et al.* Adult medulloblastoma comprises three major molecular variants. *J. Clin. Oncol.* **29**, 2717–23 (2011).

61. Gilbertson, R. J. & Ellison, D. W. The Origins of Medulloblastoma Subtypes. *Annu. Rev. Pathol. Mech. Dis.* **3**, 341–365 (2008).

62. Yang, Z.-J. *et al.* Medulloblastoma Can Be Initiated by Deletion of Patched in Lineage-Restricted Progenitors or Stem Cells. *Cancer Cell* **14**, 135–145 (2008).

63. Northcott, P. A. *et al.* Pediatric and adult sonic hedgehog medulloblastomas are clinically and molecularly distinct. *Acta Neuropathol.* **122**, 231–240 (2011).

64. Kool, M. *et al.* Genome Sequencing of SHH Medulloblastoma Predicts Genotype-Related Response to Smoothened Inhibition. *Cancer Cell* **25**, 393–405 (2014).

65. Jones, D. T. W. *et al.* Dissecting the genomic complexity underlying medulloblastoma. *Nat. 2012 4887409* **488**, 100 (2012).

66. Rausch, T. *et al.* Genome Sequencing of Pediatric Medulloblastoma Links Catastrophic DNA Rearrangements with TP53 Mutations. *Cell* **148**, 59–71 (2012).

67. Waszak, S. M. *et al.* Spectrum and prevalence of genetic predisposition in medulloblastoma: a retrospective genetic study and prospective validation in a clinical trial cohort. *Lancet Oncol.* **19**, 785–798 (2018).

68. Ramaswamy, V. *et al.* Risk stratification of childhood medulloblastoma in the molecular era: the current consensus. *Acta Neuropathol.* **131**, 821–831 (2016).

69. Remke, M. *et al.* TERT promoter mutations are highly recurrent in SHH subgroup medulloblastoma. *Acta Neuropathol.* **126**, 917–929 (2013).

70. Northcott, P. A. *et al.* Medulloblastomics: the end of the beginning. *Nat. Rev. Cancer* **12**, 818–34 (2012).

71. Raybaud, C., Ramaswamy, V., Taylor, M. D. & Laughlin, S. Posterior fossa tumors in children: developmental anatomy and diagnostic imaging. *Child's Nerv. Syst.* **31**, 1661–1676 (2015).

72. Kawauchi, D. *et al.* A Mouse Model of the Most Aggressive Subgroup of Human Medulloblastoma. *Cancer Cell* **21**, 168–180 (2012).

73. Pei, Y. *et al.* An Animal Model of MYC-Driven Medulloblastoma. *Cancer Cell* **21**, 155–167 (2012).

74. Tseng, Y.-Y. *et al.* PVT1 dependence in cancer with MYC copy-number increase. *Nature* **512**, 82–86 (2014).

75. Northcott, P. A. *et al.* Enhancer hijacking activates GFI1 family oncogenes in medulloblastoma. *Nature* **511**, 428–434 (2014).

76. Shih, D. J. H. *et al.* Cytogenetic prognostication within medulloblastoma subgroups. *J. Clin. Oncol.* **32**, 886–96 (2014).

77. Pietsch, T. *et al.* Prognostic significance of clinical, histopathological, and molecular characteristics of medulloblastomas in the prospective HIT2000 multicenter clinical trial cohort. *Acta Neuropathol.* **128**, 137–149 (2014).

78. Ramaswamy, V. *et al.* Recurrence patterns across medulloblastoma subgroups: an integrated clinical and molecular analysis. *Lancet Oncol.* **14**, 1200–1207 (2013).

79. Bandopadhayay, P. *et al.* BET Bromodomain Inhibition of MYC-Amplified Medulloblastoma. *Clin. Cancer Res.* **20**, 912–925 (2014).

80. Pei, Y. *et al.* HDAC and PI3K Antagonists Cooperate to Inhibit Growth of MYC-Driven Medulloblastoma. *Cancer Cell* **29**, 311–323 (2016).

81. Ecker, J. *et al.* Targeting class I histone deacetylase 2 in MYC amplified group 3 medulloblastoma. *Acta Neuropathol. Commun.* **3**, 22 (2015).

82. Hill, R. M. *et al.* Combined MYC and P53 Defects Emerge at Medulloblastoma Relapse and Define Rapidly Progressive, Therapeutically Targetable Disease. *Cancer Cell* **27**, 72–84 (2015).

83. Hanaford, A. R. *et al.* DiSCoVERing Innovative Therapies for Rare Tumors: Combining Genetically Accurate Disease Models with In Silico Analysis to Identify Novel Therapeutic Targets. *Clin. Cancer Res.* **22**, 3903–14 (2016).

84. Northcott, P. A. *et al.* The whole-genome landscape of medulloblastoma subtypes. *Nature* **547**, 311–317 (2017).

85. Khorasanizadeh, S. The Nucleosome: From Genomic Organization to Genomic Regulation. *Cell* **116**, 259–272 (2004).

86. Bannister, A. J. & Kouzarides, T. Regulation of chromatin by histone modifications. *Cell Res.* **21**, 381–395 (2011).

87. Seto, E. & Yoshida, M. Erasers of Histone Acetylation: The Histone Deacetylase Enzymes. *Cold Spring Harb. Perspect. Biol.* **6**, a018713 (2014).

88. Eberharter, A. & Becker, P. B. Histone acetylation: a switch between repressive and permissive chromatin. Second in review series on chromatin dynamics. *EMBO Rep.* **3**, 224–9 (2002).

89. Choudhary, C. *et al.* Lysine Acetylation Targets Protein Complexes and Co-Regulates Major Cellular Functions. *Science* **324**, 834–840 (2009).

90. Narita, T., Weinert, B. T. & Choudhary, C. Functions and mechanisms of non-histone protein acetylation. *Nat. Rev. Mol. Cell Biol.* **20**, 156–174 (2019).

91. Millard, C. J., Watson, P. J., Fairall, L. & Schwabe, J. W. R. Targeting Class I Histone Deacetylases in a 'Complex' Environment. *Trends Pharmacol. Sci.* **38**, 363–377 (2017).

92. Juan, L. J. *et al.* Histone deacetylases specifically down-regulate p53-dependent gene activation. *J. Biol. Chem.* **275**, 20436–43 (2000).

93. Dasgupta, T., Antony, J., Braithwaite, A. W. & Horsfield, J. A. HDAC8 Inhibition Blocks SMC3 Deacetylation and Delays Cell Cycle Progression without Affecting

Cohesin-dependent Transcription in MCF7 Cancer Cells. *J. Biol. Chem.* **291**, 12761–70 (2016).

94. Witt, O., Deubzer, H. E., Milde, T. & Oehme, I. HDAC family: What are the cancer relevant targets? *Cancer Lett.* **277**, 8–21 (2009).

95. Fischle, W. *et al.* Enzymatic Activity Associated with Class II HDACs Is Dependent on a Multiprotein Complex Containing HDAC3 and SMRT/N-CoR. *Mol. Cell* **9**, 45–57 (2002).

96. Lahm, A. *et al.* Unraveling the hidden catalytic activity of vertebrate class IIa histone deacetylases. *Proc. Natl. Acad. Sci. U. S. A.* **104**, 17335–40 (2007).

97. Oehme, I. *et al.* Histone deacetylase 10 promotes autophagy-mediated cell survival. *Proc. Natl. Acad. Sci.* **110**, E2592–E2601 (2013).

98. Hai, Y., Shinsky, S. A., Porter, N. J. & Christianson, D. W. Histone deacetylase 10 structure and molecular function as a polyamine deacetylase. *Nat. Commun.* **8**, 15368 (2017).

99. Kutil, Z. *et al.* Histone Deacetylase 11 Is a Fatty-Acid Deacylase. *ACS Chem. Biol.* **13**, 685–693 (2018).

100. Li, Y. & Seto, E. HDACs and HDAC Inhibitors in Cancer Development and Therapy. *Cold Spring Harb. Perspect. Med.* **6**, (2016).

101. West, A. C. & Johnstone, R. W. New and emerging HDAC inhibitors for cancer treatment. *J. Clin. Invest.* **124**, 30–39 (2014).

102. Bolden, J. E., Peart, M. J. & Johnstone, R. W. Anticancer activities of histone deacetylase inhibitors. *Nat. Rev. Drug Discov.* **5**, 769–784 (2006).

103. Roche, J. & Bertrand, P. Inside HDACs with more selective HDAC inhibitors. *Eur. J. Med. Chem.* **121**, 451–483 (2016).

104. Bertrand, P. Inside HDAC with HDAC inhibitors. *Eur. J. Med. Chem.* **45**, 2095–2116 (2010).

105. Giannini, G., Cabri, W., Fattorusso, C. & Rodriquez, M. Histone deacetylase inhibitors in the treatment of cancer: overview and perspectives. *Future Med. Chem.* **4**, 1439–1460 (2012).

106. Vansteenkiste, J. *et al.* Early phase II trial of oral vorinostat in relapsed or refractory breast, colorectal, or non-small cell lung cancer. *Invest. New Drugs* **26**, 483–488 (2008).

107. Hummel, T. R. *et al.* A pediatric phase 1 trial of vorinostat and temozolomide in relapsed or refractory primary brain or spinal cord tumors: a Children's Oncology Group phase 1 consortium study. *Pediatr. Blood Cancer* **60**, 1452–7 (2013).

108. Lee, E. Q. *et al.* Phase II study of panobinostat in combination with bevacizumab for recurrent glioblastoma and anaplastic glioma. *Neuro. Oncol.* **17**, 862–7 (2015).

109. Bradley, D. *et al.* Vorinostat in advanced prostate cancer patients progressing on prior chemotherapy (National Cancer Institute Trial 6862). *Cancer* **115**, 5541–5549 (2009).

110. Molife, L. R. *et al.* Phase II, two-stage, single-arm trial of the histone deacetylase inhibitor (HDACi) romidepsin in metastatic castration-resistant prostate cancer (CRPC). *Ann. Oncol.* **21**, 109–113 (2010).

111. Whitehead, R. P. *et al.* Phase II trial of romidepsin (NSC-630176) in previously treated colorectal cancer patients with advanced disease: a Southwest Oncology Group study (S0336). *Invest. New Drugs* **27**, 469–75 (2009).

112. Balasubramanian, S., Verner, E. & Buggy, J. J. Isoform-specific histone deacetylase inhibitors: The next step? *Cancer Lett.* **280**, 211–221 (2009).

113. Somoza, J. R. *et al.* Structural Snapshots of Human HDAC8 Provide Insights into the Class I Histone Deacetylases. *Structure* **12**, 1325–1334 (2004).

114. Lauffer, B. E. L. *et al.* Histone deacetylase (HDAC) inhibitor kinetic rate constants correlate with cellular histone acetylation but not transcription and cell viability. *J. Biol. Chem.* **288**, 26926–43 (2013).

115. Watson, P. J. *et al.* Insights into the activation mechanism of class I HDAC complexes by inositol phosphates. *Nat. Commun.* **7**, 11262 (2016).

116. Watson, P. J., Fairall, L., Santos, G. M. & Schwabe, J. W. R. Structure of HDAC3 bound to co-repressor and inositol tetraphosphate. *Nature* **481**, 335–340 (2012).

117. Wagner, F. F. *et al.* An Isochemogenic Set of Inhibitors To Define the Therapeutic Potential of Histone Deacetylases in β-Cell Protection. *ACS Chem. Biol.* **11**, 363–374 (2016).

118. Whitehead, L. *et al.* Human HDAC isoform selectivity achieved via exploitation of the acetate release channel with structurally unique small molecule inhibitors. *Bioorg. Med. Chem.* **19**, 4626–4634 (2011).

119. KrennHrubec, K., Marshall, B. L., Hedglin, M., Verdin, E. & Ulrich, S. M. Design and evaluation of 'Linkerless' hydroxamic acids as selective HDAC8 inhibitors. *Bioorg. Med. Chem. Lett.* **17**, 2874–2878 (2007).

120. Luckhurst, C. A. *et al.* Potent, Selective, and CNS-Penetrant Tetrasubstituted Cyclopropane Class IIa Histone Deacetylase (HDAC) Inhibitors. *ACS Med. Chem. Lett.* **7**, 34–39 (2016).

121. Santo, L. *et al.* Preclinical activity, pharmacodynamic, and pharmacokinetic properties of a selective HDAC6 inhibitor, ACY-1215, in combination with bortezomib in multiple myeloma. *Blood* **119**, 2579–89 (2012).

122. Bergman, J. A. *et al.* Selective Histone Deacetylase 6 Inhibitors Bearing Substituted Urea Linkers Inhibit Melanoma Cell Growth. *J. Med. Chem.* **55**, 9891–9899 (2012).

123. Bantscheff, M. *et al.* Chemoproteomics profiling of HDAC inhibitors reveals selective targeting of HDAC complexes. *Nat. Biotechnol.* **29**, 255–265 (2011).

124. Anighoro, A., Bajorath, J. & Rastelli, G. Polypharmacology: Challenges and Opportunities in Drug Discovery. *J. Med. Chem.* **57**, 7874–7887 (2014).

125. Qian, C. *et al.* Cancer Network Disruption by a Single Molecule Inhibitor Targeting Both Histone Deacetylase Activity and Phosphatidylinositol 3-Kinase Signaling. *Clin. Cancer Res.* **18**, 4104–4113 (2012).

126. Atkinson, S. J. *et al.* The structure based design of dual HDAC/BET inhibitors as novel epigenetic probes. *Medchemcomm* **5**, 342 (2014).

127. Bhatia, S. *et al.* Discovery of the First-in-Class Dual Histone Deacetylase–Proteasome Inhibitor. *J. Med. Chem.* **61**, 10299–10309 (2018).

128. Cai, X. *et al.* Discovery of 7-(4-(3-Ethynylphenylamino)-7-methoxyquinazolin-6-yloxy)- *N* -hydroxyheptanamide (CUDC-101) as a Potent Multi-Acting HDAC, EGFR, and HER2 Inhibitor for the Treatment of Cancer. *J. Med. Chem.* **53**, 2000–2009 (2010).

129. Guerrant, W., Patil, V., Canzoneri, J. C. & Oyelere, A. K. Dual Targeting of Histone Deacetylase and Topoisomerase II with Novel Bifunctional Inhibitors. *J. Med. Chem.* **55**, 1465–1477 (2012).

130. Ganesan, A. Multitarget Drugs: an Epigenetic Epiphany. *ChemMedChem* **11**, 1227–1241 (2016).

131. Archin, N. M. *et al.* Interval dosing with the HDAC inhibitor vorinostat effectively reverses HIV latency. *J. Clin. Invest.* **127**, 3126–3135 (2017).

132. Janczura, K. J. *et al.* Inhibition of HDAC3 reverses Alzheimer's disease-related pathologies in vitro and in the 3xTg-AD mouse model. *Proc. Natl. Acad. Sci. U. S. A.* **115**, E11148–E11157 (2018).

133. Herman, D. *et al.* Histone deacetylase inhibitors reverse gene silencing in Friedreich's ataxia. *Nat. Chem. Biol.* **2**, 551–558 (2006).

134. Shakespear, M. R., Halili, M. A., Irvine, K. M., Fairlie, D. P. & Sweet, M. J. Histone deacetylases as regulators of inflammation and immunity. *Trends Immunol.* **32**, 335–43 (2011).

135. Collisson, E. A. *et al.* Comprehensive molecular profiling of lung adenocarcinoma. *Nature* **511**, 543–550 (2014).

136. Brennan, C. W. *et al.* The Somatic Genomic Landscape of Glioblastoma. *Cell* **155**, 462–477 (2013).

137. Berger, A. C. *et al.* A Comprehensive Pan-Cancer Molecular Study of Gynecologic and Breast Cancers. *Cancer Cell* **33**, 690-705.e9 (2018).

138. Sanchez-Vega, F. *et al.* Oncogenic Signaling Pathways in The Cancer Genome Atlas. *Cell* **173**, 321-337.e10 (2018).

139. Bailey, M. H. *et al.* Comprehensive Characterization of Cancer Driver Genes and Mutations. *Cell* **173**, 371-385.e18 (2018).

140. Corces, M. R. *et al.* The chromatin accessibility landscape of primary human cancers. *Science* **362**, eaav1898 (2018).

141. Terstappen, G. C., Schlüpen, C., Raggiaschi, R. & Gaviraghi, G. Target deconvolution strategies in drug discovery. *Nat. Rev. Drug Discov.* **6**, 891–903 (2007).

142. Hopkins, A. L. & Groom, C. R. The druggable genome. *Nat. Rev. Drug Discov.* **1**, 727–730 (2002).

143. Lenci, E. *et al.* Diversity-Oriented Synthesis as a Tool for Chemical Genetics. *Molecules* **19**, 16506–16528 (2014).

144. Lipinski, C. A., Lombardo, F., Dominy, B. W. & Feeney, P. J. Experimental and computational approaches to estimate solubility and permeability in drug discovery and development settings. *Adv. Drug Deliv. Rev.* **23**, 3–25 (1997).

145. Ghose, A. K., Vellarkad N. Viswanadhan, A. & Wendoloski, J. J. A Knowledge-Based Approach in Designing Combinatorial or Medicinal Chemistry Libraries for Drug

Discovery. 1. A Qualitative and Quantitative Characterization of Known Drug Databases. *J. Comb. Chem.* **1**, 55–68 (1999).

146. Veber, D. F. *et al.* Molecular Properties That Influence the Oral Bioavailability of Drug Candidates. *J. Med. Chem.* **45**, 2615–2623 (2002).

147. Congreve, M., Carr, R., Murray, C. & Jhoti, H. A 'Rule of Three' for fragment-based lead discovery? *Drug Discov. Today* **8**, 876–877 (2003).

148. Paul, S. M. *et al.* How to improve R&D productivity: the pharmaceutical industry's grand challenge. *Nat. Rev. Drug Discov.* **9**, 203–214 (2010).

149. DiMasi, J. A., Feldman, L., Seckler, A. & Wilson, A. Trends in Risks Associated With New Drug Development: Success Rates for Investigational Drugs. *Clin. Pharmacol. Ther.* **87**, 272–277 (2010).

150. Hay, M., Thomas, D. W., Craighead, J. L., Economides, C. & Rosenthal, J. Clinical development success rates for investigational drugs. *Nat. Biotechnol.* **32**, 40–51 (2014).

151. Li, Y. Y. & Jones, S. J. Drug repositioning for personalized medicine. *Genome Med. 2012 43* **4**, 27 (2012).

152. Ashburn, T. T. & Thor, K. B. Drug repositioning: identifying and developing new uses for existing drugs. *Nat. Rev. Drug Discov.* **3**, 673–683 (2004).

153. Ashley, E. A. Towards precision medicine. *Nat. Rev. Genet.* **17**, 507–522 (2016).

154. Weber, K., Bartsch, U., Stocking, C. & Fehse, B. A Multicolor Panel of Novel Lentiviral "Gene Ontology" (LeGO) Vectors for Functional Gene Analysis. *Mol. Ther.* **16**, 698–706 (2008).

155. Warren, L. *et al.* Highly Efficient Reprogramming to Pluripotency and Directed Differentiation of Human Cells with Synthetic Modified mRNA. *Cell Stem Cell* **7**, 618–630 (2010).

156. Wilson, A. A. *et al.* Lentiviral Delivery of RNAi for In Vivo Lineage-Specific Modulation of Gene Expression in Mouse Lung Macrophages. *Mol. Ther.* **21**, 825–833 (2013).

157. Foucquier, J. & Guedj, M. Analysis of drug combinations: current methodological landscape. *Pharmacol. Res. Perspect.* **3**, e00149 (2015).

158. Chou, T.-C. Drug Combination Studies and Their Synergy Quantification Using the Chou-Talalay Method. *Cancer Res.* **70**, 440–446 (2010).

159. Stenzel, K. *et al.* Alkoxyurea-Based Histone Deacetylase Inhibitors Increase Cisplatin Potency in Chemoresistant Cancer Cell Lines. *J. Med. Chem.* **60**, 5334–5348 (2017).

160. Marek, L. *et al.* Histone Deacetylase (HDAC) Inhibitors with a Novel Connecting Unit Linker Region Reveal a Selectivity Profile for HDAC4 and HDAC5 with Improved Activity against Chemoresistant Cancer Cells. *J. Med. Chem.* **56**, 427–436 (2013).

161. Reßing, N. *et al.* Design, synthesis and biological evaluation of β-peptoid-capped HDAC inhibitors with anti-neuroblastoma and anti-glioblastoma activity. *Medchemcomm* **10**, 1109–1115 (2019).

162. Diedrich, D. *et al.* Rational design and diversity-oriented synthesis of peptoid-based selective HDAC6 inhibitors. *Chem. Commun.* **52**, 3219–3222 (2016).

163. Krieger, V. *et al.* Design, Multicomponent Synthesis, and Anticancer Activity of a Focused Histone Deacetylase (HDAC) Inhibitor Library with Peptoid-Based Cap Groups. *J. Med. Chem.* **60**, 5493–5506 (2017).

164. Kaletsch, A. *et al.* Effects of novel HDAC inhibitors on urothelial carcinoma cells. *Clin. Epigenetics* **10**, 100 (2018).

165. Furumai, R. *et al.* FK228 (depsipeptide) as a natural prodrug that inhibits class I histone deacetylases. *Cancer Res.* **62**, 4916–21 (2002).

166. Atadja, P. Development of the pan-DAC inhibitor panobinostat (LBH589): Successes and challenges. *Cancer Lett.* **280**, 233–241 (2009).

167. Diedrich, D. Peptoidbasierte HDAC6-Inhibitoren und α -Aminoxyoligopeptide – Neuartige peptidomimetische Substanzklassen mit Antitumoraktivität. (Heinrich-Heine University Düsseldorf, 2017).

168. Martirosyan, A. R. *et al.* Differentiation-inducing quinolines as experimental breast cancer agents in the MCF-7 human breast cancer cell model. *Biochem. Pharmacol.* **68**, 1729–1738 (2004).

169. Martirosyan, A. *et al.* Actions of a histone deacetylase inhibitor NSC3852 (5-nitroso-8-quinolinol) link reactive oxygen species to cell differentiation and apoptosis in MCF-7 human mammary tumor cells. *J. Pharmacol. Exp. Ther.* **317**, 546–52 (2006).

170. Ivanov, D. P., Coyle, B., Walker, D. A. & Grabowska, A. M. In vitro models of medulloblastoma: Choosing the right tool for the job. *J. Biotechnol.* **236**, 10–25 (2016).

171. Milde, T. *et al.* HD-MB03 is a novel Group 3 medulloblastoma model demonstrating sensitivity to histone deacetylase inhibitor treatment. *J. Neurooncol.* **110**, 335–348 (2012).

172. Krieger, V. Synthese, Konformationsanalyse und biologische Evaluierung von neuartigen antitumoraktiven Peptoid-Derivaten. (Heinrich-Heine University, 2017).

173. Stenzel, K. *et al.* Design and Synthesis of Terephthalic Acid-Based Histone Deacetylase Inhibitors with Dual-Stage Anti- *Plasmodium* Activity. *ChemMedChem* **12**, 1627–1636 (2017).

174. Matthay, K. K. *et al.* Neuroblastoma. *Nat. Rev. Dis. Prim.* **2**, 16078 (2016).

175. Rickman, D. S., Schulte, J. H. & Eilers, M. The Expanding World of N-MYC-Driven Tumors. *Cancer Discov.* **8**, 150–163 (2018).

176. Alves Avelar, L. A. Design and Synthesis of Histone Deacetylase Inhibitors with Antiplasmodial and Anticancer Activities. (Heinrich-Heine University).

177. Riva, L. *et al.* Pharmacokinetics and cerebrospinal fluid penetration of CI-994 (N-acetyldinaline) in the nonhuman primate. *Clin. Cancer Res.* **6**, 994–7 (2000).

178. Kaspers, G. *et al.* CI-994 (N-acetyl-dinaline) in combination with conventional anti-cancer agents is effective against acute myeloid leukemia in vitro and in vivo. *Oncol. Rep.* **19**, 1517–1523 (2008).

179. Loprevite, M. *et al.* In vitro study of CI-994, a histone deacetylase inhibitor, in non-small cell lung cancer cell lines. *Oncol. Res.* **15**, 39–48 (2005).

180. Gediya, L. K., Belosay, A., Khandelwal, A., Purushottamachar, P. & Njar, V. C. O. Improved synthesis of histone deacetylase inhibitors (HDIs) (MS-275 and CI-994)

and inhibitory effects of HDIs alone or in combination with RAMBAs or retinoids on growth of human LNCaP prostate cancer cells and tumor xenografts. *Bioorg. Med. Chem.* **16**, 3352–3360 (2008).

181. Seelig, M. H. & Berger, M. R. Efficacy of dinaline and its methyl and acetyl derivatives against colorectal cancer in vivo and in vitro. *Eur. J. Cancer* **32**, 1968–1976 (1996).

182. Nemunaitis, J. J. *et al.* Phase I Study of Oral CI-994 in Combination with Gemcitabine in Treatment of Patients with Advanced Cancer. *Cancer J.* **9**, 58–66 (2003).

183. Pauer, L. R. *et al.* Phase I study of oral CI-994 in combination with carboplatin and paclitaxel in the treatment of patients with advanced solid tumors. *Cancer Invest.* **22**, 886–96 (2004).

184. Prakash, S. *et al.* Chronic oral administration of CI-994: a phase 1 study. *Invest. New Drugs* **19**, 1–11 (2001).

185. Undevia, S. D. *et al.* A phase I study of the oral combination of CI-994, a putative histone deacetylase inhibitor, and capecitabine. *Ann. Oncol.* **15**, 1705–1711 (2004).

186. Richards, D. A. *et al.* Gemcitabine plus CI-994 offers no advantage over gemcitabine alone in the treatment of patients with advanced pancreatic cancer: results of a phase II randomized, double-blind, placebo-controlled, multicenter study. *Ann. Oncol.* **17**, 1096–1102 (2006).

187. Delmore, J. E. *et al.* BET Bromodomain Inhibition as a Therapeutic Strategy to Target c-Myc. *Cell* **146**, 904–917 (2011).

188. Xia, Y., Shen, S. & Verma, I. M. NF-κB, an active player in human cancers. *Cancer Immunol. Res.* **2**, 823–30 (2014).

189. Godwin, P. *et al.* Targeting nuclear factor-kappa B to overcome resistance to chemotherapy. *Front. Oncol.* **3**, 120 (2013).

190. Mann, A. P. *et al.* Overexpression of Tissue Transglutaminase Leads to Constitutive Activation of Nuclear Factor-κB in Cancer Cells: Delineation of a Novel Pathway. *Cancer Res.* **66**, 8788–8795 (2006).

191. Zhang, H., Chen, Z., Miranda, R. N., Medeiros, L. J. & McCarty, N. TG2 and NF-κB Signaling Coordinates the Survival of Mantle Cell Lymphoma Cells via IL6-Mediated Autophagy. *Cancer Res.* **76**, 6410–6423 (2016).

192. Hwang, J. Y. *et al.* Clinical and biological significance of tissue transglutaminase in ovarian carcinoma. *Cancer Res.* **68**, 5849–58 (2008).

193. Verma, A. *et al.* Increased Expression of Tissue Transglutaminase in Pancreatic Ductal Adenocarcinoma and Its Implications in Drug Resistance and Metastasis. *Cancer Res.* **66**, 10525–10533 (2006).

194. Fok, J. Y., Ekmekcioglu, S. & Mehta, K. Implications of tissue transglutaminase expression in malignant melanoma. *Mol. Cancer Ther.* **5**, 1493–1503 (2006).

195. Yin, J. *et al.* Transglutaminase 2 Inhibition Reverses Mesenchymal Transdifferentiation of Glioma Stem Cells by Regulating C/EBPβ Signaling. *Cancer Res.* **77**, 4973–4984 (2017).

196. Yuan, L. *et al.* Tissue transglutaminase 2 inhibition promotes cell death and chemosensitivity in glioblastomas. *Mol. Cancer Ther.* **4**, 1293–1302 (2005).

197. Li, C., Cai, J., Ge, F. & Wang, G. TGM2 knockdown reverses cisplatin chemoresistance in osteosarcoma. *Int. J. Mol. Med.* **42**, 1799–1808 (2018).

198. Park, K.-S. *et al.* Transglutaminase 2 as a cisplatin resistance marker in non-small cell lung cancer. *J. Cancer Res. Clin. Oncol.* **136**, 493–502 (2010).

199. Kumar, A. *et al.* Tissue Transglutaminase Promotes Drug Resistance and Invasion by Inducing Mesenchymal Transition in Mammary Epithelial Cells. *PLoS One* **5**, e13390 (2010).

200. Mehta, K., Fok, J., Miller, F. R., Koul, D. & Sahin, A. A. Prognostic Significance of Tissue Transglutaminase in Drug Resistant and Metastatic Breast Cancer. *Clin. Cancer Res.* **10**, 8068–8076 (2004).

201. Konopleva, M. *et al.* Novel triterpenoid CDDO-Me is a potent inducer of apoptosis and differentiation in acute myelogenous leukemia. *Blood* **99**, 326–35 (2002).

202. Shishodia, S., Sethi, G., Konopleva, M., Andreeff, M. & Aggarwal, B. B. A Synthetic Triterpenoid, CDDO-Me, Inhibits IKBA Kinase and Enhances Apoptosis Induced by TNF and Chemotherapeutic Agents through Down-Regulation of Expression of Nuclear Factor kB-Regulated Gene Products in Human Leukemic Cells. *Clin. Cancer Res.* **12**, 1828–1838 (2006).

203. Palombella, V. J., Rando, O. J., Goldberg, A. L. & Maniatis, T. The ubiquitin-proteasome pathway is required for processing the NF-kappa B1 precursor protein and the activation of NF-kappa B. *Cell* **78**, 773–85 (1994).

204. Pergola, P. E. *et al.* Bardoxolone Methyl and Kidney Function in CKD with Type 2 Diabetes. *N. Engl. J. Med.* **365**, 327–336 (2011).

205. Yore, M. M., Kettenbach, A. N., Sporn, M. B., Gerber, S. A. & Liby, K. T. Proteomic Analysis Shows Synthetic Oleanane Triterpenoid Binds to mTOR. *PLoS One* **6**, e22862 (2011).

206. Garnett, M. J. *et al.* Systematic identification of genomic markers of drug sensitivity in cancer cells. *Nature* **483**, 570–575 (2012).

207. Barretina, J. *et al.* The Cancer Cell Line Encyclopedia enables predictive modelling of anticancer drug sensitivity. *Nature* **483**, 603–607 (2012).

208. Iorio, F. *et al.* A Landscape of Pharmacogenomic Interactions in Cancer. *Cell* **166**, 740–754 (2016).

209. Yang, W. *et al.* Genomics of Drug Sensitivity in Cancer (GDSC): a resource for therapeutic biomarker discovery in cancer cells. *Nucleic Acids Res.* **41**, D955–D961 (2012).

7 Appendix

7.1 Supplementary Figures and Tables

Supplementary Figure 1. Heatmap of inhibitors with low or no activity.
A total of 102 inhibitors showed either no activity across all cell lines or mean $IC_{50} > 20$ µM and were therefore omitted from the initial analysis.
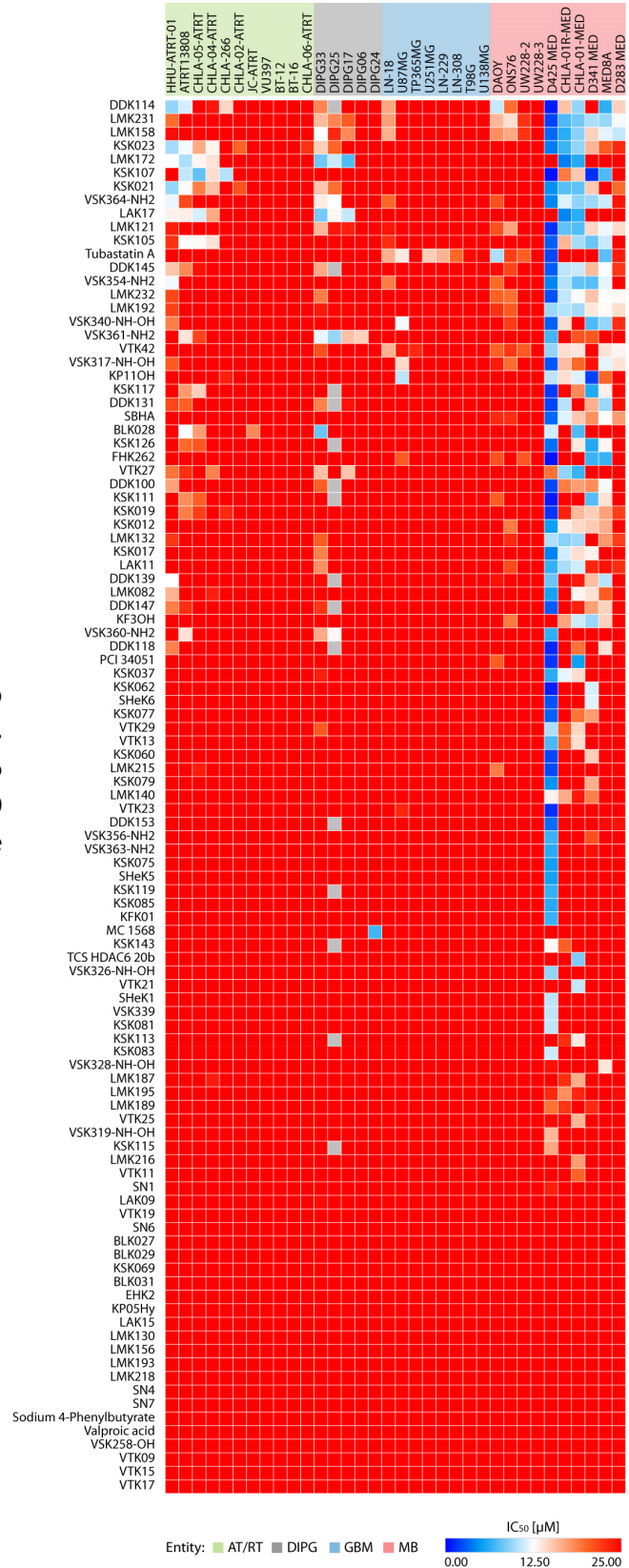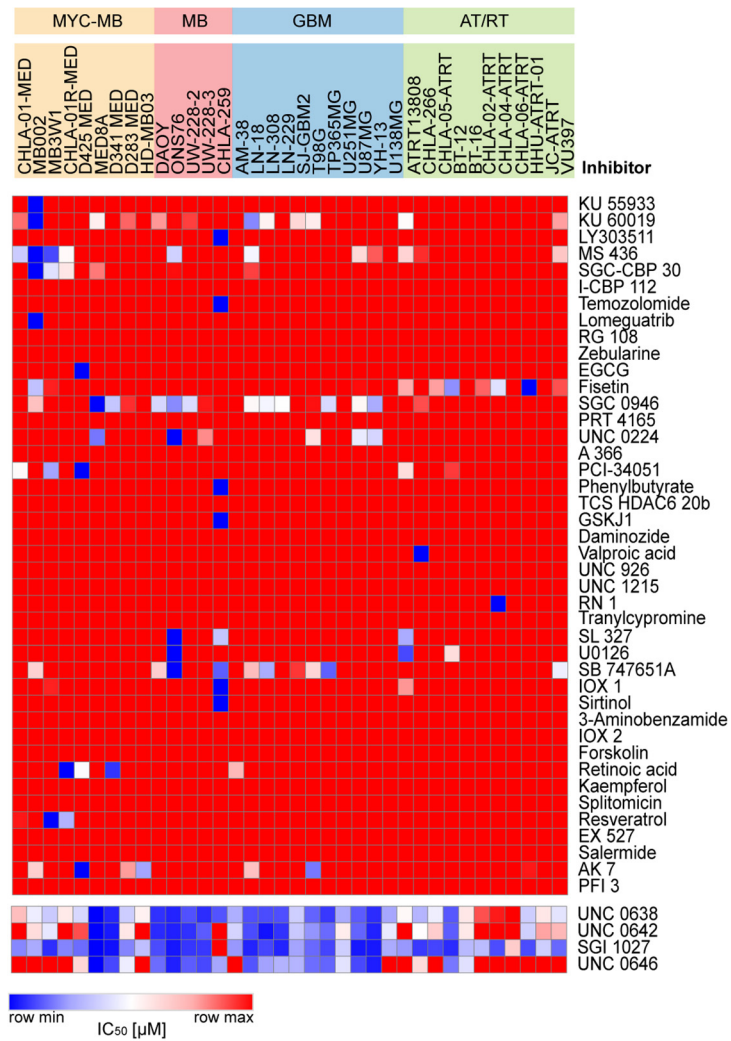
Supplementary Figure 2. Inhibitors from epigenetic library screen with low overall activity or higher mean activity in GBM. 42 inhibitors showed low or no activity across the tested cell lines and four inhibitors were preferential active in GBM.

Supplementary Table 1. Overview of significant inhibitors identified from entity comparison

Names	total	elements
MYC MB vs AT/RT *MYC* MB vs DIPG *MYC* MB vs GBM *MYC* MB vs non-*MYC* MB	14	KSK027 FHK257 DDK122 KP15OH VSK365-NH2F FHK281 DDK119 DDK142 KSK031 VSK341-NH-OH DDK140 KSK029 LMK204 LMK210
MYC MB vs AT/RT *MYC* MB vs GBM *MYC* MB vs non-*MYC* MB	12	VSK327-NH-OH VSK335-NH-OH DDK117 KP08Hy CI994 VSK336-NH-OH LAK07 LMK230 LAK25 LMK131 TC-H 106 LMK220
MYC MB vs DIPG *MYC* MB vs GBM *MYC* MB vs non-*MYC* MB	1	KSK035
MYC MB vs AT/RT *MYC* MB vs DIPG *MYC* MB vs GBM	26	LMK101 KSK043 VSK322-NH-OH LAK19 DDK116 KK21OH Pyroxamide DDK141 RVK2 KSK045 VTK39 LMK162 KSK047 VSK334-NH-OH KSK049 LMK214 KSK064 KK19OH KP16OH DDK146 LMK200 LAK31 NSC 3852 VSK333-NH-OH LMK231 DDK138
MYC MB vs GBM *MYC* MB vs non-*MYC* MB	6	KSK025 KSK013 KP04Hy KSK007 LMK173 LMK168
MYC MB vs AT/RT *MYC* MB vs GBM	36	SN2-NH-OH DDK133 DDK115 KD5170 KSK041 LAK05 DDK113 Entinostat LAK13 LMK163 LMK233 LMK225 M344 Vorinostat LMK208 KK20OH KP14OH KSK056 KP06Hy LMK157 EHKXII LAK21 VSK347-NH-OH DDK144 LAK23 KSK145 LAK29 VSK258-NH-OH LAK03 LMK121 KSK135 LAK27 DDK143 Scriptaid LMK158 DDK148
MYC MB vs AT/RT *MYC* MB vs DIPG	3	LMK235 VTK36 Belinostat
MYC MB vs DIPG *MYC* MB vs GBM	2	DDK121 DDK137
MYC MB vs AT/RT	1	DDK120
MYC MB vs GBM	3	KSK033 KSK139 DDK132
MYC MB vs DIPG	1	Panobinostat

Supplementary Table 2. Overview of inhibitors identified from synergy screen

Names	total	elements
D425 MED IC10 D425 MED IC25 MED8A IC10 MED8A IC25	17	Decitabine Clofarabine Daunorubicin hydrochloride Rigosertib sodium Epirubicin hydrochloride Bardoxolone methyl Teniposide Mitomycin C Valrubicin Etoposide GSK126 Irinotecan Bortezomib Mitoxantrone dihydrochloride Uramustine MLN9708 Melphalan
D425 MED IC10 D425 MED IC25 MED8A IC10	2	LY2835219 6-Mercaptopurine

D425 MED IC10 D425 MED IC25 MED8A IC25	4	Panobinostat Homoharringtonine CI-994 Tubastatin A hydrochloride
D425 MED IC25 MED8A IC10 MED8A IC25	7	Trifluorothymidine Idarubicin hydrochloride 5-Azacytidine Topotecan hydrochloride Olaparib Doxorubicin hydrochloride Cladribine
D425 MED IC10 MED8A IC10 MED8A IC25	2	Pacritinib Cytarabine
D425 MED IC10 D425 MED IC25	16	ABT-199 Lapatinib Entinostat Vorinostat TAK-715 LDK378 Carfilzomib Erlotinib hydrochloride Belinostat Vinflunine tartrate BIBF 1120 INK 128 Lonafarnib Alisertib Volasertib API-2
D425 MED IC10 MED8A IC25	1	Oxaliplatin
MED8A IC10 MED8A IC25	12	3-Deazaneplanocin A hydrochloride Gemcitabine Everolimus LY3009120 Fosbretabulin disodium Deforolimus GSK 525762A Elesclomol Linsitinib Floxuridine Obatoclax Palbociclib
D425 MED IC25	12	Gefitinib Retinoic acid WP1066 Canertinib Imatinib mesylate Staurosporine PF-04691502 Temozolomide Cabazitaxel R406 Amonafide Dinaciclib
D425 MED IC10	1	CYT387
MED8A IC10	4	Pazopanib hydrochloride Bosutinib Quizartinib Dasatinib
MED8A IC25	5	Thioridazine hydrochloride OTX-015 Rapamycin Verteporfin Tivozanib

7.2 Abbreviations

µg	Microgram
µl	Microliter
AT/RT	Atypical teratoid/rhabdoid tumor
ATP	Adenosine triphosphate
BET	Bromodomain and extraterminal domain
BSA	Bovine serum albumin
cDNA	Complementary DNA
CNS	Central nervous system
CoREST	Co-repressor of REST
CREBBP	CREB binding protein
CSF	Cerebrospinal fluid
CTCL	Cutaneous T-cell lymphoma
CTG	CellTiter Go
CTNNB1	Catenin beta 1
CU	Connecting unit
D/N	Desmoplastic-nodular
DIPG	Diffuse intrinsic pontine glioma
DMEM	Dulbecco's Modified Eagle Medium
DMSO	Dimethyl sulfoxide
DNA	Deoxyribonucleic acid
dNTP	Deoxynucleotide
EGF	Epidermal growth factor
EGFR	Epidermal growth factor receptor
EtOH	Ethanol
FBS	Fetal bovine serum
FDA	Food and Drug Administration
FGFR	Fibroblast growth factor
FITC	Fluorescein isothiocyanate
g	g Force

GBM	Glioblastoma
GFP	Green fluorescent protein
GLI	Glioma-associated oncogenes
h	Hours
HAT	Histone acetyltransferase
HDAC	Histone deacetylase
HTS	High-troughput screening
IC_{50}	Half maximal inhibitory concentration
IPA	Ingenuity Pathway Analysis
KDM	histone lysine demethylases
LCA	Large-cell-anaplastic
MB	Medulloblastoma
MBEN	Medulloblastoma with extensive nodularity
MiDAC	Mitotic deacetylase
min	Minutes
mL	Milliliter
mM	Millimole
MPNST	Malignant peripheral nerve sheath tumor
mRNA	Messenger ribonucleic acid
NAD+	Nicotinamide adenine dinucleotide
NB	Neuroblastoma
NFκB	Nuclear factor kappa-light-chain enhancer of activated B cells
NuRD	Nucleosome remodeling and deacetylase
OTX2	Orthodenticle homeobox 2
PBS	Phosphate buffered saline
PGK1	Phosphoglycerate kinase 1
PI	Propidium iodide
PI3K	Phosphatidylinositol 3-kinase
PPIA	Peptidylprolyl isomerase A
PTCH1	Patched 1

PTCL	Peripheral T-cell lymphoma
PTEN	Phosphatase and tensin homolog
PVT1	Plasmacytoma variant translocation 1
qPCR	Quantitative polymerase chain reaction
RNA	Ribonucleic acid
RPMI	Roswell Park Memorial Institute
RT	Room temperature
SAR	Structure-activity relationship
SD	Standard deviation
SEM	Standard error of the mean
SHH	Sonic hedgehog
SMO	Smoothened
SMRT/NCoR	Cuclear receptor corepressor
SUFU	Suppressor of fused
TGM2	Transglutaminase 2
TNFa	Tumor necrosis factor
WB	Western Blot
WHO	World Health Organization
WNT	Wingless
YAP1	Yes-associated protein 1
ZGB	Zinc binding group

7.3 List of figures

7.4 List of tables

Curriculum Vitae

Personal Data

Name: Viktoria Marquardt

Date of birth: 02.06.1987, Kassel

Education

01/2015 – present   PhD student, Heinrich-Heine University Düsseldorf, Scholarship by the Düsseldorf School of Oncology (DSO)

Thesis: Evaluation of novel HDAC inhibitors for epigenetic therapy of brain tumors. (Prof. T. Kurz, PD J. Felsberg, Dr. M. Remke, Institute for Pharmaceutical and Medicinal Chemistry, Institute of Neuropathology, Pediatric Neuro-Oncogenomics)

10/2011 – 12/2013   M.Sc. Chemical Biology, Technical University Dortmund

Master Thesis: Design, synthesis and biological evaluation of b-annelated dihydropyridines as inhibitors of the TGFβ signaling pathway (Prof. D. Schade, Prof. D. Rauh, Medicinal Chemistry)

10/2008 – 09/2011   B.Sc. Chemical Biology, Technical University Dortmund

Bachelor Thesis: Bioconjugation of proteins via oxime ligation (Prof. C. Niemeyer, Biochemical Microstructure Technology)

06/2007   Abitur

Engelsburg Gymnasium Kassel

Publications and presentations

Publication included in this thesis

Marquardt V, Theruvath J, Pauck D, Picard D, Qin N, Blümel L, Maue M, Bartl J, Ahmadov U, Langini M, Meyer FD, Graef CM, Wölfl M, Milde T, Witt O, Erdreich-Epstein A, Leprivier G, Kahlert U, Stefanski A, Stühler K, Keir ST, Bigner DD, Hauer J, Beez T, Knobbe-Thomsen CB, Fischer U, Felsberg J, Hansen FK, Cheshier SH, Reifenberge Gm Borkhardt A, Kurz T, Mitra S, Remke M. *HDAC and NFκB antagonists synergistically inhibit growth of MYC-driven medulloblastoma.* Submitted

Other publications

Tjaden B, Baum K, <u>Marquardt V</u>, Simon M, Trajkovic-Arsic M, Kouril T, Siebers B, Lisec J, Siveke JT, Schulte JH, Benary U, Remke M, Wolf J, Schramm A. *MYCN-induced metabolic rewiring creates novel therapeutic vulnerabilities in neuroblastoma.* BioRxiv, doi: https://doi.org/10.1101/423756.

Reßing N, <u>Marquardt V</u>, Gertzen C. G. W, Schöler A, Schramm A, T. Kurz, H. Gohlke, A. Aigner, M. Remke and F. K. Hansen. *Design, Synthesis and Biological Evaluation of β-Peptoid-Capped HDAC Inhibitors with Anti-Neuroblastoma and Anti-Glioblastoma Activity.* Med. Chem. Commun. 2018 Oct 23;10(7):1109-1115.

Bhatia S, Diedrich D, Frieg B, Ahlert H, Stein S, Bopp B, Lang F, Zang T, Kröger T, Ernst T, Kögler G, Krieg A, Lüdeke S, Kunkel H, Rodrigues Moita AJ, Kassack MU, <u>Marquardt V</u>, Opitz FV, Oldenburg M, Remke M, Babor F, Grez M, Hochhaus A, Borkhardt A, Groth G, Nagel-Steger L, Jose J, Kurz T, Gohlke H, Hansen FK, Hauer J. *Targeting HSP90 dimerization via the C terminus is effective in imatinib-resistant CML and lacks the heat shock response.* Blood. 2018 Jul 19;132(3):307-320.

Stenzel K, Hamacher A, Hansen FK, Gertzen CGW, Senger J, <u>Marquardt V</u>, Marek L, Marek M, Romier C, Remke M, Jung M, Gohlke H, Kassack MU, Kurz T. *Alkoxyurea-Based Histone*

Deacetylase Inhibitors Increase Cisplatin Potency in Chemoresistant Cancer Cell Lines. J Med Chem. 2017 Jul 13;60(13):5334-5348.

Maciaczyk D, Picard D, Zhao L, Koch K, Herrera-Rios D, Li G, Marquardt V, Pauck D, Hoerbelt T, Zhang W, Ouwens DM, Remke M, Jiang T, Steiger HJ, Maciaczyk J, Kahlert UD. *CBF1 is clinically prognostic and serves as a target to block cellular invasion and chemoresistance of EMT-like glioblastoma cells.* Br J Cancer. 2017 Jun 27;117(1):102-112.

Selt F, Hohloch J, Hielscher T, Sahm F, Capper D, Korshunov A, Usta D, Brabetz S, Ridinger J, Ecker J, Oehme I, Gronych J, Marquardt V, Pauck D, Bächli H, Stiles CD, von Deimling A, Remke M, Schuhmann MU, Pfister SM, Brummer T, Jones DT, Witt O, Milde T. *Establishment and application of a novel patient-derived KIAA1549:BRAF-driven pediatric pilocytic astrocytoma model for preclinical drug testing.* Oncotarget. 2017 Feb 14;8(7):11460-11479.

Poster and oral presentations

HDAC and NFκB antagonists synergistically inhibit growth of MYC-driven medulloblastoma.
V. Marquardt, J. Theruvath, D. Pauck, D. Picard, N. Qin, L. Blümel, F. K. Hansen, J. Felsberg, S. Cheshier, G. Reifenberger, A. Borkhardt, T. Kurz, S. Mitra, M. Remke.

Poster, 5th Pediatric Neuro-Oncology Basic & Translational Research Conference, 03.-04.05.2019, San Francisco, USA.

Talk at poster highlight session, 18th International Symposium Pediatric Neuro-Oncology (ISPNO), 01.-03.07.2018, Denver, USA.

Identification of a selective histone deacetylase inhibitor for MYC-driven medulloblastoma by high-throughput drug screening.
V. Marquardt, J. Theruvath, F. K. Hansen, D. Pauck, D. Picard, J. Felsberg, S. Cheshier, G. Reifenberger, A. Borkhardt, T. Kurz, S. Mitra, M. Remke.

1st poster award, 6th Retreat Düsseldorf School of Oncology (DSO), 03.05.2018, Düsseldorf, Germany.

Poster, 1st Translational Oncology Symposium (ETOS), 12.1.2018, Essen, Germany.

Talk, 1st Taiwan-German Epigenetics, Cancer Biology, and Therapy symposium", 26-29.06.2017, Taipei, Taiwan.

Poster, 4th Pediatric Neuro-Oncology Basic and Translational Research Conference, 15.-16.06.2017, New York, USA.

Talk, 5th Retreat Düsseldorf School of Oncology, 06.04.2017, Düsseldorf, Germany.

High throughput screening of novel histone deacetylase inhibitors for epigenetic therapy of primary brain tumors.

V. Marquardt, F. K. Hansen, D. Picard, J. Felsberg, G. Reifenberger, A. Borkhardt, T. Kurz, M. Remke.

Talk at poster highlight session, 48th Congress of the International Society of Pediatric Oncology (SIOP), 19.-22.10.2016, Dublin, Ireland.

Talk, 25th GPOH Arbeitstagung Experimentelle Neuroonkologie, 29.-30.04.2016, Minden, Germany

Talk, 4th Retreat Düsseldorf School of Oncology, 03.03.2016, Düsseldorf, Germany.

Acknowledgements

Affirmation

Hereby, I declare on oath that I composed this dissertation independently by myself. I used only the references and resources indicated in this thesis. With the exception of such quotations, the work presented in this thesis is my own. I have accredited all the sources of help. This PhD thesis was never submitted or presented in a similar form to any other institution or examination board. I have not undertaken a doctoral examination without success so far.

_____

Viktoria Marquardt